FORSCHUNGSZENTRUM ROSSENDORF FZR - 212

Institute of Ion Beam Physics and Materials Research

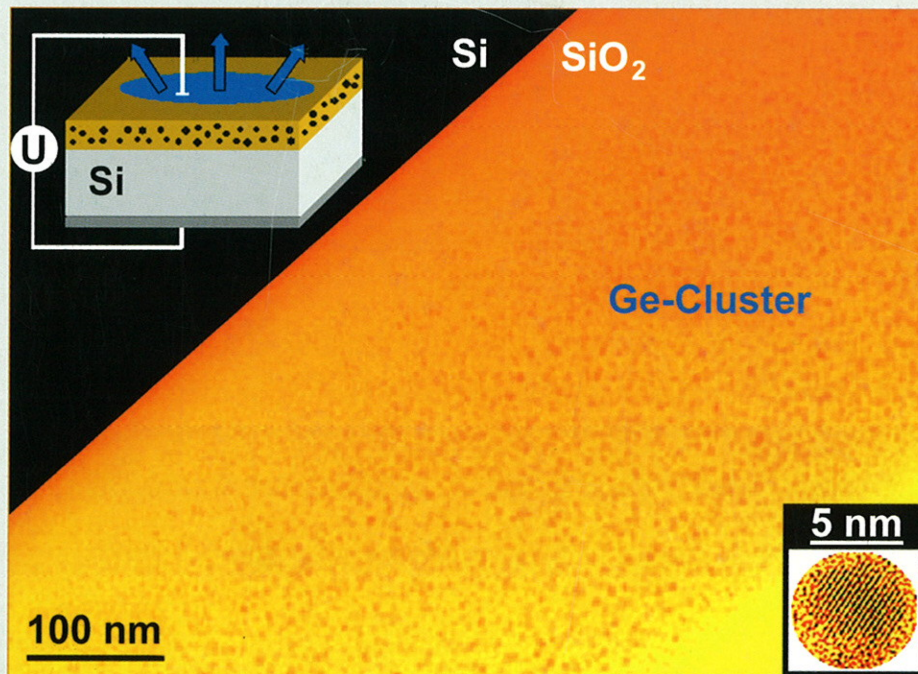

Annual Report 1997

Postfach 510119
D-01314 Dresden, Germany
Tel. +49-351-260-22 45
Fax +49-351-260-32 85

Forschungszentrum
D 120
-Bibliothek-
Rossendorf e.V.

BRD

FORSCHUNGSZENTRUM ROSSENDORF
INSTITUT FÜR IONENSTRAHLPHYSIK UND MATERIALFORSCHUNG

Annual Report 1997

Editors:
J. von Borany, H.-U. Jäger, W. Möller, E. Wieser

FZR-212
Februar 1998

For further information on the research projects described in the present annual report, please address the director or one of the authors at the institute.

Front cover:
Cross-sectional transmission electron micrograph of a Si/SiO_2 structure with Ge nanoclusters formed by ion-beam synthesis. The high-resolution image (bottom right) shows an individual cluster with its (111) lattice planes.The structure exhibits an intensive UV and blue photo- and electroluminescence (schematic top left). See p. 31.

Director: Prof. Dr. Wolfhard Möller

P. O. B. 51 01 19
D-01314 Dresden
Germany

Tel.: +49 351 260 2245
Fax: +49 351 260 3285
E-mail: w.moeller@fz-rossendorf.de

Preface

The Research Center Rossendorf (Forschungszentrum Rossendorf, FZR) represents the largest governmental research institution in the "new" states of the Federal Republic of Germany. Its presently about 600 employees, organized in five institutes, study problems of basic and applied science in the fields of biomedicine, environmental research and materials science. The FZR is a member of the "Gottfried Wilhelm Leibniz Society" (WGL), with the federal government and the state of Saxony contributing 50 % of the basic funding each.

The Institute of Ion Beam Physics and Materials Research (IIM) has 76 permanent positions of scientists (32), technicians and engineers (42) and administration personnel (2). In average about 40 additional employees are funded from PhD student and PostDoc programs, guest funds, and governmental and industrial projects. The aim of the institute is to combine basic research and application-oriented studies in the fields of ion surface modification and ion beam surface analysis. According to the German Science Council, the institute shall represent a national ion beam center, which, in addition to its own scientific research, offers services and transfers know-how on ion beam techniques to universities, other research institutes, and industry.

For these purposes, a broad range of ion-related equipment is available, delivering ion energies from about 10 eV (plasma treatment) to several 10 MeV (electrostatic accelerators). For the diagnostics of ion-treated surfaces, standard analytical techniques are available such as transmission electron microscopy, X-ray diffraction, Auger and photoelectron spectroscopy, and a number of chemical, optical, electrical, and mechanical diagnostics. Sample preparation is available for a large number of different materials including standard silicon processing.

The main R&D activities of the institute are subdivided into the fields of New Materials (Hard Coatings, Phases and Defects, Nanoclusters) and New Processes (Focused Ion Beam, Plasma Immersion Implantation, MeV Ion Beam Analysis) as shown in the figure.The present Annual

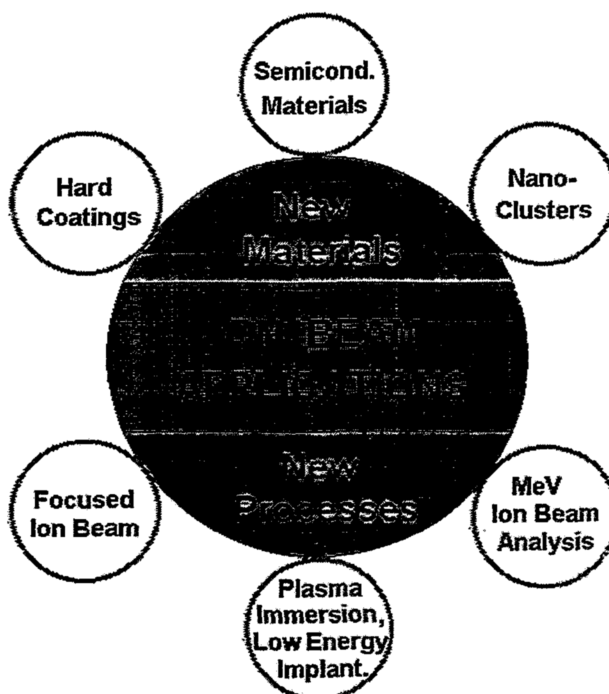

Report documents the scientific progress of the institute in these areas. In 1997, the number of scientific publications has still been increasing, in particular in the most renowned international journals and on the base of intense national and international collaborations. These collaborations are also substantiated by numerous guests at the institute, and in turn by many visits of our researchers at other institutions. A number of invited lectures, given at international conferences by members of the institute, confirm its progress towards an internationally highly competitive ion beam research center.

This progress is also confirmed by the placement of the 14th International Conference on Ion Beam Analysis in connection with the 6th European Conference on Accelerators in Applied Research and Technology, which will be organized by the institute to be held at Dresden in summer 1999, and for which more than 400 participants are expected. In 1997, the institute (supported by the Dresden Fraunhofer Institutes of Materials and Beam Techniques, and of Electron and Plasma Techniques) organized successfully the 8th German Conference on Plasma Technology with about 200 scientists and exhibitors from universities, research institutes, and industry. Furthermore, a summer school "Nuclear Probes and Ion Beams" was organized in cooperation with the Hahn-Meitner Institute, Berlin, and held in Bad Blankenburg (Thuringia) with 35 students and 12 lecturers.

The research efficiency of the institute relies essentially on the engagement of young scientists, in particular of the PhD students and PostDocs. Six PhD students finished their theses and passed their doctoral examinations with mostly excellent results. At present and for the future, we hope to maintain the very high standard of our young researchers, in spite of the dramatically decreased number of university students in physics all over Germany.

A number of new projects were acquired in 1997 from different governmental funding organisations in Germany and from the European Union, partly involving cooperation with industry. The participation in a European Network in the field of thin-film deposition will especially promote the cooperation of young researchers from different European nations.

The ion beam service activities of the institute have been significantly extended in 1997. Ion beam analysis services for universities and industry cover a wide range of materials such as metals, semiconductors, hard coatings, oxides and perovskites, and are related to a broad spectrum of activities for mechanical and electronic applications and in energy research, biomedicine, information technology, geology, and extraterrestrial research. Ion implantation service, including the plasma immersion technique and the focused ion beam, was performed in cooperation with about 40 partner institutions from research and industry. Comparatively minor activities also involved furnace annealing, optical and mechanical diagnostics, X-ray diffraction, transmission electron microscopy and Auger electron and Mössbauer spectroscopy.

The GESIM small enterprise, which had been founded in 1995 based on research activities of the institute, received the Innovation Award 1997 of the German Industry for the development of microfluidic components ("World's smallest pump"). GESIM still cooperates with the institute in a common project and makes use of its services. We congratulate our former coworkers and hope that their success will encourage further initiatives promoting industrial applications of successful developments at the institute.

The construction works for the new aceelerator building of the institute are near completion. A major fraction of the beamline components and experimental facilities to be installed there has been purchased in 1997. The 5 MV Tandem accelerator celebrated its 25th anniversary and

received a new injector system including remote control. In addition, the control panel and a number of power supplies were modernized. The 300 kV transmission electron microscope was equipped with a two-dimensional CCD camera. Two new devices were installed for plasma immersion implantation, for an increased process volume (0.3 m^3) and for the combination with filtered arc deposition of thin films.

The installation of the Rossendorf Beamline (ROBL) at the ESRF (Grenoble, France) has proceeded in a very efficient and successful way. The complete X-ray optics and a 6-axis goniometer for x-ray diffraction studies including control and data acqusition were installed and commissioned. First diffraction experiments demonstrated an energy resolution close to the calculated data.

The present report will first describe the most important scientific results achieved in 1997, in the form of letter contributions. Subsequently, short summaries of the individual research activities will be given, followed by a statistical section.

The institute would like to thank all friends and organisations who supported its progress in 1997. Special thanks are due to the directors of the Forschungszentrum Rossendorf, the minister of science and arts of the Free State of Saxony, and the minister of research and technology of the Federal Government of Germany. Our partners from industry and other research institutes play an essential role for the Rossendorf ion beam center. Last but not least, the director would like to thank all members and guests of the institute for their active and often excellent contributions to a successful development in 1997.

Prof. Wolfhard Möller

Contents

Page

Highlights

First Synchrotron Light at ROBL 11

Molecular-Dynamics Studies of a-C:H Film Growth by Energetic Hydrocarbon Molecule Impact 15

On the Role of Laminate Architecture in Al/AlN Multilayers Synthesized by Ion Beam Assisted Deposition 19

Detection of Metastable Defects in Ion-Implanted Silicon by Means of Metal Gettering 23

A New Approach to Full Atomistic Simulation of Ion Implantation within a Commercial Process Simulator 27

Strong Blue and Violet Photo- and Electroluminescence from Germanium- and Silicon-Implanted Silicon Dioxide Layers 31

Damage-Related Dwell-Time Effects in Focused Ion Beam Synthesis of Cobalt Disilicide 35

Ion Nitriding of Austenitic Stainless Steel: Influence of the Surface Oxide Layer on the Nitriding Kinetics 40

Biocompatibly Reactive Titanium Surface Endowed by Ion Implantation 44

Short Contributions

Abbreviations 51

Hard Coatings 53

Semiconductor Materials 55

Nanoclusters 62

Focused Ion Beam 66

Plasma Immersion Ion Implantation 68

Ion Beam Analysis 70

Equipment 73

Other Activities 74

Statistics

Publications 81

Conference Contributions 90

Lectures 102

Reports 106

Laboratory Visits 107

Guests 110

Awards 113

PhD Theses 113

Diploma Thesis 113

Meetings Organized by the Institute 113

Patents 114

New Projects 114

Departments of the Institute 115

Experimental Equipment 116

List of Personnel 117

Highlights

First Synchrotron Light at ROBL

W. Matz, N. Schell, F. Prokert, F. Eichhorn and M. Betzl

The Forschungszentrum Rossendorf is constructing a synchrotron radiation beamline at the bending magnet BM20 of the European Synchrotron Radiation Facility (ESRF) in Grenoble [1]. The project of the *RO*ssendorf *B*eam*L*ine (ROBL) consists of two experimental end-stations for radiochemistry and materials research, respectively [2]. It is the only beamline at the ESRF directly built by a German institution. Moreover, the radiochemistry set-up, which allows experiments with low radioactivity (liquid and solid samples) will be unique in the world. During 1997 the beamline optics as well as the main equipment of the materials research hutch (MRH) were installed and commissioned. This report describes the installations in the MRH and the first results obtained.

The beamline optics is designed for delivering monochromatic synchrotron radiation in the energy range from 5 to 35 keV. The energy resolution will be better than 10^{-3} for all energies. For the double crystal monochromator two pairs of silicon crystals with the orientations (311) and (111), respectively, are available. The suppression of harmonics is performed by two X-ray mirrors in front of and behind the monochromator. Both mirrors carry two strips with coatings of platinum and silicon, respectively. The silicon coated mirror will be used for experiments in the low-energy range (<12 keV) while the platinum coated mirror is for the high-energy range. Normally, the beam has a height of 3 mm and a width up to 70 mm. Focusing the beam to a size less than 1x1 mm^2 is foreseen, but not yet installed. A detailed description of the optics layout and the design principles is given in [3].

The materials research end station is designed mainly for X-ray diffraction and reflectometry. An overview of MRH is given in Fig. 1. The basic instrument is a 6-circle goniometer with a heavy-load sample table (up to 15 kg). The sample may be mounted in the goniometer circle, on a x-y-z-table or on a powder sample support. The high-load design is necessary for a high-temperature chamber allowing experiments up to 2000°C.

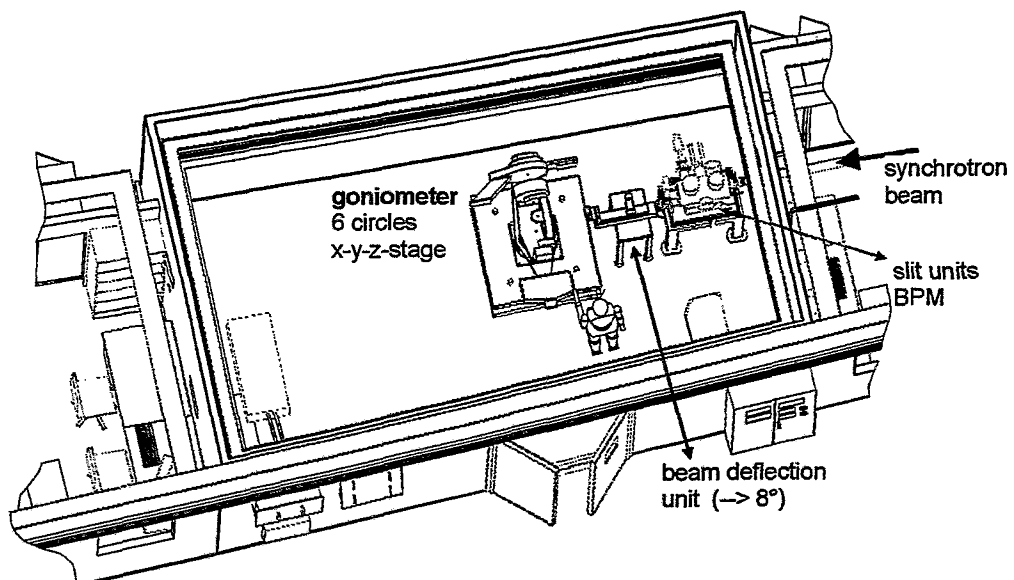

Fig. 1: Birds eye view of the materials research hutch (MRH) of ROBL.

The intended applications cover structural investigations on surfaces and buried thin films produced by ion beam techniques in Rossendorf. An additional option is the diffraction on liquids with free surfaces (e.g. melts) for which a deflection unit is installed in front of the goniometer to allow angles of incidence up to 8° onto the sample.

The first diffraction experiments were performed mainly with standard or already studied samples in order to test the performance of the instrument. The diffraction pattern of pure Si powder allows a simple estimate of the resolution by comparing the FWHM of the Bragg peaks. Fig. 2 shows the experimental resolution for diffraction expressed by $\Delta d/d$ in dependence on the lattice plane spacing d of crystals. The data from ROBL are compared with the typical resolution of a laboratory X-ray diffractometer for standard powder diffraction (Bragg-Brentano configuration; URD BB in Fig. 2) and for thin film studies with grazing incidence (URD DSA in Fig. 2). In the latter case one has to realise a parallel beam geometry which limits the resolution in the laboratory instrument for reasons of intensity. The synchrotron source delivers this parallel beam condition a priori which explains the resolution improvement by a factor of about 10. It should be noted that the reported values do not represent the instrumental resolution of ROBL for diffraction experiments. The instrumental contribution to the peak width was measured with perfect silicon single crystal. The value of 0.005° at 8 keV shows that the actual peak width in the diffraction pattern of polycrystals is determined by the sample under investigation.

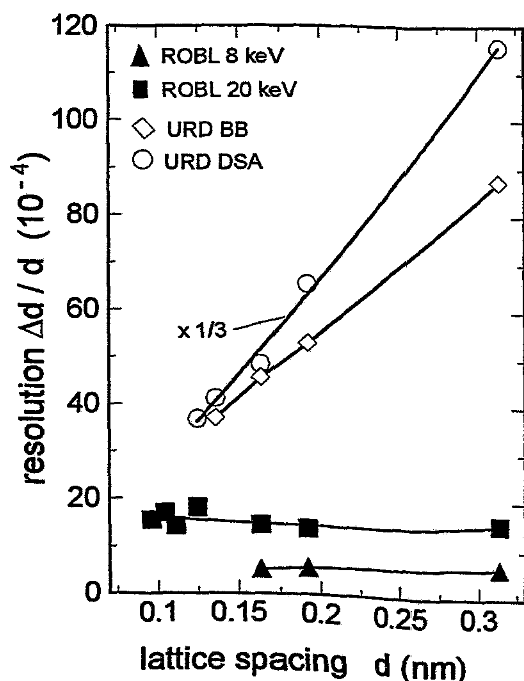

Fig. 2:
Experimental resolution $\Delta d/d$ in dependence on lattice spacing d for comparison of a X-ray diffraction laboratory equipment (URD BB; URD DSA) with the materials research set-up at ROBL for 8 and 20 keV, respectively.

Besides general structural studies of thin films, the identification and size estimation of nanocrystals in amorphous matrices is a very demanding point for X-ray diffraction. We have studied the formation of nanocrystals of AgX (X = Cl, I, Br) after ion co-implantation of Ag and X into an amorphous SiO_2 layer of 70 nm thickness [4]. The size evolution of the nanocrystals in dependence on the annealing temperature was deduced from the line broadening of Bragg peaks. Fig. 3 compares the parts of diffraction patterns from the system Ag+I, where Ag nanoclusters are formed, measured at ROBL (a) and with laboratory X-ray equipment (b). The conventional X-ray measurement was performed with Cu-K_α-radiation (8.02 keV) whereas for the synchrotron experiments 15.6 keV radiation was used. Due to the high resolution the intensity gain at ROBL is here only a factor of 4. However, the measuring time at ROBL was half of that in the laboratory experiment, so that the overall gain factor is near ten, although the intensity suffers from the air scattering (about 2.5 m) at ROBL. From

the line broadening of the Bragg reflections a mean crystallite size of (18±1) nm was estimated for the ROBL experiment. This is in good agreement with the earlier data of (20.5±2.5) nm. In this case the high resolution of the synchrotron experiment is not necessary since line broadening is much greater than the instrumental line width. On the other hand it will allow to follow the size evolution of nanocrystals up to crystallite sizes of 100 nm, where line broadening effects are significantly reduced.

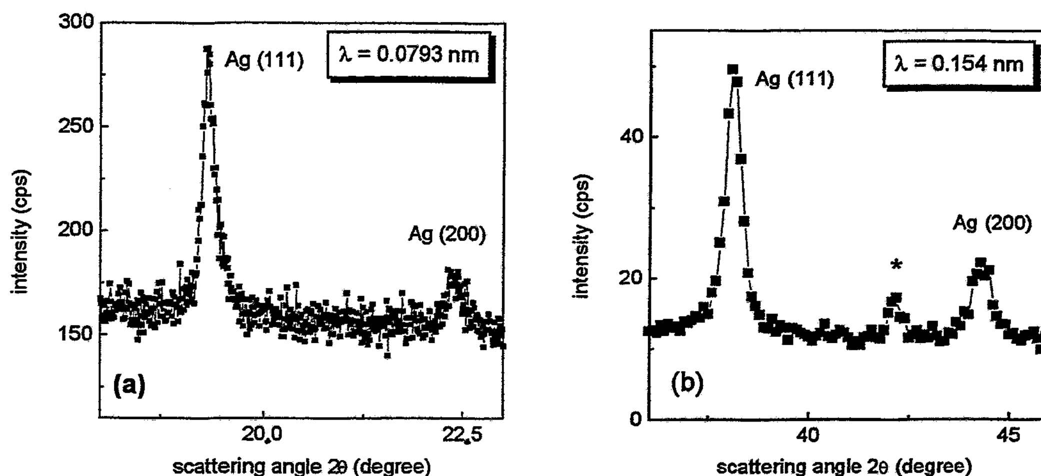

Fig. 3: The first two diffraction peaks from silver nanocrystals in a SiO_2 matrix produced by ion implantation and annealing at 600°C. (a) experiment at ROBL with λ=0.0793 nm, (b) laboratory experiment at IIM with λ=0.1514 nm (the additional peak marked by an asterisk (*) results from the Si substrate).

Furthermore, we have studied SiC particles synthesised by high-dose carbon implantation into silicon. The (100) Si wafer was implanted with a dose of 4×10^{17} C/cm^2 at an energy of 195 keV and a temperature of 500°C. Due to the small volume concentration of the formed 3C-SiC particles only the strongest diffraction peak (111) could be detected under laboratory conditions (sealed Cu tube, λ=0.154 nm) with a rather low accuracy in intensity and in angular position. Fig. 4 shows the (200) peak obtained at ROBL with λ=0.07927 nm with a reasonable intensity and a small half-width. With these conditions it is possible to study in future the size and the orientation of 3C-SiC particles formed at different implantation parameters.

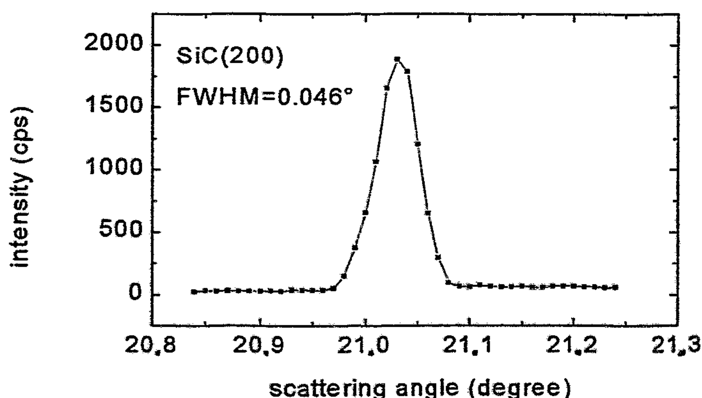

Fig. 4: (200) diffraction peak of 3C-SiC particles formed by carbon ion implantation into silicon.

In summary, the first experiments with the materials research goniometer at ROBL are very encouraging and promise many sophisticated experiments during the forthcoming years. It should be noted that at present not all design features for resolution and intensity optimisation are implemented in the beamline optics, sò that in future still better conditions will be available.

Acknowledgements

The authors thank Dr. W. Oehme, P. Reichel, Dr. D. Pröhl, and S. Dienel for the design and installation of control and measuring electronics at MRH. The construction of ROBL is a joint project of the Institute for Ion Beam Physics and Materials Research, the Institute for Radiochemistry as well as the Central Department of Research and Information Technology of the Forschungszentrum Rossendorf.

References

[1] For general information see: http://www.esrf.fr
[2] Beamline description in: http://www.fz-rossendorf.de/FWE/project_group.html
[3] W. Matz, F. Prokert, R. Schlenk, J. Claußner, N. Schell, F. Eichhorn, G. Bernhard, The Rossendorf Beamline at the ESRF, Report FZR-158, Rossendorf 1996
[4] W. Matz, M.T. Pham, A. Mücklich, J. Mat. Science **33** (1998) 155

Molecular-Dynamics Studies of a-C:H Film Growth by Energetic Hydrocarbon Molecule Impact

H.-U. Jäger

There is great interest in the deposition of amorphous carbon (a-C and a-C:H) films because of their smoothness, transparency, hardness, low friction and chemical inertness [1]. These properties are strongly related to the ratio of sp^3 to sp^2 bonded carbon atoms in the films. The higher the amount of C-C sp^3 bonds the closer the film properties are to those of crystalline diamond. The most highly sp^3 bonded form of a-C, known as tetrahedral amorphous carbon (ta-C), is prepared from mass-filtered beams of medium energy ions ($E \approx 100$ eV per C atom). According to the phenomenological subplantation deposition model, the sp^3 bonding arises from C ions entering subsurface atomic sites and producing a quenched-in density increase.

The hydrogenated analogue of ta-C, i.e. ta-C:H films, has recently been prepared by plasma deposition using a low pressure plasma beam source with acetylene C_2H_2 as source gas [2, 3]. The properties of ta-C:H films as function of the incident ion energy and the substrate temperature have been widely studied. At room temperature the diamond-like character reaches a maximum at an energy of about 200 eV per $C_2H_2^+$ ion, or 92 eV per C atom. This optimum energy per C atom is similar to that found for the deposition of ta-C, which suggests that the subplantation model also describes the deposition of a-C:H [4].

To obtain a further, more detailed insight into the formation of a-C and a-C:H films by energetic particles, molecular dynamics studies can be used. Such investigations were performed for C atom impact [5, 6], for methyl radical deposition [7], but have not as yet been applied to C_2H_2 beams. The empirical hydrocarbon potential of Brenner [8] provides a possibility to analyse C_2H_2 beam deposition. This many-body potential was originally developed for use in simulating the chemical vapor deposition of diamond films. It describes chemical bonding in a variety of hydrocarbon molecules as well as graphite and diamond lattices. The potential function is short ranged and rather quickly evaluated, so the demand for computer time is not an essential restriction in performing systematic investigations, also for impacts of more energetic particles. Using parameter set I of Brenner's potential-energy expression, we performed molecular dynamics simulations for impacts of neutral energetic C_2H_2 molecules onto hydrogen-terminated diamond surfaces [9].

The evolution of the atoms in time and space is calculated by the numerical solution of the classical equations of motion. Diamond target slabs of two different surface orientations, {111} and {001}, are considered. Periodic boundary conditions are used for the two directions perpendicular to the surface. The slabs have 30 or 32 carbon atoms per layer, respectively. Totally the number of substrate carbon atoms taken into account varies between 360 and 640 atoms, in dependence on incidence energy and crystal orientation. A monolayer of hydrogen atoms is placed above the diamond surface atoms. The Brenner potential correctly predicts that a hydrogen-covered bulk-terminated diamond {111} surface is favored over other possible surface states. So it is reasonable to use in our investigations a diamond target with a hydrogen-covered bulk-terminated {111} surface where all carbon atoms are initially 4-fold coordinated. For similar reasons, the {001} slab which we use has a hydrogen-covered dimer reconstructed {001}(2x1) surface. Only normal incidence of the C_2H_2 molecules is considered.

Effects (averaged values, per C_2H_2 impact)	diamond {111}:H				diamond {001}(2x1):H		
	C_2H_2 impact energy E(eV)						
	40eV	80eV	120eV	200eV	40eV	120eV	200eV
numbers of deposited projectile atoms:							
C	1.98	2.00	2.00	2.00	1.99	2.00	2.00
H	1.79	1.45	1.17	0.78	1.80	1.14	0.91
sputtering:							
H atoms	0.96	1.97	2.52	2.93	0.72	1.97	2.51
H_2 molecules	0.02	0.07	0.22	0.30	0.01	0.17	0.23
averaged $E_{kin}(eV)$ of H	1.56	3.26	4.06	5.55	1.22	3.43	4.17
resultant numbers of C atoms with coordinations other than 4:							
minimum-maximum(found)	0-8	0-14	2-17	3-24	0-9	2-27	6-33
2-fold coordinated	0.09	0.12	0.16	0.38	0.14	0.52	1.00
3-fold coordinated	2.67	4.25	6.60	11.21	2.82	8.75	15.21
5-fold coordinated	0.17	0.42	0.63	1.09	0.34	0.57	1.04

Tab. 1: Simulation results for the average effects of energetic C_2H_2 molecule impacts into diamond targets.

In this short contribution, some results for the impact of one energetic C_2H_2 molecule are presented. In ref. [9] film growth is also modelled, but only for low-energy (80 eV) C_2H_2 molecule impacts. At a beam energy of 80 eV, corresponding to ≈37 eV per C atom, highly tetrahedral a-C:H layers are not formed [3]. Extensive computations which are more relevant to ta-C:H deposition are still in progress.

In view of the real experimental conditions, which average over all possible impact points and initial molecule axis orientations, we characterize the single molecule impact by average quantities calculated for a sequence of 100 events with random impact parameters. Tab. 1 summarizes such simulation results: these are predictions for the numbers of deposited projectile atoms, for sputtering, and for the resultant numbers of carbon atoms with coordinations other than 4. C_2H_2 molecule kinetic energies ranging from 40 to 200 eV are taken into account. Fig. 1 shows range distributions for the deposited projectile carbon and hydrogen atoms. At a beam energy of 40 eV, the projectile atoms are adsorbed preferentially as C-H radicals at the surface. Therefore, the 40-eV profiles in Fig. 1 are peaked above the surface carbon layer. Our range profiles are expected to be more accurate than TRIM profiles [10] for such low projectile energies. In addition to the usual projectile energy effect, the computed profiles reflect, to some extent, differences of carbon atomic density in the immediate surface region of the crystal. From the depth distributions a penetration probability can be defined by normalizing the area under the deeper part of the curve to the whole integral value. As limit we have choosen the depth positions of subsurface carbon atoms (see the bold vertical lines in Fig. 1). Our penetration probabilities are plotted in Fig. 2 versus the projectile energies. In order to compare these data with the results of preceding investigations, Fig. 2 also shows the carbon penetration probability reported by Weiler *et al.* [2, 3] which was obtained from plasma beam deposition of ta-C:H under the assumption that only subplantation induced densification leads to the formation of sp^3 bonded carbon. For the low C_2H_2 projectile energies (<80 eV), an agreement of the penetration probabilities concluded from these different investigations cannot be expected. Our range profiles refer to periodically structured diamond targets and contain a component due to "channeling" through the upper

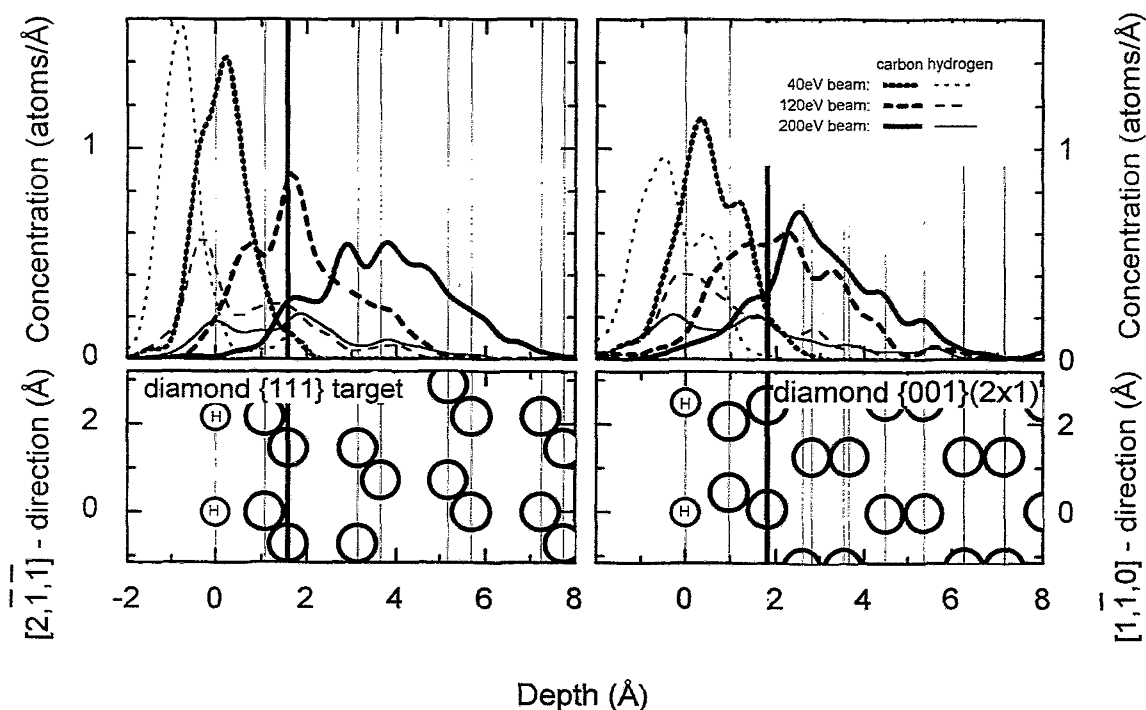

Fig. 1: C_2H_2 projectile atoms depth distributions in hydrogen-covered diamond {111} and {001}(2x1) targets. The bottom graphs and the thin vertical lines show the atomic structure of the target. The thick vertical lines mark the two depths which are used to define atom penetration probabilities.

two carbon layers (compare Fig. 1). This component, which dominates our penetration probabilities at low energies, will be absent from amorphous film data. It is a reasonable result, however, that the different carbon curves shown in Fig. 2 approach each other for penetration probabilities larger than 0.5. This result gives further evidence that subsurface implantation is the basic mechanism for the formation of sp^3 bonded carbon during C_2H_2 plasma beam deposition.

According to our calculated penetration probability for hydrogen (see also Fig. 2), the amount of hydrogen in growing films is expected to be not higher than ≈20%. This is in agreement with the experimental results [11] obtained by plasma beam deposition of highly tetrahedral bonded amorphous carbon.

The model predictions presented in Tab. 1 and Figs. 1, 2 for atom deposition and sputtering prove to depend rather weakly on the orientation of the diamond target. This does not hold true, however, of the impact-induced changes in carbon atom coordinations. In the present analysis, the coordinations are defined by the assumption that carbon-carbon and carbon-hydrogen atom pairs are bonded if the distances between them are less than 1.85 and 1.55 Å, respectively. The choice of these limit values is not critical, such atomic distances are suppressed by the potential and does practically not appear after projectile energy dissipation in the simulation cell. Considering the impact-induced numbers of C atoms in the slab with coordinations other than 4, some trends are obvious from Tab. 1. After a single impact, the number of such carbon atoms varies significantly depending on the respective impact parameters; a minimum value of 0 and a maximum of 33 appear in the table. The average

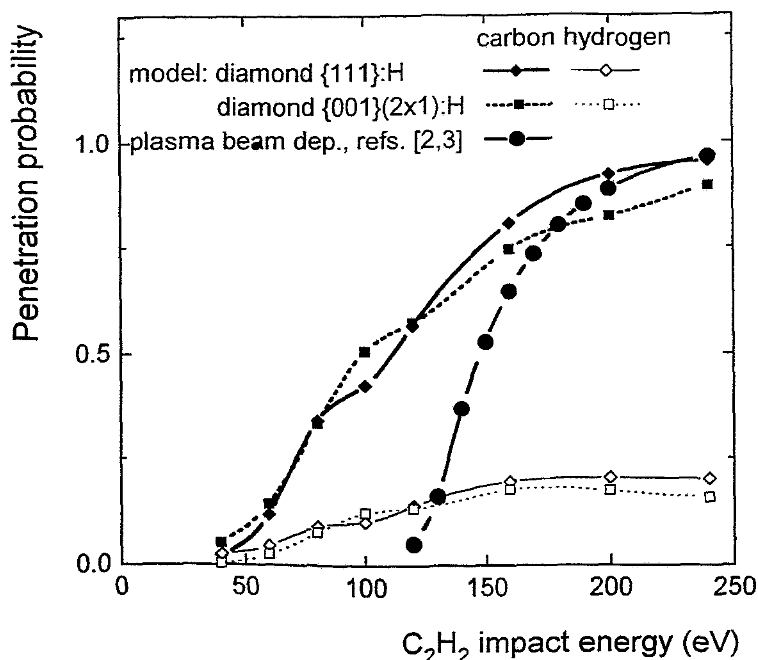

Fig. 2: C_2H_2 projectile atoms penetration probabilities versus projectile energy. Present simulation results for hydrogen-covered diamond {111} and {001}(2x1) targets are shown, together with results from C_2H_2 plasma beam deposition.

value per impact is predicted to be nearly proportional to projectile energy. With increasing projectiles energies, this "damage" in the carbon atom coordinations becomes significantly higher for the diamond {001}(2x1) surface than for the {111} orientation. This result should be caused by the formation of 3-fold coordinated carbon atoms at the {001}(2x1) surface after removal of surface-bonded hydrogen atoms.

References

[1] J. Robertson, Surface Coating Technol. 50 (1992) 185; J. Robertson, Phil. Trans. Roy. Soc. A 342 (1993) 277

[2] M. Weiler, S. Sattel, K. Jung, H. Ehrhardt, V.S. Veerasamy, J. Robertson, Appl. Phys. Lett. 64 (1994) 2797

[3] M. Weiler, S. Sattel, T. Giessen, K. Jung, H. Ehrhardt, V.S. Veerasamy, J. Robertson, Phys. Rev. B 53 (1996) 1594

[4] M. Weiler, J. Robertson, S. Sattel, V.S. Veerasamy, K. Jung, H. Ehrhardt, Diamond Relat. Mater. 4 (1995) 268

[5] D.R. McKenzie, D. Muller, B.A. Pailthorpe, Phys. Rev. Lett. 67 (1991) 773; B.A. Pailthorpe, J. Appl. Phys. 70 (1991) 543

[6] H.P. Kaukonen, R.M. Nieminen, Phys. Rev Let. 68 (1992) 620; Surface Science 331 - 333 (1995) 975

[7] S. Uhlmann, T. Frauenheim, Diamond Relat. Mater. 5 (1995) 169

[8] D.W. Brenner, Phys. Rev. B 42 (1990) 9458; 46 (1992) 1948

[9] H.U. Jäger, M. Weiler, Diamond Relat. Mater., in press

[10] W. Eckstein, Computer Simulations of Ion Solid Interactions, Springer, New York 1990

[11] R. Stief, J. Schafer, J. Ristein, L. Ley, W. Beyer, J. Non Cryst. Solids 198 (1996) 636

On the Role of Laminate Architecture in Al/AlN Multilayers Synthesized by Ion Beam Assisted Deposition

X. Wang, A. Kolitsch, A. Mücklich, F. Prokert and W. Möller

Today multilayer coatings are used in very different fields of application. In addition to combination of single layer materials with very different properties and functions, the most fundamental background for the multilayer concept is to interrupt columnar grain growth [1], which usually occurs in conventional physical vapor deposition (PVD) processes. Improved mechanical hardness of the multilayer coatings is the direct result of the interruption of the columnar growth, according to the Hall-Petch model [2, 3].

While thin films can be tailored by laminate architectures, their structure, and hence properties and performance, can also be improved by ion beam assisted deposition [4]. Little work on the ion beam assisted deposition of multilayers has been reported [5-7]. Actually, the films reported in these references are bilayer, trilayer or multiple layer coatings (3 - 13 single layers), instead of multilayers, and the thickness of the sublayers is larger than 100 nm. Thus, these studies are devoted to the combination of sublayer materials with different functions, without considering the structural modification by laminate architectures.

Here we report on the ion beam assisted deposition (IBAD) of Al/AlN multilayers with a periodic thickness ranging from 6 to 24 nm. We demonstrate how the multilayers prepared by IBAD behave in comparison with their constituent monolithic films, mainly concentrating on the mechanical hardness and its dependence on the structural variation of films. AlN is chosen as the model material because the nitrogen content is not over-stoichiometric, even if the ratio of the nitrogen ion current to the aluminium evaporative flux in the IBAD process is very high [8], which implies that no composition caused structural variation exists when the ion-to-atom ratio is changed in a wide range.

The experimental procedure of IBAD of Al/AlN multilayers and monolithic AlN films has been described in detail elsewhere [8]. The AlN monolithic films were grown by evaporating aluminium under simultaneous nitrogen ion bombardment. During deposition of the Al/AlN multilayers, the N_2^+ ion beam was alternately switched on and off, corresponding to the AlN and Al sublayer deposition periods. The independent control of ion energy, ion beam current and evaporative flux in the IBAD process makes it possible to vary the degree of ion impact during the deposition in a wide range.

In this work, two sets of ion energy E and ion-to-atom arrival rate ratio R were used: $E = 200$ eV and $R = 1.45$, $E = 500$ eV and $R = 3.60$. With each set of E and R, one AlN monolithic film and several Al/AlN multilayers of varying periodic thicknesses λ were prepared.

Tab. I: Preparation parameters for the monolithic AlN films and Al/AlN multilayers.

	Monolithic AlN films		Al/AlN multilayers
	E (eV)	R	λ (nm)
Set I	200	1.45	6, 12, 18, 24
Set II	500	3.60	6, 9, 12

The thicknesses of the Al and AlN sublayers were maintained to be equal. Table I presents the preparation parameters for the two sets of films. The overall film thickness was varied from 500 nm to 900 nm. Depositions were carried out at room temperature.

Fig. 1 comparatively illustrates the hardness of the two sets of AlN monolithic films and Al/AlN multilayers. The hardness of a monolithic Al film is also presented for reference. The hardness was measured using a dynamic ultra-microhardness tester. The load used in the hardness measurement was chosen to be sufficiently small (3 mN) to avoid substrate effects. It is seen that the hardness of the monolithic AlN films can be greatly improved by increasing the ion bombardment. When comparing the Al/AlN multilayers with their constituent monolithic AlN films, two features are noteworthy. First, the two sets show as a common feature that the hardness of the multilayers increases with decreasing λ. Second, there is a remarkable difference between the two sets. In the case of E = 200 eV and R = 1.45, all the multilayers are harder than the corresponding monolithic AlN film within the studied range of λ, in spite of the inclusion of very soft Al sublayers. In contrast, at E = 500 eV and R = 3.60, the multilayers even can not reach the hardness of the constituent AlN film. In other words, the mechanical hardness of the AlN monolithic film in set II can not be improved any more within a multilayer configuration.

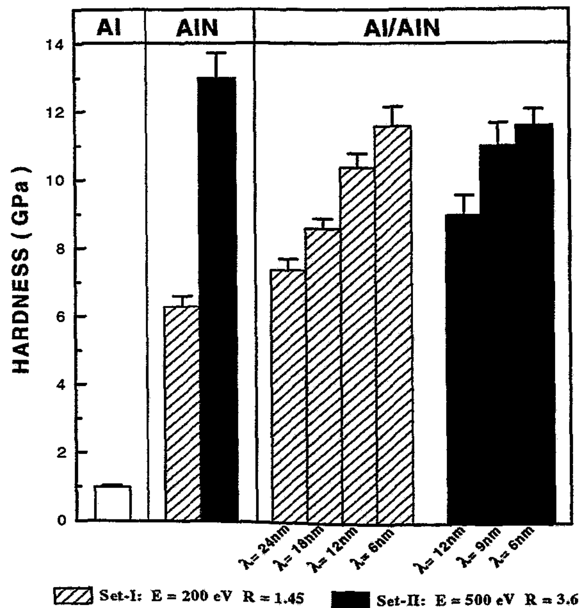

Fig. 1: Hardness of the two sets of the Al/AlN multilayers, along with their constituent monolithic AlN and Al films of equal thickness.

In order to understand the hardness behaviour of the two sets of the AlN and Al/AlN films, X-ray diffraction (XRD) and cross-sectional transmission electron microscopy (TEM) have been performed to examine the structure of the films. XRD analysis shows that the monolithic AlN film of set I exhibits (002) preferred orientation [8]. The hexagonal basal plane (002) of AlN is the most densely packed crystalline plane, grains of this orientation have the lowest surface free energy. It is suggested that the film structure is growth-controlled under the preparation condition of this AlN monolithic film, where the ion impingement is relatively weak, characterized by low E and small R. Fig. 2a shows the cross-sectional TEM view of this monolithic AlN film. It is seen that the film exhibits a pronounced columnar structure, the columns being separated by a large number of porous boundaries. This structural feature with extended microvoids along the column boundaries develops due to atomic self-shadowing by protruding clusters and small ledges as a consequence of insufficient surface mobility of the deposited atoms. The direct TEM observation of the film structure further confirms the above growth-controlled model for the low E and small R case. Each of the columns in Fig. 2a may consist of several crystalline grains, as XRD analysis indicates that the mean AlN crystallite size is smaller than the "columnar grain" size in Fig. 2a. This has also been verified by high resolution TEM observation. From this structure, it is understandable that the AlN monolithic film of set I exhibits a relatively low hardness.

When a laminate architecture is introduced to the films by alternating deposition of Al and AlN, the formed Al/AlN multilayers (of set I) show a considerably changed structure. Fig. 2b is the cross-sectional TEM micrograph of one Al/AlN multilayer of set I with λ = 18 nm. Although the Al and AlN sublayers are not well defined, the layered structure is visible, showing the periodic thickness of 16.3 nm, a little smaller than the pre-set value of 18 nm. The entire film exhibits very slight columnar structure, without microvoids between the

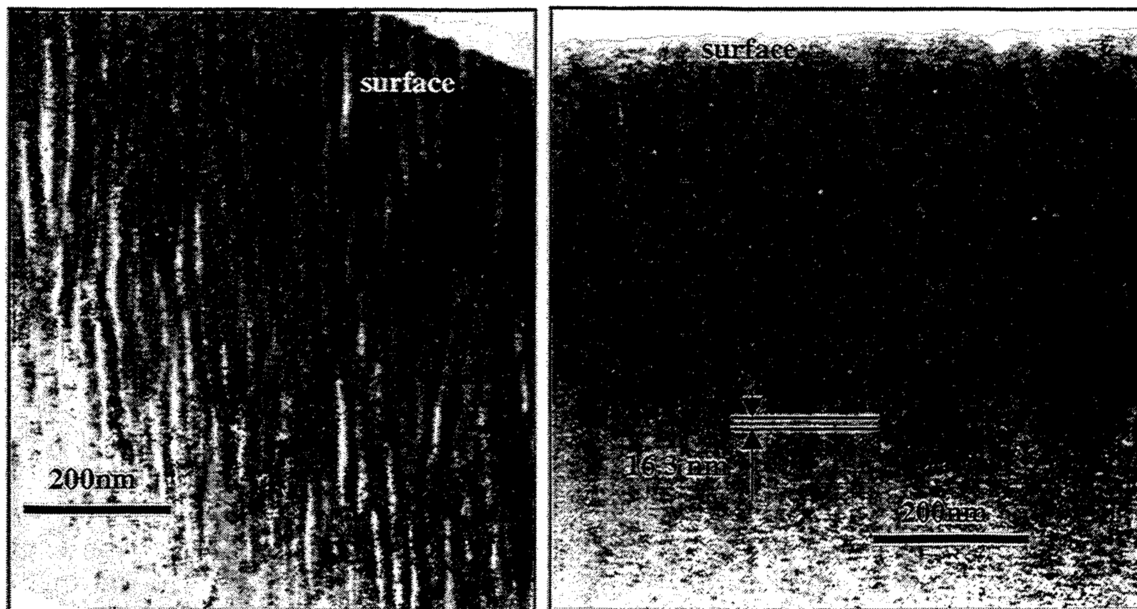

a) **b)**

Fig. 2: Cross-sectional TEM micrographs of
a) the monolithic AlN film, b) one Al/AlN multilayer in set I (E = 200 eV, R = 1.45, λ = 18 nm).

poorly-defined columns. The film is much denser than the corresponding AlN monolithic film. Atomic force microscopy investigation revealed that the surface of the multilayer is exceptional smooth, while the surface of the monolithic AlN is relatively rough [9]. Topography and structure of the multilayer clearly indicate that the loose columnar structure existing in the monolithic AlN film prepared with low E and small R has been modified. Since the ion bombardment level and the deposition temperature are not varied, the structural modification can only be correlated with the alternating deposition process. The formed multilayers, therefore, benefit from the laminate architecture with respect to the film structure, which results in an enhanced mechanical hardness. This is commonly observed in many conventional plasma based deposition processes, where the assisting energetic ion bombardment during deposition is mild.

In the case of high E and large R, the loose columnar structure has not been observed even in the monolithic AlN film (of set II), as shown in Fig. 3. It has been proposed that the structure of the formed monolithic AlN film in this case is ion-beam controlled with the following two evidences [8]: First, the final film thickness in this case is almost the half of that expected from the arrival rate of aluminium, indicating that considerable ion beam sputtering occurs under this condition. Second, XRD examination shows AlN crystallites with preferred (100) orientation in this film. The configuration of the (100) orientation in a h.c.p. lattice, like AlN allows a more open structure with respect to the ion beam. The incoming ions can be accommodated in this structure with less radiation damage, or in other words, the sputtering yield for (100) oriented grains is smaller than that for grains with different orientation. Under

the condition where the ion bombardment controls the film growth, the interruption of the loose columnar structure has been theoretically studied by Müller using Monte Carlo and molecular dynamic calculations [10-12]. The intense energetic ion bombardment during vapor deposition removes overhanging atoms, which cause shadowing effects, leaving void regions open until they are filled by new depositing atoms. This results in elimination of the porous columnar network, favouring the growth of a dense packed structure. As a consequence, there is no room for improvement of the film structure by means of the laminate architecture, and the hardness of the Al/AlN multilayers cannot surpass that of the corresponding monolithic AlN film.

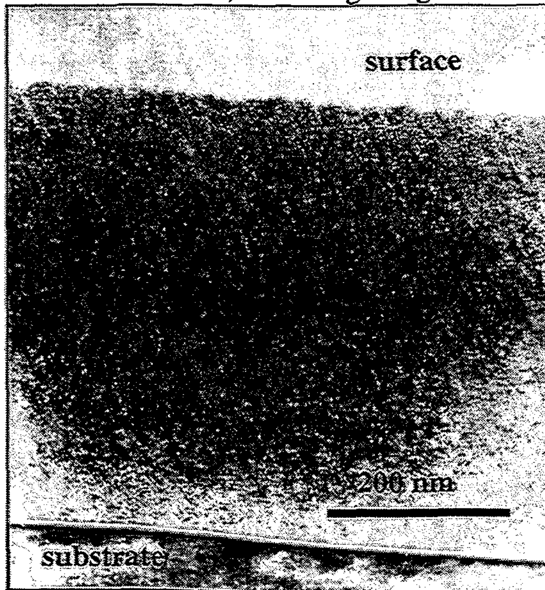

Fig. 3: Cross-sectional TEM micrograph of the monolithic AlN film of set II ($E = 500$ eV, $R = 3.60$).

In summary, laminate architecture can avoid the columnar growth when the ion impingement during deposition is relatively weak, which is the usual case for many plasma based coating techniques. In contrast, when a compact structure is obtained due to intense ion bombardment during deposition, which can be achieved in the IBAD process under suitable conditions, a laminate architecture will not further improve the structure, and hence, the mechanical hardness of the films.

References

[1] H. Holleck,V. Schier, Surf. Coat. Technol. 76-77 (1995) 328
[2] E.O. Hall, Nature 173 (1954) 848
[3] W.J. Petch, J. Iron Steel Inst. 173 (1953) 25
[4] J.J. Cuomo, S.M. Rossnagel, H.R.Kaufmann, Handbook of Ion Beam Processing and Technology, Noyes, Park Ridge, NJ, 1989
[5] G.S. Was, C.E. Kalnas, H. Ji, J.W. Jones, Nucl. Instr. Meth. B106 (1995) 147
[6] R. Hübler, A. Schröer, W. Ensinger, G. K. Wolf, W. H. Schreiner, I. J. R. Baumvol, Surf. Coat. Technol. 60 (1993) 561
[7] S. Nishiyama, N. Kuratani, A. Ebe, K. Ogata, Nucl. Instr. Meth. B80/81 (1993) 1485
[8] X. Wang, A. Kolitsch, F. Prokert, W. Möller, 10th Inter. Conf. on Surface Modification of Metals by Ion Beams, Gatlinburg, Tennessee, USA, 1997
[9] X. Wang, A. Kolitsch, W. Möller, Appl. Phys. Lett. 71 (1997) 1951
[10] K.-H. Müller, J. Vac. Sci. Technol. 4 (1986) 184
[11] K.-H. Müller, J. Appl. Phys. 59 (1986) 2803
[12] K.-H. Müller, Phys. Rev. B35 (1987) 7906

Detection of Metastable Defects in Ion-Implanted Silicon by Means of Metal Gettering

R. Kögler, R.A. Yankov, J.R. Kaschny, P. Werner*, A.B. Danilin** and W. Skorupa
*Max Planck Institut für Mikrostrukturphysik, Haale/Saale, Germany
**Center for Analysis of Substances, Moscow, Russia

The post-anneal lattice disorder resulting from MeV implants in Si is known to act as a sink for transition-metal atoms [1-6] as well as for intrinsic oxygen [6-8]. Conversely, the accumulation of impurities in a certain region of Si can be taken as evidence for the presence of radiation-induced damage therein.

A new approach is presented here to explore implantation induced post-anneal damage evolution by means of metal gettering. Gettering of Cu, to a low dose controllably introduced in MeV-implanted Si, offers a unique means of detecting residual point defects and simple defect clusters which cannot be directly observed by techniques sensitive to the lattice structure, such as transmission electron microscopy (TEM) and Rutherford backscattering/channeling spectrometry (RBS/C) [5]. Cu atoms are able to decorate such defects, thus making them detectable by secondary ion mass spectrometry (SIMS). Metal impurities segregate to either the defects in the depth of the projected range of the implanted ions, R_P, or to the extended defects at the implant end-of-range.
The reason for employing Cu is that it is the fastest diffuser among the transition metals in Si and its gettering occurs via a relaxation induced mechanism. Cu is dissolved in Si at high temperatures. The decoration of defects takes place during the temperature drop. In this way the process of defect evolution at high temperature is not disturbed by the presence of Cu.
Using this method, unanticipated residual defects have been detected midway between the surface and R_P in a depth range which is commonly believed to be free of damage. This phenomenon has been called the $R_P/2$ effect [5,8]. Metal trapping around $R_P/2$ occurs always irrespective of both, the type of ions and the gettering species as shown in Tab. 1. This points towards the operation of a universal physical process of damage nucleation and growth occurring between the surface and R_P in ion-implanted Si during annealing.

Tab. 1: Implants into Si for which the $R_P/2$ effect has been observed.

Implanted species (annealing temperature /°C)	Gettered species	Reference
F (1000), Si (900*,1000**), P (1000), Ge (1000, 1150), As (1000)	Intrinsic O	[7],*[6],**[8]
He (800)**, C (700, 850), Si (800*, 850, 1000), Ge (1150)	Cu	[12],*[6],**[9]
C (700, 850, 950, 1000), Si (900)*, Ge (1150)	Fe	[5],*[6]

A typical example of the $R_P/2$ effect is demonstrated in Fig. 1. A composite of Cu depth distributions is shown after Si^+ ion implantation and annealing. With the exception of the highest temperature (1150 °C) a well separated double band structure is always observed.

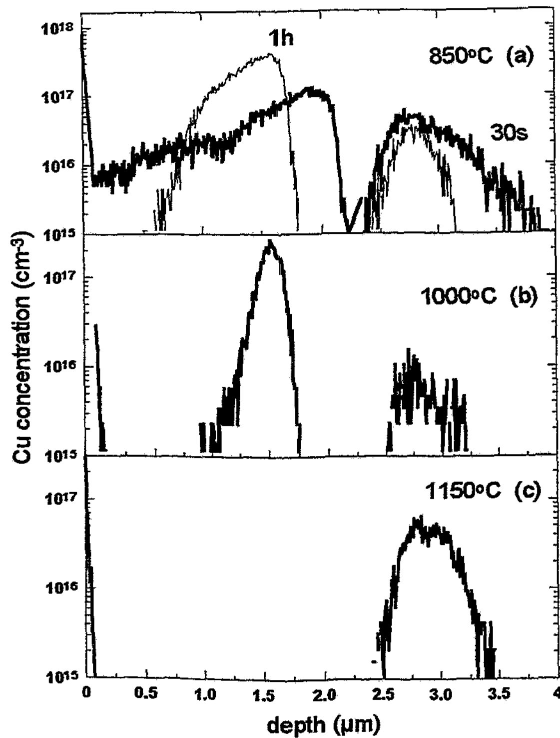

Fig. 1: SIMS Cu depth profiles after implantation of 3.5 MeV, 5×10^{15} Si^{+} cm^{-2} in Si contaminated with 45 keV, 2.5×10^{13} Cu^{+} cm^{-2}, after RTA at different temperatures for 30 sec.

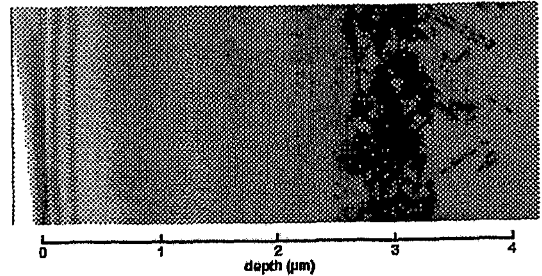

Fig. 2: XTEM brigth field micrograph of Si implanted with 3.5 MeV Si^{+} ions. The sample is the same as shown in Fig. 1b.

The deeper region is located within the secondary-defect band around R_P. However, in the depth range forward of R_P a second band exists which is centered at about $R_P/2$ and becomes narrower at higher temperatures (Figs. 1a and 1b) or for a longer annealing time (see Fig. 1a, 30 s and 1 h). By an annealing at 1000 °C, the amount of Cu gettered around R_P is considerably reduced (Fig. 1b). The reason for this will be discussed below. After annealing at even higher temperature of 1150 °C the gettering band at $R_P/2$ has disappeared. This means that the Si defects acting as gettering sites have been removed by the annealing cycle used.

The microstructure of the sample after annealing at 1000 °C is shown in Fig. 2. At the depth of the gettering band around $R_P/2$, where the main content of Cu is gettered, no defects are observed by XTEM, whereas around R_p a well-defined dense band of extrinsic dislocations has formed. Contrary to what one would expect, in this case SIMS measurements (Fig. 1b) show very weak gettering of Cu in the vicinity of R_P. Instead, appreciable accumulation of Cu is occurred well ahead of R_P exhibiting a narrow distribution with a maximum at $R_P/2$, irrespective of the lack of any other defects being resolvable by XTEM in the depth region between the surface and R_P. Obviously the defects acting as gettering sites are of different types in the two gettering regions around $R_P/2$ and R_P. The damage at $R_P/2$ should be in the form of very small defect complexes as they are not resolved by XTEM.

The total amount of gettered Cu is shown in Fig. 3 together with the fraction trapped in the gettering band around $R_P/2$. The amount of Cu accumulated in the whole layer modified by the self-ion implantation increases with temperature up to 850 °C. Further increase in the

annealing temperature leads to a decrease in the amount of gettered Cu. At the same time, the fraction of Cu gettered around $R_P/2$ related to the total amount of Cu increases progressively in the temperature range of 850 to 1000 °C.

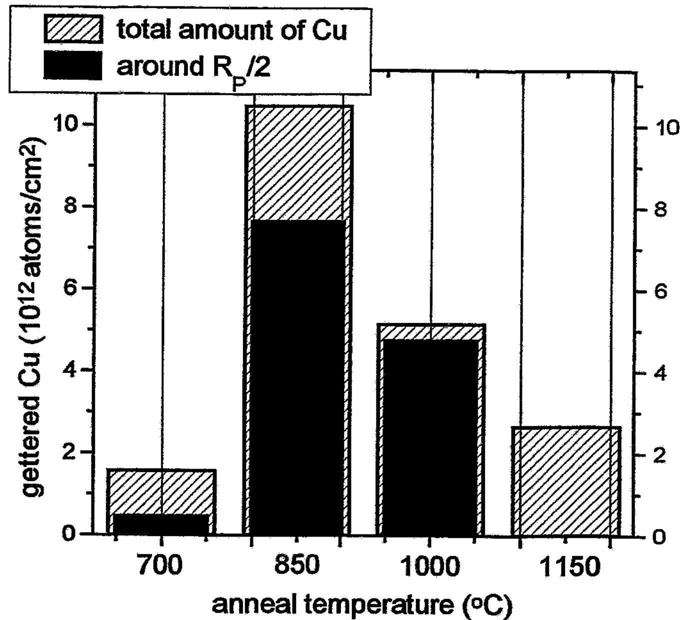

Fig. 3: Total amount of gettered Cu and the fraction of Cu gettered around $R_P/2$ after RTA for 30 sec at temperatures of 700, 850, 1000 and 1150 °C.

In fact, the total amount of gettered Cu for anneals at different temperature should not be compared to each other. This value depends on the temperature drop as a function of time because of the relaxation induced gettering. However, the fraction of Cu gettered around $R_P/2$ in relation to the total amount of Cu can be compared. This quantity shows an increasing fraction of Cu gettered at $R_P/2$ with increasing temperature up to that temperature where the $R_P/2$ band disappears.

The following conclusions can be drawn from these results. The gettering sites for Cu atoms around $R_P/2$ are very small defect complexes. Therefore, these defect complexes cannot be resolved by XTEM and RBS/C [5]. They are formed at temperatures of 700 to 850 °C and disappear at temperatures in excess of 1000 °C. There is a competition between the different gettering defects at $R_P/2$ and R_P. The trapping of Cu around $R_P/2$ clearly outperforms that at R_P. The gettering ability of the extended defects around R_P is much smaller as compared to that of the small defect complexes around $R_P/2$, as is clearly seen in Fig. 1b. This higher gettering ability at $R_P/2$ may be explained by a higher number of preferred gettering sites for Cu exhibited by the small defect complexes. The question for the nature of these defects remains open at present.
The reason for trapping of intrinsic O at $R_P/2$ has been explained in terms of the formation of VO defect complexes [7,8]. However, not only vacancy-type defects, but also Si interstitial-type defects may be responsible for the $R_P/2$ gettering. There is evidence that metal impurities are gettered in ion-beam processed Si in regions where the supersaturation of Si interstitials clearly exists. Such regions are the end-of-range region of Si^+-implanted Si [10], the deeper SiO_2/Si interface of SIMOX structures [11] and the bulk-Si side of an amorphous-crystalline interface [12]. The gettering of intrinsic O and the gettering of metal

impurities are propably independent processes. Because of the much higher mobility of metals in Si compared to O, the metal gettering occurs at lower anneal temperatures as can be seen from Tab. 1. Large numbers of Frenkel-pairs (vacancies and Si interstitials) are created by displacements during ion implantation in Si. Both types of defects are highly mobile and can either recombine or agglomerate during thermal treatment to form larger defect complexes. Assuming that the gettering sites at $R_P/2$ are such small agglomerates of Si interstitials formed at temperatures T>700 °C one may explain the formation of the defect depth profile in Fig. 1 by the precipitate kinetics via Ostwald ripening [13] which leeds to such a stratification of the defect profile. Basically, the described $R_P/2$-R_P structure is only one specific example of this kind. A suitable variation of the experimental conditions should also result in more complicated stratifications. Further investigations are necessary to verify this assumption.

In summary, it has been shown by means of metal gettering that it is possible to gain an insight into the defect evolution of radiation defects in Si during annealing. The appearance of an unanticipated defective band around $R_P/2$ has been observed to occur within the temperature window which is preferably used in advanced device processing. Despite the fact that the real nature of the defects acting as gettering centres is still obscure, the methode is sensitive just for these defects which may pose a problem for the viability of any high-dose (>10^{14} cm^{-2}) ion implantation. In most cases not the defect structure itself deteriorates the characteristics of devices, but its ability to getter metal impurities. To avoid unwanted metal gettering in the vicinity of active device areas the $R_P/2$-effect has to be taken into account.

References

[1] H.Wong, N.W. Cheung, P.K. Chu, J. Liu, J.W. Mayer, Appl. Phys. Lett. 52 (1988) 1023
[2] W. Skorupa, R. Kögler, K. Schmalz, H. Bartsch, Nucl. Instr. Meth. B 55 (1991) 224
[3] T. Kuroi, Y. Kawasaki, S. Komori, K. Fukumoto, M. Inuishi, K. Tsukamoto, H. Shinyashiki, T. Shingyoji, Jpn. J. Appl. Phys. 32 (1993) 303
[4] P.A. Stolk, H.J. Gossman, D.J. Eaglesham, H.S. Luftman, Appl. Phys. Lett. 66 (1995) 568
[5] R. Kögler, D. Panknin, W. Skorupa, P. Werner, A. Danilin, Proc. XI Int. Conf. Ion Implantation and Technology 96, IEEE Publ. 96TH8182, Piscataway, NJ, 1996
[6] O. Kononchuk, R.A. Brown, S. Koveshnikov, K. Beamen, F. Gonzalez, G.A. Rozgonyi, Solid State Phenomena 57/58 (1997) 69
[7] M. Tamura, T. Ando, K. Ohyu, Nucl. Instr. Meth. B 59 (1991) 572
[8] A. Agarwal, K. Christiensen, D. Venables, D.M. Maher, G.A. Rozgonyi, Appl. Phys. Lett. 69 (1996) 3899
[9] J.R. Kaschny, A. Mücklich, U. Kreißig, R.A. Yankov, R. Kögler, W. Skorupa, P. Fichtner, A.B. Danilin, Mat. Res. Soc. Symp. Proc. 469 (1997) 451
[10] R. Kögler, M. Posselt, R.A. Yankov, J.R. Kaschny, W. Skorupa, A.B. Danilin, Mat. Res. Soc. Symp. Proc. 469 (1997) 463
[11] W. Skorupa, N. Hatzopulos, R.A. Yankov, A.B. Danilin, Appl. Phys. Lett. 67 (20) (1995) 2992
[12] R. Kögler, unpublished results
[13] V.A. Borodin, K.-H. Heinig, S. Reiss, Phys. Rev. B 56 (1997) 5332

A New Approach to Full Atomistic Simulation of Ion Implantation within a Commercial Process Simulator

Bruno Schmidt, M. Posselt, N. Strecker* and T. Feudel**
* Swiss Federal Institute of Technology, Zürich, Switzerland
** ISE Integrated Systems Engineering AG, Zürich, Switzerland

2D and 3D dopant distributions in complex target structures are hardly accessible to measurements. Their precise prediction by computer simulations is therefore of great importance. On the other hand, it is well known that as-implanted profiles can be calculated accurately by atomistic methods based on binary collision (BC) codes. Such inherently three-dimensional codes can describe ion channeling as well as damage accumulation and amorphization in single-crystalline Si. The physically based approaches, which are used for that, are independent of the dimensionality of the problem. A review on these models, which have been verified for the 1D case, has been given recently [1,2]. To be capable to simulate the ion implantation step in today's semiconductor technology, the BC code Crystal-TRIM [1,2,3] was implemented into the 2D process simulator DIOS [4] as an optional module. In contrast to previous concepts of combining BC-calculations and 2D-process simulation a complete integration was performed. The target structure given by the process simulator is directly irradiated. Nearly all thinkable implantation conditions, geometries and material arrangements can be considered. The data produced during the BC simulation of ion trajectories are stored in triangular cells. In most of the other process steps a point grid is used for data registration however. Therefore, before and after the simulation of implantation the data must be transformed from points to triangles and vice versa. The simulation grid can be refined or coarsened before, after and sometimes also during the simulation of process steps either explicitly by user definitions or automatically by given criteria like dopant gradients. For the kind of simulation presented here a fixed mesh with triangles of equal size is chosen.

Because the actual number of implanted ions is usually very high, pseudoprojectiles representing many real ions are used in the BC simulation. These projectiles are started from a line significantly above the top of the 2D target structure. This line is subdivided into equidistant intervals. Within each interval the lateral coordinates of the starting points are chosen randomly. A major issue for this kind of simulation is the computational efficiency. In particular this problem arises if, as usual, the dopant concentration has to be predicted precisely for several orders of magnitude. The regions of low concentration are mainly due to deep channeling tails and lateral channeling branches which are caused by a small number of projectiles with long trajectories. The use of splitting algorithms in BC codes [5,6,7,8] can reduce the statistical problem of bad depth resolution without introducing physical errors. The basic idea of splitting consists in "importance sampling", i.e. the number of trajectories calculated in regions with a low trajectory density is increased artificially. If a projectile reaches a region of small concentration where the trajectory density is low, a splitting point is set: The current status of the particle e.g. position, energy, direction of motion as well as the positions of neighbouring target atoms, in particular those of the last collision partners, is stored and used several times to start "daughter" projectiles. Because all "daughter" particles start under identical conditions the differences in the trajectories are solely caused by the thermal vibrations of the collision partners found beyond the splitting point. As an proper splitting criterion we found the following one: For each registration cell J (area A_J) the weighted sum over the particle trajectory

density is determined and stored

$$s_J = \frac{1}{A_J} \sum_i w_i \, l_i \tag{1}$$

where w_i is the weight of a particle i depending on its splitting level L_i ($w_i = 1/2^{L_i}$) and l_i the length of the trajectory section lying within the cell J. The sum is over all particles previously registered in this cell. If a particle enters a new cell K the ratio of the value of s_K and of s_s for the first cell at the target surface entered by the original projectile is compared with the instantaneous weight w_m of the particle considered. A splitting point is set if

$$\frac{s_K}{s_s} < 2w_m \tag{2}$$

The only user input required is the maximum splitting level N per particle, i.e. how many subsequent splitting points are allowed.

In 2D process simulations the target structures under consideration are usually very vast. Since a high density of starting points is required to obtain statistically significant results the CPU time is considerably higher than in 1D-calculations. However, in most applications different starting intervals correspond to regions at the target surface which have very similar properties, e.g. nearly the same lateral environment and depth structure. This fact can be employed for the lateral duplication of ion trajectories. At the beginning of the implantation all starting intervals are labeled with the same index assigning them to only one equivalence class. When the motion of a projectile is followed, for each registration cell passed, the material composition as well as the change of damage and dopant concentrations in this cell are stored. Having finished the simulation of the history of a projectile it is tried to transfer the 2D range and damage profile obtained by this projectile to all other starting intervals of the same equivalence class. The material arrangement in the region of the transferred 2D profiles is compared to that in the area of the original distribution. If sufficiently large deviations occur the considered interval obtains a new index, otherwise the transfer of the 2D profile is performed.

Fig.1 shows a small section of the simulation area for a pMOS process simulation. The target setup at this process stage is quite simple and can be described as a (100) Si substrate with an oxide layer of about 6 nm at the surface and 5 nm between the substrate and the polycrystalline Si of the gate. The height and the width of the polysilicon gate are 0.25 μm and 0.2 μm, respectively. The lateral dimension was chosen from -1.5 μm to 1.5μm which is essential for the later process steps. Ground doping was set to zero to get a better visibility of the implantation results. The registration cells of the triangulated simulation area have an typical edge length of 10 nm. This value was chosen for various reasons: The resulting depth resolution is still acceptable. Doubling the resolution would not only mean that the memory consumption is increased by a factor of 4 but also 4 times more particle trajectories had to be followed to gain the same statistics for the registration cells. In Fig. 1a the 2D dopant profile for a 200 keV arsenic implant at 30° tilt and 0° rotation is shown. This is the first of 4 successive implantations which differ only by their rotation angle. The influence of the pre-damage caused by an preceding boron implant was investigated by comparing the results to an implantation where no pre-damage was regarded.

Fig. 1: 200 keV ($8.75 \times 10^{12} cm^{-2}$, 30° tilt and 0° rotation) As^+ implant.

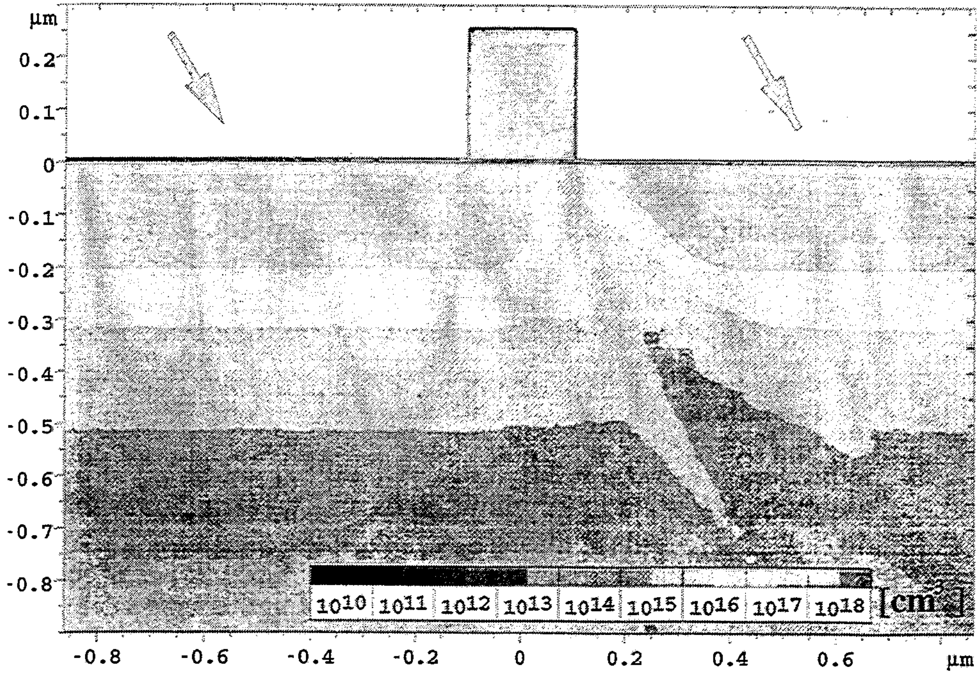

Fig. 1a: 2D range profile in a target predamaged by 15 keV ($3.5 \times 10^{14} cm^{-2}$) zero tilt BF_2^+ implantation.

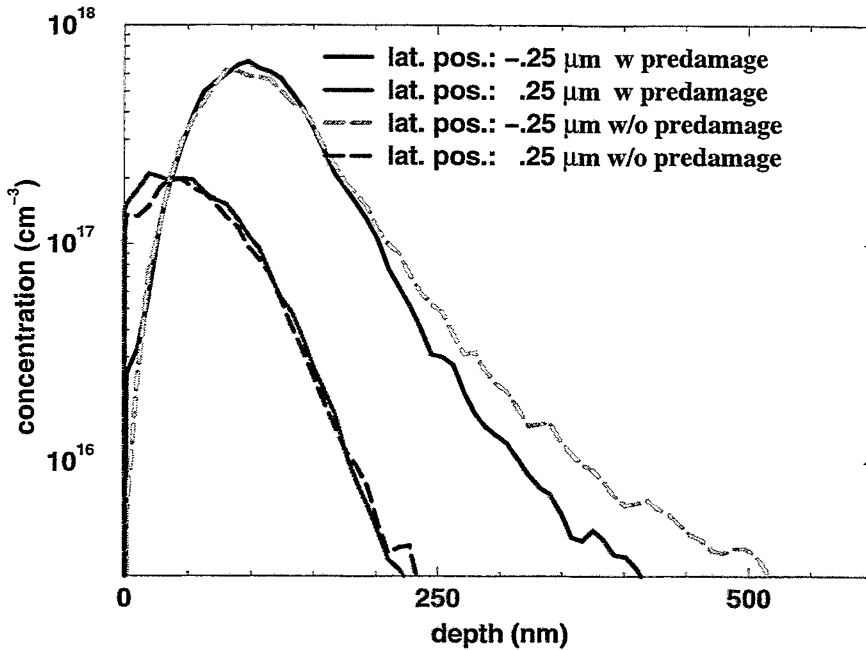

Fig. 1b: Comparison of vertical 1D-cuts regarding and not regarding the predamage.

The pre-damage reduces channeling which is demonstrated by the vertical 1D-cuts of Fig. 1b. Considered is a lateral position (-0.25 μm) which lies totally within a directly irradiated area. The calculation with regarding pre-damage leads to a depth profile with a higher maximum dopant concentration and a smaller concentration for greater depths than the simulation without considering pre-damage. This is due to the damage buildup which results in a stronger dechanneling and therefore a shortened range. The second lateral position (+0.25 μm) is close to the border of the region "shadowed" by the gate. The much smaller dopant concentration is mainly due to laterally straggled particles. As far as the poor statistics in that part of the simulation area allows to state, this effect seems not to be strongly influenced by the pre-damage.

In summary, it was shown that the BC module of DIOS is applicable for precise calculations of 2D dopant profiles in complex and vast target structures. Different irradiation conditions and damage effects can be regarded. Even the influence of pre-damage caused by a preceding implant is accessible to investigation. The use of trajectory splitting and lateral duplication algorithms ensures a high computational efficiency. Nevertheless, the present restrictions of standard workstations concerning memory and CPU-time require a careful planning what should be calculated by the BC module or in which cases conventional methods should be employed.

References

[1] M. Posselt, B. Schmidt, C.S. Murthy, T. Feudel, K. Suzuki, J. Electrochem. Soc. 144 (1997) 1496

[2] C.S. Murthy, M. Posselt, T. Frei, J. Vac. Sci. Techn. B14 (1996) 276

[3] M. Posselt, Rad. Eff. Def. Sol. 130/131 (1994) 87

[4] N. Strecker, DIOS-ISE, ISE TCAD Release 4.0, User's Manual, Zürich 1997

[5] W. Bohmayr, A. Burenkov, J. Lorenz, H. Ryssel, S. Selberherr, IEEE Trans. Semiconductor Man. 8 (1995) 402

[6] S.H. Yang, D. Lim, S. Morris, A.F. Tasch, Proc. NUPAD 1994, p. 97

[7] T. Feudel, A. Höfler, TESIM, ISE TCAD Release 4.0, Version 4.5, Zürich 1997

[8] B. Schmidt, M. Posselt, T. Feudel, N. Strecker, Comp. Mat. Sci., to be published

Strong Blue and Violet Photo- and Electroluminescence from Germanium- and Silicon-Implanted Silicon Dioxide Layers

L. Rebohle, J. von Borany, R.A. Yankov, W. Skorupa, I.E. Tyschenko*, H. Fröb** and K. Leo**
* Institute of Semiconductor Physics, 630090 Novosibirsk, Russia
** Institut für Angewandte Photophysik, Technische Universität, D-01062 Dresden, Germany

Because of its indirect bandgap silicon is not suitable for fabricating light-emitting devices. The desire to adhere to the standard Si technology has motivated extensive research on the development of Si-related materials for optoelectronic applications. After the observation of efficient photoluminescenece (PL) from porous silicon [1] much interest has beeen initially generated in this material. Many authors [2-4] have reported on electroluminescence (EL) in the red spectral region with wavelengths longer than 600 nm. However, the possible application for light-emitting devices in various chemical ambients or under thermal stress has focused the interest on alternative materials which show better compatibility with current Si processing than porous silicon.

One promising approach of forming luminescent Si-based structures is the ion implantation of semiconductor species into thin SiO_2 films thermally-grown on Si substrates, because of the robustness of the matrix and the very good control over the fabrication process. Furthermore, ion implantation is a dry process which, as distinct from the wet procedures utilized in the production of porous silicon, is fully compatible with microelectronic technology. Various studies have used the implantation of Si to obtain structures exhibiting PL in the red region [5-8]. Recently, results pertinent to blue PL from Si-implanted SiO_2 layers have been reported [9-13]. Bao *et al.* [14] have shown that violet PL can also be achieved from Ge-implanted SiO_2 layers, but no comparison between the Ge-induced PL intensity and that from Si-implanted SiO_2 has been attempted. To date, there have been only few EL studies of Si- or Ge-implanted SiO_2 layers. Shcheglov *et al.* [15] have implanted Ge at very high doses into thermally-grown SiO_2 and have recorded a broad EL spectrum peaking in the infrared region. In the present study we demonstrate that the violet PL from Ge-implanted SiO_2 is much higher in intensity than the blue PL from Si-implanted SiO_2. Furthermore, we show that the Ge-rich structure exhibits strong EL with the same emission characteristics like the PL.

500 nm thick SiO_2 films on (100) n-type Si substrates were grown in a wet ambient at 1000 °C. The SiO_2 films were implanted with Ge^+ ions at an energy of 350 keV to a dose of 3×10^{16} cm^{-2} followed by a second Ge implant at 200 keV to a dose of 1.8×10^{16} cm^{-2}. The substrate temperature during implantation was maintained between -120 °C and -150 °C by mounting the samples on a LN_2-cooled stage. For the sake of comparison, Si^+ ions were implanted at an energy of 200 keV followed by a second Si implant at 100 keV using the same doses and substrate temperatures as in the case of Ge. As calculated by TRIM, under these conditions a broad implant profile of an average density of excess Si or Ge atoms of about 3 at. % would be achieved over a depth region of 100 to 400 nm below the oxide surface. After implantation the structures prepared for PL measurements were furnace-annealed (FA) in the temperature range of 400 °C to 1200 °C for 30 min in an N_2 ambient. The SiO_2 films to be examined for EL were annealed at 1000 °C for 60 min in an N_2 ambient to recover the SiO_2 network using the same temperature as for the oxide growth. MOS dot structures for EL studies were prepared using sputtered layers of indium tin oxide (ITO) and Al as front and rear side electrodes with a thickness of 300 nm, respectively. The oxide on the rear side of the wafer was removed before Al metallization. The transmission of ITO is higher than 80 % in the wavelength region from 340 nm to 2 μm. The dot matrix with a dot diameter of 1 mm was made by photolithographic patterning. Finally, an annealing procedure of 400 °C for 30 min was performed to improve the ohmic behavior of the contacts. EL and PL measurements were performed at room temperature in a Spex Fluoromax spectrometer with an R 928 Hamamatsu photomultiplier.

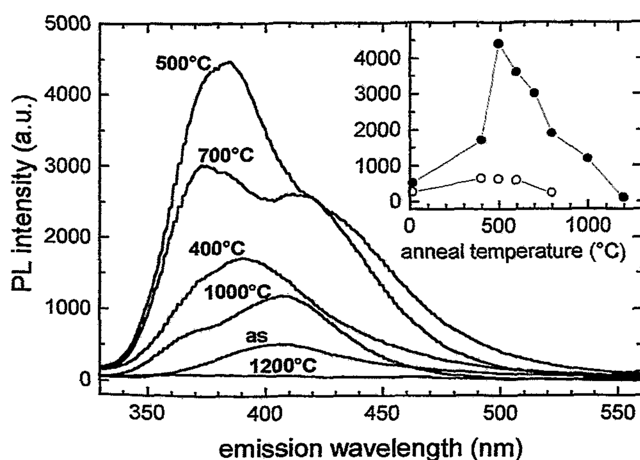

Fig. 1: The PL spectra from Ge-implanted SiO_2 films after implantation (as) and at different anneal temperatures under 240 nm excitation. The inset shows the PL intensity maximum from both Ge- (closed circles) and Si- (open circles) implanted SiO_2 films depending on anneal temperature.

Fig. 1 shows PL spectra from Ge-implanted SiO_2 films at different anneal temperatures under 240 nm excitation. The inset compares the PL intensity maximum from both Ge- and Si-implanted SiO_2 films depending on anneal temperature. Maximum PL intensity is achieved for both Ge- and Si-implanted layers at 500 °C for 30 min, consistent with previous results [13]. At this anneal temperature the PL intensity for Ge exceeds that of Si by a factor of 7, thus becoming visible with the naked eye. The main emission from the Ge-implanted layers occurs between 350 and 450 nm, but the increase in the anneal temperature causes apparent changes in the shape of the violet PL spectra. This behavior differs distinctly from that of the Si-implanted oxide which shows always a single emission peak around 460 nm [13]. While the PL signal recorded from the as-implanted oxide exhibits a single broad peak of low intensity around 410 nm, after annealing at 500 °C a peak around 380 nm becomes dominant and a „shoulder" around 410 nm is also evident indicating the presence of a second peak. For $T > 600$ °C the bimodal behavior is retained, but the intensity ratio of these two peaks is seen to change in favor of the 410 nm peak, accompanied by a decrease in the overall intensity of the violet emission. At an anneal temperature of 800 °C the longer-wavelength peak now dominates in the PL signal and its maximum occurs at 407 nm.

Our previous investigations have shown that the PL from Si-implanted SiO_2 films is not simply caused by radiation damage, but is rather related to the non-stoichiometric composition of the silicon dioxide [12]. This was concluded from the very weak PL of the Ar-implanted oxide compared to the PL signal from Si-implanted SiO_2. Tohmon *et al.* [16] have interpreted the blue PL from Si-rich glasses in terms of oxygen-defect centers and suggested that the neutral oxygen vacancy is the main luminescent center. Recently, it has been shown that the neutral oxygen vacancy is also responsible for the blue PL in Si-implanted SiO_2 [10]. This luminescing center is a product of Si-Si bond formation in the SiO_2 network and will be denoted hereafter as ≡Si-Si≡ center.

In the framework of our interpretation the PL may be explained as excitation from the singlet ground state, S_0, to the first excited singlet state, S_1, followed by intersystem crossing to the first excited triplet state, T_1, and a radiative deexcitation to the ground state. In the case of Ge-implanted SiO_2 films we believe that one or both Si atoms of the ≡Si-Si≡ center are substituted by Ge atoms forming a ≡Ge-Si≡ and ≡Ge-Ge≡ center, respectively. The formation of two different defect centers can also explain the presence of two main subpeaks in the emission spectra of Ge-implanted material. As is known from molecular spectroscopy [17], substituting an atom of a given molecule with a heavier atom of isoelectronic configuration leads to an increase in the spin-orbit coupling. This in turn raises the probability of the triplet-to-singlet transition ($T_1 \rightarrow S_0$) and normally increases the transition energy as well. Therefore, assuming that the blue PL from a Si-rich oxide is due to a $T_1 \rightarrow S_0$ transition of the ≡Si-Si≡ center, one would expect a blue shift of the peak position in the order ≡Ge-Si≡ and ≡Ge-Ge≡. The energy of the $S_0 \rightarrow S_1$ excitation band would not be influenced appreciably by the spin-orbit coupling and, in fact, we find only a small shift of the optimum excitation energy, namely from 250 nm (Si) to 240 nm (Ge).

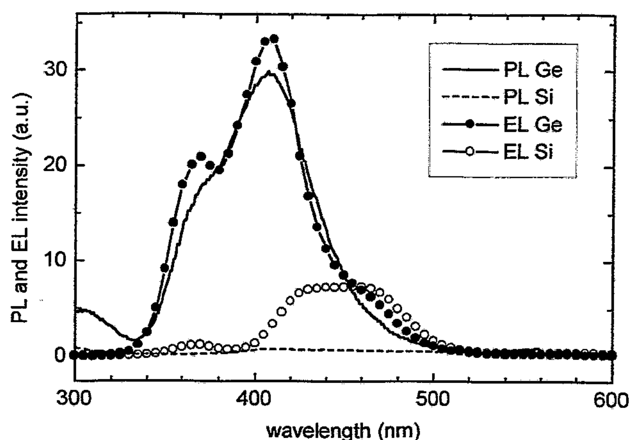

Fig. 2: The EL spectra from Ge- (closed circles) and Si- (open circles) implanted SiO_2 films in comparison to the PL spectra from Ge- (solid line) and Si- (dashed line) implanted oxide. All structures were furnace-annealed at 1000 °C. The PL spectra for Ge- and Si-rich oxide were recorded under an excitation wavelength of 240 nm and 250 nm, respectively.

Fig. 2 shows the EL and PL spectra of Si-and Ge-implanted SiO_2 films. The EL was stimulated using an injection current of about 100 nA by applying a voltage of either 370 V (Si) or 380 V (Ge). The EL spectrum from the Ge-rich layers shows a double-peak structure with maxima at 366 nm and 407 nm, whereas the Si-implanted oxide exhibits a broader distribution between 420 nm and 470 nm. The EL intensity from the Ge-implanted SiO_2 films for the same current is by a factor of 5 larger than that in the case of Si-implanted structures, and for currents higher than 250 nA the EL emission becomes readily visible with the naked eye. It should be noted that unimplanted SiO_2 films exhibit no EL.

The corresponding PL spectra from Ge- and Si-implanted layers shown in Fig. 2 were recorded using an excitation wavelength of 240 nm and 250 nm, respectively. For Ge-implanted layers a peak structure similar to that of EL is observed implying that both PL and EL of Ge-implanted SiO_2 films are caused by one and the same luminescing center. To verify this hypothesis, a basic peak fit analysis was carried out assuming that the peak structure can be described as a sum of Gaussian distributions on the energy scale. Both spectra can be fitted well by means of three subbands peaking at 3.39 eV (366 nm), 3.05 eV (407 nm) and 2.72 eV (455 nm). They differ slightly in two features: (i) the intensity ratio between the 3.39 eV and the 3.05 eV peak is 1.66 for the EL spectrum, but 3.1 for PL spectra; (ii) all subpeaks in the EL spectra have the same full width at half maximum (FWHM) of 0.3 eV, whereas in the PL spectra the FWHM of the 3.39 eV peak is broadened to 0.38 eV. On the basis of the preceding considerations we attribute the three subbands at 3.39 eV , 3.05 eV and 2.72 eV to the ≡Ge-Ge≡, ≡Ge-Si≡ and ≡Si-Si≡ center, respectively. For the Si-implanted oxide layers annealed at 1000 °C only weak PL with a broad distribution between 400 and 500 nm was recorded.

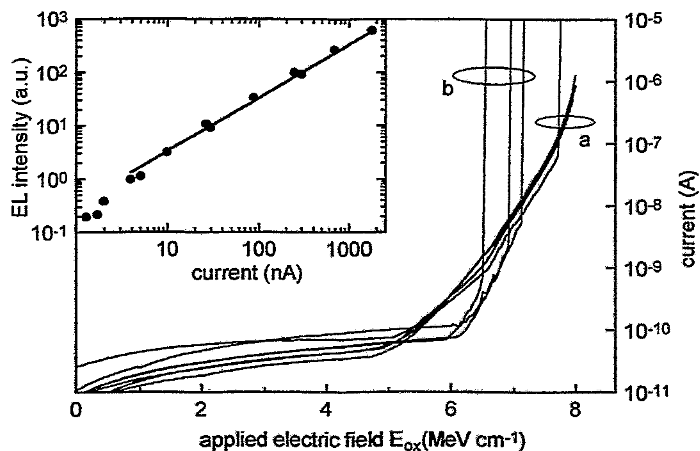

Fig. 3: The dependence of injection current on the applied electrical field E_{ox} for Ge-rich SiO_2 furnace-annealed at 1000 °C (a) and pure oxide (b). The inset shows the EL intensity for the Ge-implanted SiO_2 films as a function of current. The solid line represents a linear fit between 3.9 nA and 1.8 µA.

Fig. 3 shows variation of the current with applied electrical field E_{ox} for Ge-rich SiO_2 (a) and pure oxide (b). The curve is divided into three different regions. For low E_{ox} a nearly constant displacement current below 100 pA is measured. For high E_{ox} the potential difference between the oxide surface and the Si substrate is so high that a considerable amount of electrons can cross the oxide layer via Fowler Nordheim (FN) tunneling and the current increases following an exponential law. Finally, E_{ox} is high enough to induce a breakdown of the oxide layer (marked with a vertical line). In comparison to

the pure oxide the region of FN tunneling for the implanted oxide starts at a lower E_{ox}, the current increases with a slightly lower exponential constant and the breakdown voltage is higher. We assume that the luminescence centers will be excited by the impact of hot electrons. As can be seen from the inset to Fig. 3, the EL intensity shows a nearly linear dependence on the injection current. The EL spectra obtained at different injection currents are characterized by an identical spectral shape. The term „EL efficiency" is defined as the ratio of the light output power to the applied electric power, and the respective value obtained in our experiments is estimated to be about $5x10^{-4}$.

In summary, we have demonstrated that Ge-implanted SiO_2 exhibits strong violet PL as well as intense EL, and that in both cases one and the same luminescence centers are excited. To the best of our knowledge, such a coincidence of PL and EL has been reported for the first time. The value of the PL efficiency has been estimated to be 5×10^{-4}. The PL and EL spectra consist of two main subpeaks which can be attributed to the presence of ≡Ge-Si≡ and ≡Ge-Ge≡ defect centers, respectively. The dependence of the EL on the injection current follows a linear relationship over a wide range of three orders of magnitude and can be explained by electron impact excitation of hot electrons injected from the Si substrate via FN tunneling. Both the PL and the EL from Ge-rich oxide layers are much higher in intensity than the respective emissions from Si-implanted oxides.

References

[1] L.T. Canham, Appl. Phys. Lett. 57 (1990) 1046

[2] A. Richter, P. Steiner, F. Kozlowski, W. Lang, IEEE Electr. Dev. Lett. 12 (1991) 691

[3] L. Tsybeskov, S.P. Duttagupta, K.D. Hirschman, P.M. Fauchet, Appl. Phys. Lett. 68 (1996) 2058

[4] N. Lalic, J. Linnros, J. Appl. Phys. 80 (1996) 5971

[5] T. Shimizu-Iwayama, K. Fujita, S. Nakato, K. Saitoh, T. Fujita, N. Itoh, J. Appl. Phys. 75 (1994) 7779

[6] H.A. Atwater, K.V. Sheglov, S.S. Wong, K.J. Vahala, R.C. Flagan, M.L. Brongersma, A. Polman, Mat. Res. Soc. Symp. Proc. 321 (1994) 363

[7] T. Fischer, V. Petrova-Koch, K. Shcheglov, M.S. Brandt, F. Koch, Thin Solid Films 276 (1996) 100

[8] G.A. Kachurin, I.E. Tyschenko, K.S. Zhuravlev, N.A. Pazdnikov, V.A. Volodin, A.K. Gutakovsky, A.F. Leier, W. Skorupa, R.A. Yankov, Nucl. Instr. Meth. B122 (1997) 571

[9] P. Mutti, G. Ghislotti, S. Bertoni, L. Bonoldi, C.F. Cerofolini, L. Meda, E. Grilli, M. Guzzi, Appl. Phys. Lett. 66 (1995) 851

[10] L.S. Liao, X.M. Bao, X.Q. Zheng, N.S. Li, N.B. Min, Appl. Phys. Lett. 68 (1996) 850

[11] W. Skorupa, R.A. Yankov, I.E. Tyschenko, H. Fröb, T. Böhme, K. Leo, Appl. Phys. Lett. 68 (1996) 2410

[12] W. Skorupa, R.A. Yankov, L. Rebohle, H. Fröb, T. Böhme, K. Leo, I.E. Tyschenko, G.A. Kachurin, Nucl. Instr. Meth. B120 (1996) 106

[13] L. Rebohle, I.E.Tyschenko, H. Fröb, K. Leo, R.A. Yankov, J. von Borany, W. Skorupa, Microelectr. Engineering 36 (1997) 107

[14] X.M. Bao, T. Gao, F. Yan, S. Tong, Mat. Res. Soc. Symp. Proc. 438 (1997) 477

[15] K.V. Shcheglov, C.M. Yang, K.J. Vahala, H.A. Atwater, Appl. Phys. Lett. 66 (1995) 745

[16] R. Thomon, Y. Shimogaichi, H. Mizuno, Y. Ohki, K. Nagasawa, Y. Hama, Phys. Rev. Lett. 62 (1989) 1388

[17] S.P. McGlynn, T. Azumi, M. Kinoshita, Molecular Spectroscopy of the Triplet State, Prentice Hall, Englewood Cliffs, NJ, 1969

Damage-Related Dwell-Time Effects in Focused Ion Beam Synthesis of Cobalt Disilicide

S. Hausmann, L. Bischoff, M. Voelskow, D. Grambole, F. Herrmann and J. Teichert

Cobalt disilicide is one of the promising silicides for future device metallization and the development of new metal-semiconductor devices. $CoSi_2$ is perfectly suited for silicon technology due to its cubic CaF_2 lattice structure with a mismatch of only -1.2 % relative to the silicon lattice. It shows metallic behavior with a resistivity of only 15 μΩcm and has a Schottky barrier height of 0.64 eV in contact to n-type silicon. To our knowledge the production of high-quality buried $CoSi_2$ layers on Si(111) and Si(100) is only possible by ion beam synthesis (IBS) [1] or allotaxy [2]. Allotaxy is a combination of epitaxial growth of the host material (silicon) and the controlled deposition of a precipitating compound by coevaporating a second component (cobalt) at a substrate temperature of about 500 °C. A subsequent annealing leads to a continuous buried layer, but the patterning has to be done after the layer preparation e.g. by local oxidation [3]. When using IBS at sufficiently high ion energy, a high dose cobalt ion implantation results in a buried distribution of $CoSi_2$ precipitates. To avoid target amorphization a substrate temperature of about 400 °C is required. During subsequent annealing, the precipitates ripe and coalesce to form a continuous buried $CoSi_2$ layer. For a detailed description of the IBS process, see, e.g., reference [4]. In the case of IBS the patterning of the layer can simply be done by implantation through a mask. However, e.g. for prototyping of new devices, a maskless implantation is also possible with a focused ion beam (FIB) system. The FIB offers the additional possibility of changing the implantation parameters, like the dose or the energy, on any single area of the silicon wafer. Aoki *et al.* [5] showed the possibility of forming $CoSi_2$ layers by high dose implantation using a FIB. Later, Bischoff *et al.* [6] formed $CoSi_2$ layers with a FIB successfully. However, broad beam and FIB implantation cannot be compared directly due to the large difference of the characteristic current densities. For conventional implantation, typical current densities are about 10 μAcm^{-2}, compared to about 1 Acm^{-2} and more for FIB. For the extremely high current densities associated with FIB, one might further anticipate dose-rate effects in case of continuous writing and dwell-time effects for the patterning by pixels. In the present paper a clear indication of such a dwell-time effect is presented and discussed in terms of damage accumulation and dynamic annealing.

The implantations have been performed with the IMSA-100 FIB system [7] using a mass separated 70 keV Co^{2+} beam with a total ion current of about 0.7 nA, extracted from a $Co_{36}Nd_{64}$ liquid metal ion source and focused to a spot size of about 300 nm. The corresponding current density is about 1 Acm^{-2}. The tilt angle was 0° and the target material was n-Si(111) heated to a temperature of 400 °C. The beam was scanned meander-like on an area of 40 x 40 μm^2 using subsequent pixels with a distance of 80 nm. The total dose was about 10^{17} ions/cm^2, corresponding to $3 \cdot 10^1$ and $3 \cdot 10^3$ frames at dwell-times of 100 μs and 1 μs, respectively. The switching of the beam between subsequent pixel positions takes 0.1 μs. For characterization, Rutherford backscattering spectroscopy (RBS) of the as-implanted samples was performed with a nuclear microprobe [8] using a 3 MeV Li^{2+} beam with a spot size of about 5 μm. The annealed samples (60 min at 600 °C, and 30 min at 1000 °C in a nitrogen atmosphere) were investigated by scanning electron microscopy (SEM) after removal of the silicon top layer by CF_4 reactive ion etching (RIE) for 6 minutes. Exact knowledge of the thickness of the silicon top layer is not necessary because $CoSi_2$ acts as an etch stop for CF_4 RIE [9]. The SEM images of the annealed samples in Fig. 1 show that continuous $CoSi_2$ layers can only be formed using sufficiently short pixel dwell-times. When

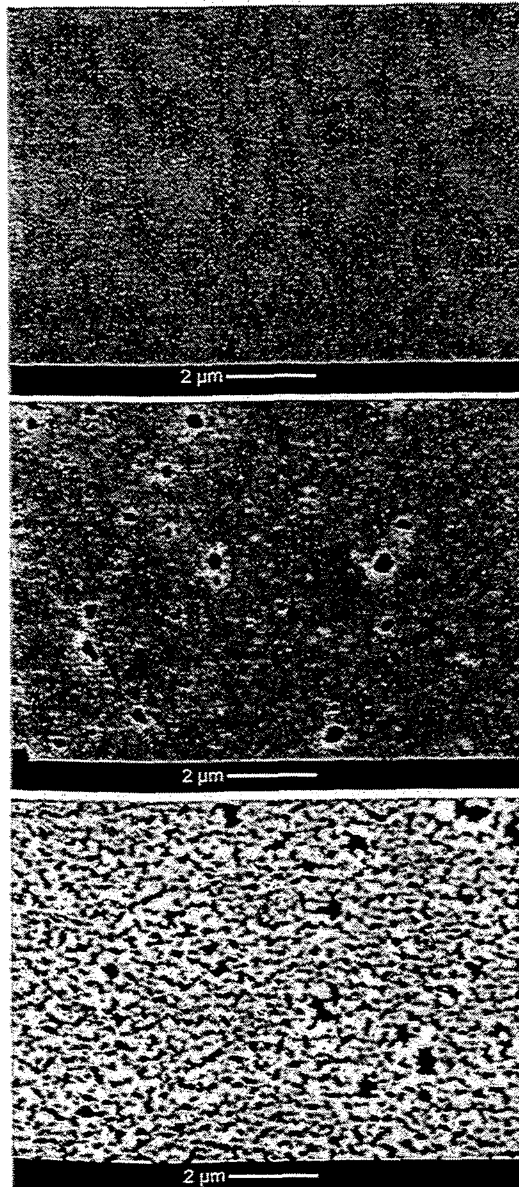

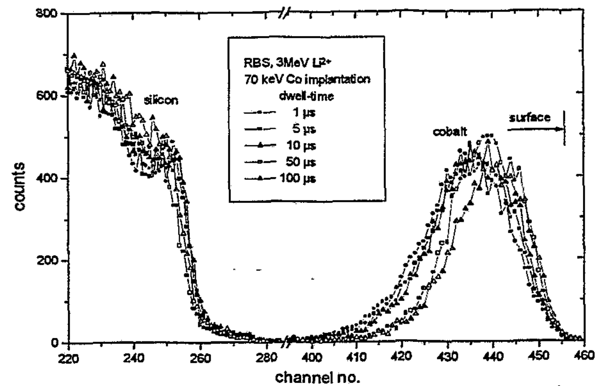

Fig. 2: RBS spectra obtained from a nuclear microprobe of as-implanted samples fabricated with different dwell-times. It can be seen that the cobalt distribution shifts deeper into the silicon with decreasing pixel dwell-times. Only the deeper cobalt distributions result in a continuous layer formation.

Fig. 1: In this series of plane view SEM images the influence of different dwell-times is shown. The upper image shows a $CoSi_2$ layer fabricated with a short pixel dwell-time of 1 µs. The layer is continuous and smooth. On the next image the dwell-time is increased to 50 µs and the layer shows some holes and an enhanced roughness. When the dwell-time is increased to 100 µs the layer is totally disintegrated as it can be seen on the lower image. Experimental parameters are: Si(111) substrate, Co^{2+} ions, energy 70 keV, dose $10^{17}cm^{-2}$. For details, see text.

the dwell-time is increased, the layers exhibit holes and become completely disintegrated at a dwell-time exceeding 100 µs. To decide whether this effect is due to annealing, SEM analysis of as-implanted samples was performed. The results prove that the disintegration is already present in the as-implanted samples. To obtain more information about the as-implanted state of the samples, RBS measurements were performed, as shown in Fig. 2, revealing a deeper distribution of the cobalt atoms for the short dwell-times than for the long ones. The change from continuous to disturbed layers is directly correlated with a shift of the as-implanted profiles of the cobalt atoms.

The reason for the shift of the cobalt profiles may be differences in damage creation in connection with dynamic annealing of the silicon target for different dwell-times. If short dwell-times would result in less damage, channeling of the cobalt atoms would occur and sputtering would be reduced. In the case of long dwell-times the reason for the insufficient formation of the layer could be a too high degree of damage of the silicon matrix up to amorphization as discussed below. Furthermore, different conditions of Ostwald ripening and coalescence might arise. The idea of a different damaging and annealing behavior is supported by the shape of the holes in the disintegrated $CoSi_2$ layer, which are not aligned along crystallographic directions of the silicon lattice. To

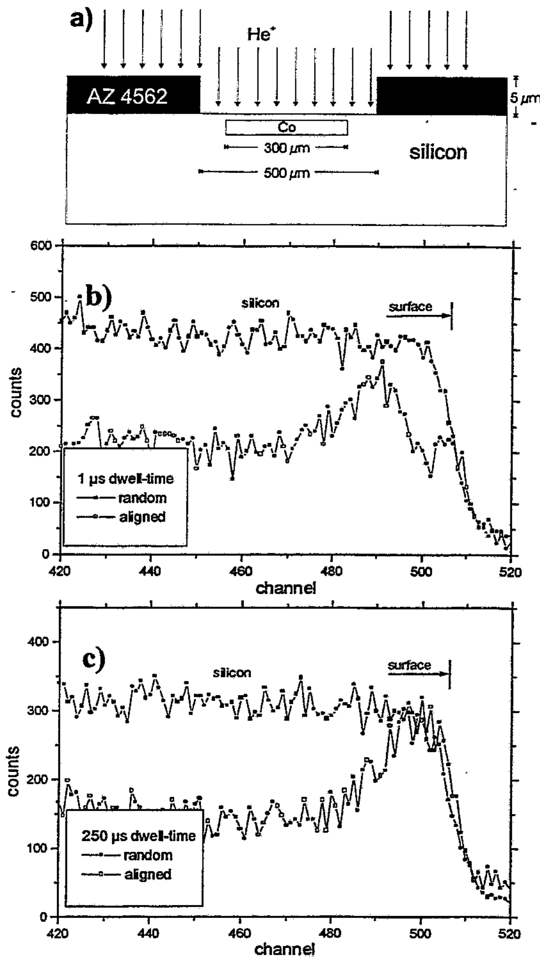

Fig. 3: a) Schematic view of the sample preparation with small implanted areas using a conventional RBS/channeling setup.
b) RBS/channeling spectrum of an as-implanted sample after implantation with $2 \cdot 10^{16}$ cm^{-2} 35 keV Co^{+} ions into Si(111) at 430°C and a dwell-time of 1 µs. The aligned spectrum is multiplied with the ratio of the total area of the hole in the resist to the implanted area (= 25/9).
c) Same as in b) except for a dwell-time of 250 µs.

further eludicate the above phenomena channeling RBS measurements were performed in order to characterize the damage buildup. A direct measurement by conventional channeling RBS was not possible for our layers as only a limited area could be implanted by the FIB within reasonable times. The application of a nuclear microprobe with a small spot size for channeling RBS measurement is prohibited because of self-damaging effects. Therefore, low cobalt doses ($2 \cdot 10^{16}$ cm^{-2}) were implanted into larger areas with a diameter of 300 µm using a 35 keV Co^{+} beam and a substrate temperature of 430 °C to investigate the early state of the layer formation. For this energy, compared to 70 keV, a slightly higher temperature is required to form a continuous layer for 1 µs dwell-time at sufficiently high doses, in accordance with results from broad-beam experiments [11]. The total implantation time for each pixel was 250 µs. Implantations were performed using 1 µs dwell-time and 250 repetitions, and 250 µs dwell-time in one cycle. RBS and channeling RBS spectra were measured with a van de Graaff accelerator using a 1.7 MeV He^{+} beam with a spot size of about 1 mm. In order to suppress the signal from the unimplanted area the wafer was masked with AZ 4562 photoresist after implantation, a hole of 500 µm diameter was opened at the irradiated area using standard optical lithography. For the evaluation of the spectra a constant helium beam profile was assumed across the 500 µm hole. The results are shown in Fig. 3. The comparison of the measurements shows that the use of short dwell-times results in a lower amount of damage. Additionally, it can be seen that for the implantation using 1 µs dwell-time the silicon surface layer remains crystalline. For a dwell-time of 250 µs the surface layer is amorphous, with respect to channeling. Thus, we conclude that different dwell-times result in a different degree of damage due to dynamic annealing.

There are some further arguments which support the idea that the different behavior of the layer formation is due to the fact that the different dwell-times result in different degrees of damage of the silicon target. Jebasinski [11] has shown for broad beam experiments that channeling implantation of cobalt is possible even for doses as high as $\sim 10^{17}$ cm^{-2}. In addition, broad beam implantation of cobalt in random direction (7° tilt angle) was successfully simulated [12] by HDTRIM (High Dose TRIM) [13], indicating that the implantation profiles are governed by collisional effects rather than diffusion. A similar dwell-time effect was also found for GaAs. Low-dose Ga FIB implantation with different dwell-times has been

investigated [14] on GaAs wafers at room temperature and the correspondig samples were analysed by RBS/channeling. The samples implanted with longer dwell-times showed a higher degree of damage than those with short dwell-times.

Thus, the damage of the silicon lattice has a strong influence on the $CoSi_2$ layer formation. For long dwell-times the damage accumulation of the silicon lattice during the cobalt implantation prevents the formation of continuous $CoSi_2$ layers. For short dwell-times the results are comparable to broad beam ion beam implantation where the thermally induced defect annihilation prevents an amorphization of the silicon wafer. It is also helpful to compare the present results to ion beam induced crystallization and amorphization experiments performed by Linnros et al. [15] with pulsed ion beams. As explained by Jackson [16], at a low pulse frequency the results are comparable to experiments with a constant beam with the same current. For high pulse frequencies the results correspond to experiments with a constant beam but with the averaged current of the pulsed beam. If this knowledge is transferred to our results, although the conditions are rather different, this means that for short dwell-times the effective ion arrival rate per pixel is reduced. In comparison with long dwell-times, when the steady-state case is assumed, the effective current density for the 40 x 40 μm^2 implanted areas with short dwell-times is a factor of $2.5 \cdot 10^5$ smaller (for 1 μs). This means that the effective current density is now in the order of μAcm^{-2} which is comparable to the current density of broad beam ion implantation.

In summary, 70 keV Co^{2+} was implanted with a focused ion beam system into a heated silicon target to form continuous cobalt disilicide layers. A strong influence of the dwell-time on the $CoSi_2$ layer formation was found. For sufficiently short dwell-times it was possible to form continuous $CoSi_2$ layers, while for long dwell-times it was shown that the increased damage accumulation of the silicon target prevent the formation of a continuous $CoSi_2$ layer.

Acknowledgements

The authors would like to thank the Deutsche Forschungsgemeinschaft for their financial support under contract no. Te 250/1-1. We gratefully acknoledge the SEM investigations by Mrs. E. Christalle and Dr. R. Müller and the technical assistance by Mrs. I. Beatus.

References

[1] A.E. White, K.T. Short, R.C. Dynes, J.P. Garno, J.M. Gibson, Appl. Phys. Lett. 50 (1987) 95
[2] S. Mantl, H.L. Bay, Appl. Phys. Lett. 61 (1992) 267
[3] S. Mantl, M. Dolle, St. Mesters, P.F.P. Fichtner, H.L. Bay, Appl. Phys. Lett. 67 (1995) 3459
[4] S. Mantl, Mater. Sci. Rep. 8 (1991) 1
[5] T. Aoki, K. Gamo, S. Namba, T. Shiokawa, K. Toyoda, H. Okabayashi, H. Mori, H. Fuijita, Nucl. Instr. Meth. B 39 (1989) 291
[6] L. Bischoff, J. Teichert, E. Hesse, D. Panknin, W. Skorupa, Vac. Sci. Technol. B 12 (1994) 3523
[7] L. Bischoff, E. Hesse, D. Janssen, K.F. Naehring, F. Nötzold, G. Schmidt, J. Teichert, Microelectron. Eng. 13 (1991) 367
[8] F. Herrmann, D. Grambole, Nucl. Instr. Meth. B 104 (1995) 26
[9] N.M. Zimmerman, J.A. Liddle, A.E. White, K.T. Short, Appl. Phys. Lett. 62 (1993) 387
[10] G. Bai, M.-A. Nicolet, J. Appl. Phys. 70 (1991) 649

[11] R. Jebasinski, PhD thesis, Universität Köln / Forschungszentrum Jülich 1993
[12] R. Jebasinski, S. Mantl, L. Vescan, Ch. Dieken, Appl. Surf. Sci. 53 (1991) 264
[13] H. Kohlhof, PhD thesis, Universität Köln / Forschungszentrum Jülich 1989
[14] C.R. Musil, J. Melngailis, S. Etchin, T.W. Haynes, J. Appl. Phys. 80 (1996) 3727
[15] J. Linnros, W.L. Brown, R.F. Elliman, Mat. Res. Soc. Symp. Proc. 100 (1988) 369
[16] K.A. Jackson, J. Mat. Res. 3 (1988) 1218

Ion Nitriding of Austenitic Stainless Steel: Influence of the Surface Oxide Layer on the Nitriding Kinetics

S. Parascandola and O. Kruse

Austenitic stainless steels (e.g. V2A steel) are widely used due to their excellent corrosion resistance based on a passivating native surface oxide layer. However, their moderate hardness leads to short life times in applications with intensive wear. Hence, surface hardening of austenitic stainless steels without adversely affecting their corrosion resistance could greatly enlarge their range of applications. However, a standard technique is missing at present, despite of research activities since some decades. Recently, it has been demonstrated that ion nitriding by plasma based techniques as plasma nitriding, beam ion implantation and plasma immersion ion implantation are promising techniques. At about 400°C the formation of a rather thick surface layer, characterized by a very high content of nitrogen in solid solution is well established, which is known to have diverse beneficial effects on the properties of austenitic stainless steels [1]. This layer may even improve the already excellent corrosion resistance. Simultaneously, the surface hardness is increased by a factor of 4 - 5 leading to wear reductions of more than two orders of magnitude [2,3,4].

Nitriding is generally described as diffusion in a semi-infinite solid at constant surface concentration. Thus, the efficiency of a selected process in combination with a given material depends on the boundary conditions at the surface which determine the retention and release of nitrogen and thereby the nitrogen flux which is available for diffusion. For ion nitriding of austenitic stainless steels the nitriding kinetics is not well understood. Extraordinary fast nitrogen diffusion has been observed during the formation of the nitrogen enriched layer and the nitrogen depth profiles do not follow the expected diffusional decay [5,6]. It has been suggested that these peculiarities are affected by the surface oxide layer [7].

In order to improve the understanding of the ion nitriding kinetics of austenitic stainless steel and to optimize it for industrial applications a crossed-beam experiment has been set up. A schematic of the experiment is given in Fig. 1. Ion nitriding is performed by a broad nitrogen ion beam from a Kaufman-type ion source [8] directed onto the sample, which is mounted on a heatable target holder. Ion energies between 0.2 and 3.0 keV and ion current densities up to $2x10^{16}$ ions $cm^{-2}s^{-1}$ can be provided homogeneously across the sample. Beam current and temperature are monitored on line. A shutter equipped with a resistive heater serves to stabilize the temperature when starting or stopping the nitriding process by minimizing the energy flux discontinuities. A residual gas analyzer and a mass flow controlled gas inlet control the residual gas atmosphere. For time and depth resolved thin film analysis the target chamber is connected to a beam line of the Rossendorf 5 MV tandem

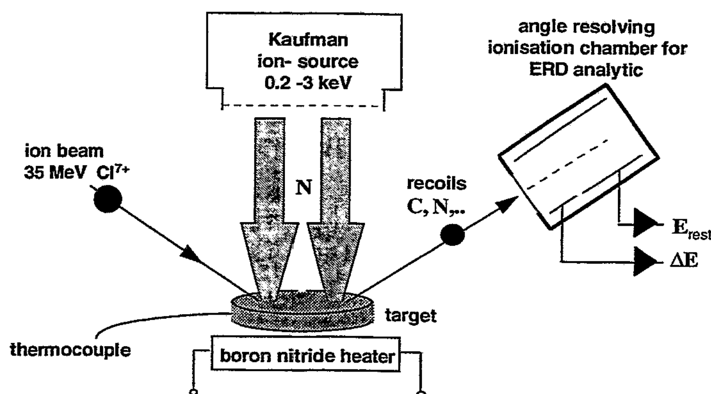

Fig. 1: Sketch of the crossed-beam experiment combining a broad ion beam from a Kaufman-type ion source for ion nitriding and a MeV-analyzing ion beam for in-situ compositional analysis of the near-surface region, using the ERDA technique.

accelerator, supplying 35 MeV Cl^{7+} projectile ions for in-situ Elastic Recoil Detection Analysis (ERDA) of the implanted samples. The detection system consists of an angle resolving gas-filled ionization chamber with a large solid angle of 5 msr. The system allows a fast acquisition time of about 30 s per spectrum. Thus, time-resolved analysis of the diffusing elements in the target becomes possible. Usually, such a large solid angle gives rise to an untolerable deterioration of the depth resolution due to kinematic errors. However, the angular resolution of the ionization chamber allows a correction for these kinematic errors and consequently a reduction of the depth resolution by one order of magnitude (10 nm for the detection of N in stainless steel).

First experiments have been performed in order to analyze the influence of the surface oxide layer on the ion nitriding kinetics of austenitic stainless steel. The re-oxidation of the surface oxide layer during ion nitriding is affected by the residual oxygen partial pressure p_{O2}. A series of samples was ion nitrided at fixed temperature (320°C ± 20°C), fixed current density (1.25×10^{15} ions $cm^{-2}s^{-1}$), fixed energy (1 keV) and at different oxygen partial pressures ranging from $p_{O2} = 1 \times 10^{-6}$ Pa up to $p_{O2} = 5 \times 10^{-3}$ Pa. For all samples the nitriding process was stopped when nitrogen approached the maximum detection depth of ERDA of about 180 nm. Fig. 2a, b and Fig. 3a show the time resolved depth distribution of oxygen, the time resolved depth distribution of nitrogen and the time resolved area densities respectively, of the two elements for $p_{O2} = 1 \times 10^{-4}$ Pa.

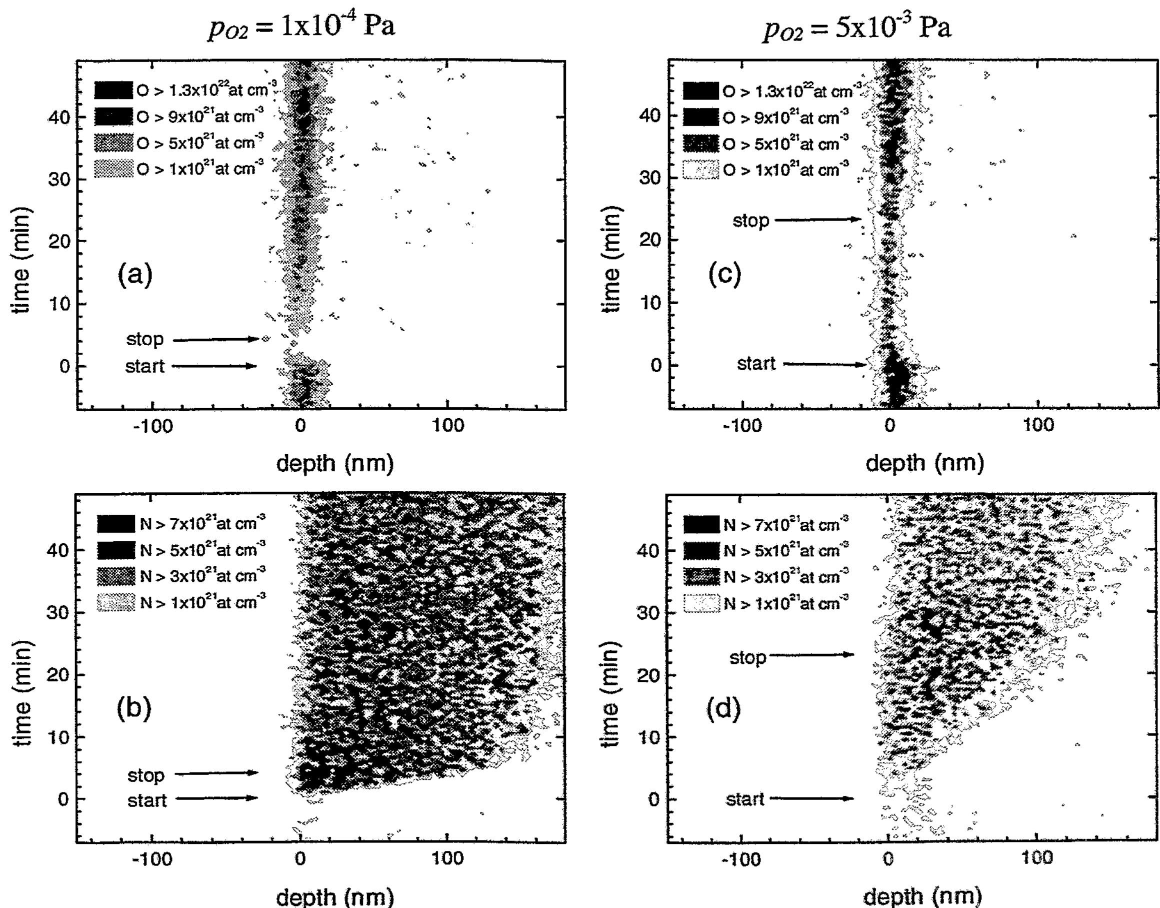

Fig. 2a -d: O (top) and N (bottom) concentration versus depth and time at different O_2 partial pressures, as measured by in-situ ERDA. Start and stop of the implantation (1 keV N, 1.25×10^{15} ions $cm^{-2}s^{-1}$) are marked.

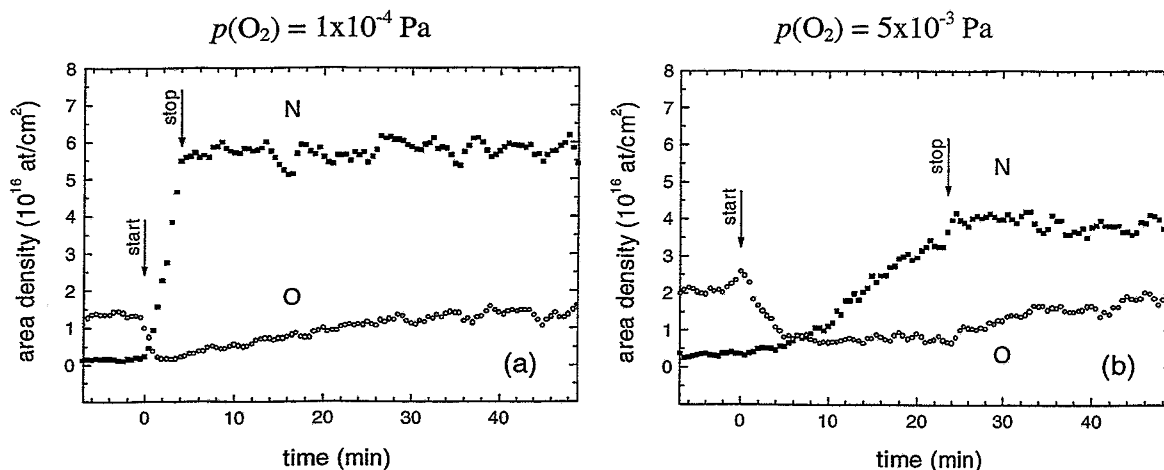

Fig. 2c: Integrated amount of retained N and O as function of time for the implantations of Fig. 2a, b and Fig. 2c, d, respectively.

The surface oxygen layer is removed within 2 minutes. High concentrations of nitrogen are established near the surface and fast nitrogen diffusion occurs. After 4 minutes nitrogen approaches the maximum detection depth. The ion nitriding is stopped and the surface oxide layer gets slowly rebuilt up to its original area density. A slight nitrogen transport into the bulk but no significant nitrogen release is seen. For oxygen pressures below $1x10^{-4}$ Pa the same scenery was observed. However, an increase of the oxygen partial pressure up to $p_{O2} = 5x10^{-3}$ Pa leads to a different behavior as shown in Fig. 2c, d and Fig. 3b. The surface oxide layer is diminished but not removed. After 5 minutes a constant oxygen area density of about $7x10^{15}$ atoms cm^{-2} is established. The nitrogen concentration near the surface is lower and the nitrogen diffuses more slowly as without a surface oxide layer. Nitrogen approaches the maximum detection depth after more than 20 minutes. Again, after stopping the ion nitriding the surface oxide layer is slowly rebuilt and a slight nitrogen transport into the bulk depth, but no significant nitrogen release is seen.

The experiments demonstrate the importance of the surface oxide layer for the kinetics of ion nitriding of austenitic stainless steels. Applying lower ion current densities ($6.25x10^{14}$ ions $cm^{-2}s^{-1}$) and lower energies (0.3 keV) an even thicker oxide surface layer and a nitrogen retention rate tending to zero has been found during the ion nitriding process. The influence of the surface oxide layer may explain the increase of the nitrogen retention rate either with ion energy or with current density found in [9]. Obviously, the nitrogen flux available for diffusion is affected by the thickness of the surface oxide layer during the ion nitriding process and depends on sputtering, re-oxidation from the residual gas and the ballistic projected range of the ions. The results fit qualitatively well with theoretical approximations of the oxygen adsorption rate, the sputter rate and the projected range of the implanted ions. However, detailed quantitative information on the influence of these mechanisms on the kinetics of ion nitriding is still missing. Further time and depth resolved ion beam analysis during the nitriding process will reveal their complicated interplay.

References

[1] R.P. Reed, J. of Met. March (1989) 16
[2] E. Menthe, K.T. Rie, J.W. Schultze, S. Simon, Surf. Coat. Technol. 74-75 (1995) 412
[3] S. Mändl, R. Günzel, E. Richter, W. Möller, Surf. Coat. Technol. (in press)
[4] M.K. Lei, Z.L. Zhang, J. Vac. Sci. Technol. A 13 (1995) 2986

[5] D.L. Williamson, O. Ozturk, R. Wei, P.J. Wilbur, Surf. Coat. Technol. 65 (1994) 15
[6] S. Parascandola, R. Günzel, E. Richter, W. Möller, Nucl. Instr. Meth. B (in press)
[7] R. Wei, Surf. Coat. Technol. 83 (1996) 218
[8] H.R. Kaufman, R.S. Robinson in: Handbook of Ion Beam Processing Technology, Eds.: J.J. Cuomo, S.M. Rossnagel, H.R. Kaufman, Noyes Publishing, New Jersey 1989
[9] D.L. Williamson, J.A. Davis, P.J. Wilbur, J.J. Vajo, R. Wei, J.N. Matossian, Nucl. Instr. Meth. B 127/128 (1997) 930

Biocompatibly Reactive Titanium Surface Endowed by Ion Implantation

M.T. Pham, H. Reuther, R. Müller, G. Steiner[1], W. Matz, I. Zyganov[2], E. Richter and E. Wieser
[1] Technische Universität Dresden, Institut für Analytische Chemie
[2] Staatliche Technische Universität Lipezk, Lipezk, Russland

Artificial hard tissue substitutes traditionally used in orthopaedics and dentistry rely on titanium and stainless steel. Their bulk material properties are highly optimized matching well those of the tissues. The interface properties in response to biological environments, however, lack the significant level of biocompatibility. Insufficient tissue bonding and low resistance to ion release are the major consequence [1]. Surface coating with hydroxyapatite (HA) is a current approach to endow these metal-based materials with some degree of biocompatibility. This strategy emerges from the *in vivo* experiment observation that Ti or stainless steel and tissue are interfaced by a thin HA film [2]. Synthetic HA coatings can be produced by a variety of technologies [3]. Inherent in the behavior of all surface films is their formation of distinct interfaces critically susceptible to detachment. This has been overcome to some extent with ion beam mixing [4]. The most severe limitation, however, is the difficulty in achieving a surface coating truely mimicking all aspects of a biologically produced interface material.

Bone is a highly organized composite material with about 70 weight % mineral carbonated apatite [5]. HA crystals are nucleated at specific sites on or within the collagen fibril growing to units of defined size, shape, and orientation [5]. These constituents are assembled, depending on the functional requirements, to hierarchical architectures over a large range of length scales which are able to remodel to adapt to the changing environment conditions [6]. All this is achieved by the biological processes in living nature. They rely on coupled material synthesis and structural assembly using matrix templating, molecular recognition, and cell processing involved in feedback loops to recognize changes and initiate responses [7]. These are features unobtainable in current available synthetic systems.

The strategy we follow is to create a biocompatibly reactive Ti surface and to exploit the biological processes for *in situ* manufacturing the tissue-bonding interface as required. The Ti surface is endowed with mineral apatite precursors capable of being actively involved in the tissue bonding reactions. This strategy is *in vitro* tested in the present experiment studying the behavior of Ca and P, the elemental constituents of bone mineral apatite, stored in a thin layer of the Ti surface. Surface-stored Ca and P are achieved by ion implantation. The reactivity of such ion implanted surfaces is examined in response to a hydrothermal treatment which provides the oxidation of Ca and P, and simulates the formation of calcium phosphates in an aqueous interfacial environment. Our results show that the initially implanted species are convertible to CaO, P_2O_5, Ca^{2+}, PO_4^{3-}. HA is formed from these precursors by an interface-liquid mediated mineralization preceded by the hydrolysis of oxygen compounds of Ca and P from the solid phase. The hydrothermal treatment demonstrates the conversion resulting in a HA doped Ti surface. The morphology and organization of the apatitic interface mineral is controlled by the fluid dynamics reflecting the adaptation to actually available local environments. Exposed to calcium and phosphate ions containing solutions, the hydrothermally treated surface templates HA growing from the solution.

Samples were plates of pure Ti sequentially implanted with Ca^+ and P^+ ions to a total dose of 1.8×10^{17} and 9×10^{16} ions per cm^2, respectively. The implantation was conducted in several energy steps at 55, 42, 30, and 15 keV for Ca and 40, 30, and 20 keV for P to achieve approximately homogeneous and overlapping concentration profiles. The hydrothermal treat-

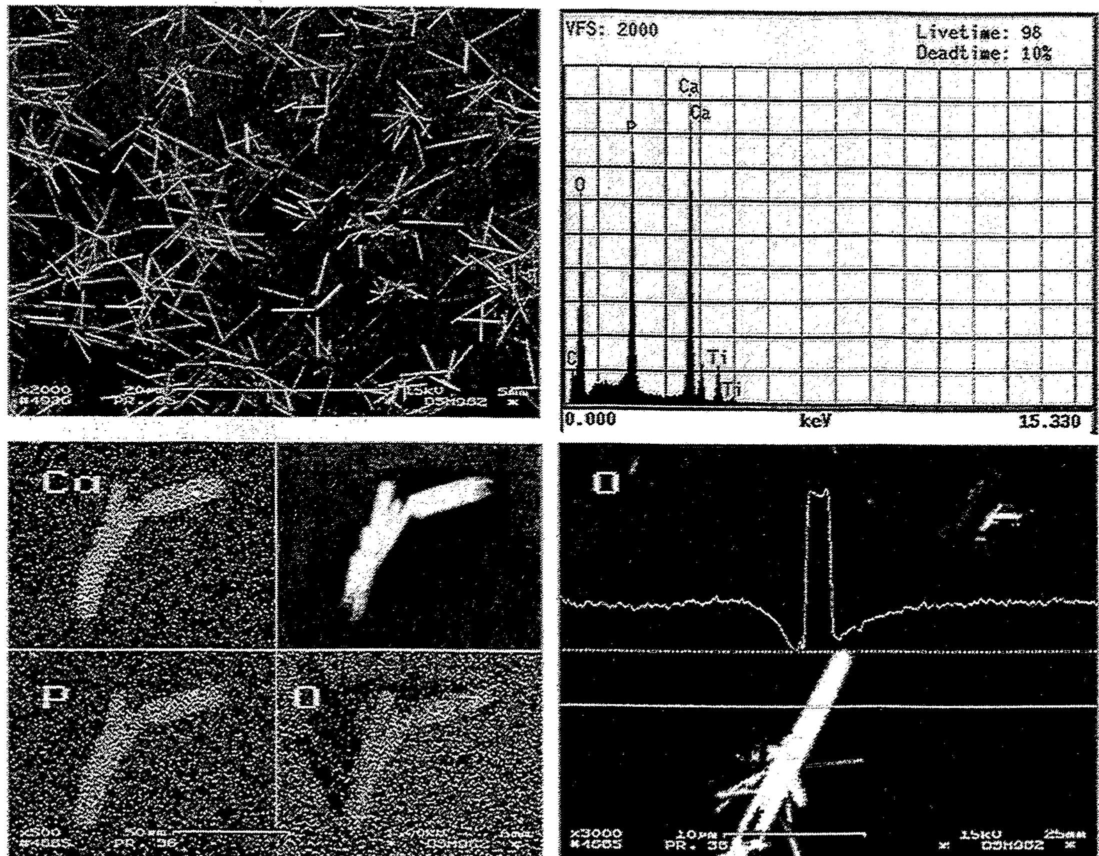

Fig. 1: HA needle crystals formed by hydrothermal treatment from Ca and P stored in Ti surface. SEM image and EDX spectrum (upper), EDX-maps for Ca, P, O distribution and oxygen EDX signal across a crystal needle (lower).

ment was carried out in a water vapor autoclave. Samples were charaterized using X-ray Diffraction (XRD), X-ray excited Photoelectron Spectroscopy (XPS), Fourier Transform Infrared Spectroscopy (FTIR), Fourier Transform Raman Scattering (FT-Raman scattering), and Scanning Electron Microscopy (SEM).

The Scanning electron micrograph of a sample after hydrothermal treatment at 200 °C, Fig. 1 reveals needle-like surface structures. The surface density and size of the crystals are controlled by the nominal ion dose indicating that the surface structure is related to the reaction products of implanted Ca and P. Such a morphology is characteristic of hydroxyapatite precipitated from chloride-free solutions. Aggregates of crystals assembled to ornamentally concentric spheres are also seen suggesting nucleation and growth of crystals at the interface with the aqueous phase mediating the formation and transport of the necessary precursor ions. The EDX spectrum (Energy dispersive X-ray microanalysis) and maps of Fig. 1 demonstrate that the components involved in the needle crystals are Ca, P, and O. Evidence for the formation of oxygen compounds follows furthermore from the line scan of the oxygen EDX signal obtained across a crystal needle.

The FTIR results shown in Fig. 2(left), indicate the presence of HA, evidenced by the absorption bands of PO_4^{3-} at 1050-950 cm^{-1} and 604 cm^{-1} and of OH^- at 3600-3500 cm^{-1} and 630 cm^{-1}.

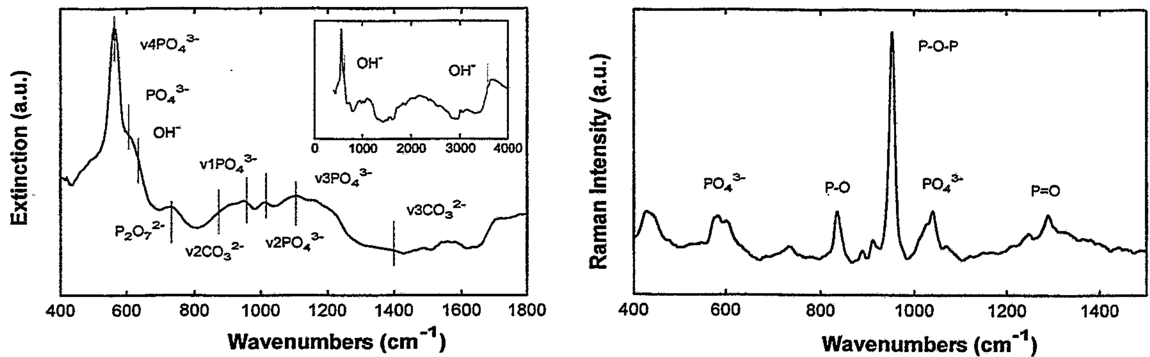

Fig. 2: FTIR (left) and FT-Raman spectra (right) of a Ca and P implanted Ti surface after hydrothermal treatment at 200 °C for 2 h. The inset shows absorption bands of OH^- at 3570 and 633 cm^{-1} from HA.

Surface carbonate is evident by CO_3^{2-} bands in the region from 1600 to 1300 cm^{-1} due to the ν3 vibrational mode of the carbonate ion and by the band at 873 cm^{-1} due to the ν2 vibrational mode. Further surface species observed are pyrophosphate $P_2O_7^{2-}$ at 753 cm^{-1}, β-tricalcium phosphate at 975 and 948 cm^{-1}, hydrogenphosphate HPO_4^{2-} at 875 cm^{-1}, $Ca(OH)_2$ and CaO at 3660 and 875 cm^{-1}. The hydrothermal treatment converts implanted precursors into HA, making the spectral features of HA becomes more obvious. The FT-Raman results confirm HA being a major product after hydrothermal oxidation. Intensive Raman bands characteristic of HA are seen from the spectrum in Fig. 2 (right). Some indications exist of Ti-substituted apatite, Ti phosphate, and CaO. Core level XPS spectra of O 1s, Fig. 3, show characteristics reflecting the the reactivity of implanted Ca and P. TiO_2 (530.2 eV) and its hydroxylation products (531.6 eV, and 533.3 eV) are the major species on the virgin Ti surface. Ca and P implantation produces spectrum changes indicating additional species CaO, $CaCO_3$, $CaTiO_3$ (131-131.7 eV), Ti phosphate (532.7-533.4 eV), $Ca(HPOP_4)_2.2H_2O$ (533.0 eV), $CaHPO_4.2H_2O$ (531.5 eV). Massive changes in the spectra are brought about by the hydrothermal treatment suggesting various reaction events occuring. The intense peak at 531.7 eV is indicative of HA, a major product of the conversion due to treatment. The TiO_2 signal is reduced in intensity relative to those of the new species pointing to the prevalent interface reactions and their products deposited onto the virgin TiO_2.

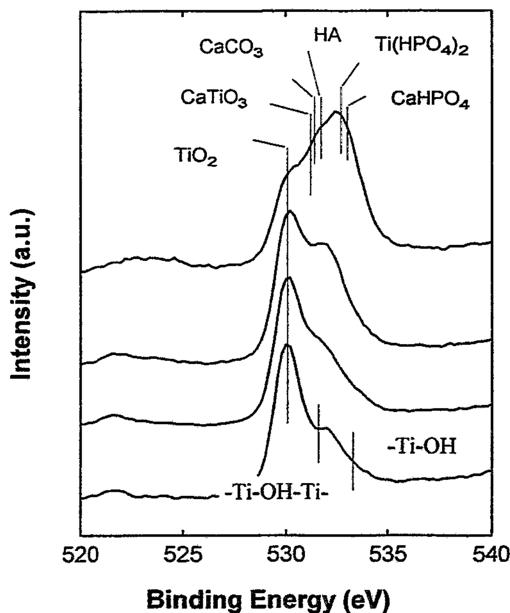

Fig.3:
Core level O 1s XPS spectra of Ti surface implanted with Ca and P and exposed to hydrothermal treatment at 200, 170, and 150 °C for 2 h (from top to bottom) in comparison with pure Ti substrate (bottom).

The XRD spectrum is shown in Fig. 4 for a sample hydrothermally oxidized and then exposed to a calcium ion and phosphate ion containing solution at 37 °C for 5 h (2.5 mM Ca^{2+} and 1 mM HPO_4^{2-} at pH 7.4). The diffraction patterns are consistent with crystalline HA. Samples before solution exposure and unimplanted control sample under the same conditions did not reveal a HA phase. The morphology examination confirmed the needle-like surface structure persisting also after exposure to the solution. This result demonstrates that the HA-doped Ti surface obtained after implantation and hydrothermal treatment templates an additional HA deposition from the solution to an amount sufficient to be detectable by XRD.

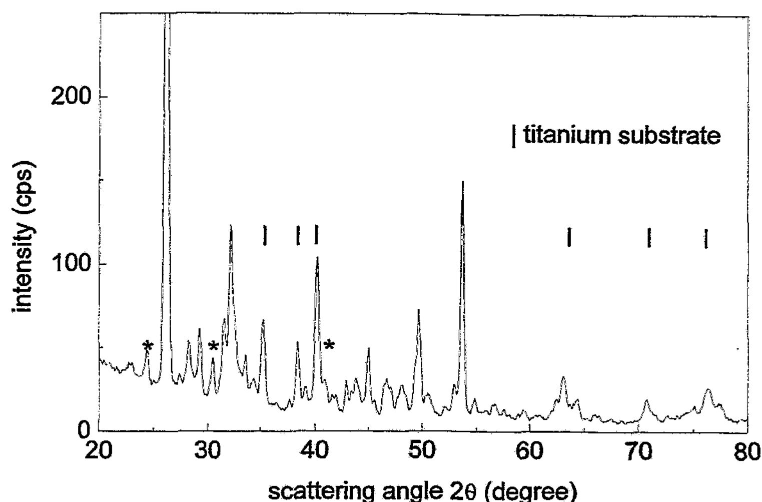

Fig. 4: XRD patterns of HA deposited from solution by templating via a Ti surface Ca-and P-implanted and thermally treated. All Bragg peaks additional to that of the Ti substrate except the marked (*) belong to HA.

References

[1] K.E. Healy, P. Duchenyne, J. Mater. Sci. Mater. Med. 4 (1993) 117; L. Sennerby, L.E. Ericson, P. Thomsen, U. Lekholm, P. Astrand, Clin. Oral. Implant Res. 2 (1991) 103

[2] T. Kokubo, in: CRC Hand Book of Bioactive Ceramics Vol. I, ed. by T. Yamamuro, L. Hench, J. Wilson, CRC Press, Boca Raton, FL, 1990, p. 41

[3] S.R. Radin, P. Ducheyne, J. Mater. Sci. Mater. Med. 3 (1992) 33; C.M. Cotell, D. B. Chrisey, K.S. Grabowski, J.A. Sprague, C.R. Grossett, J. Appl. Biomater. 3 (1992) 87; M. Shirkhanzadeh, J. Mater. Sci. Mater. Med. 6 (1995) 90

[4] Y. Ohtsuka, M. Matsuura, N. Chida, M. Yoshinari, T. Sumii, T. Derand, Surf. Coat. Technol. 65 (1994) 224; F.Z. Cui, Z.S. Luo, Q.L. Feng, J. Mater. Sci. Mater. Med. 8 (1997) 403

[5] L.T. Kuhn, D.J. Fink, A.H. Heuer, in: Biomimetic Materials Chemistry, ed. by S. Mann, VCH 1996, p. 41

[6] S. Mann, J. Mater. Chem. 5 (1995) 935; L. Addadi, S. Weiner, Angew. Chem. Int. Ed. Engl. 31 (1992) 153

[7] Hierarchical Structures in Biology as a Guide to New Materials Technology, NMAB-464, National Academy of Sciences, National Academy Press, Washington D.C., 1994

Short Contributions

ABBREVIATIONS USED IN THE SHORT CONTRIBUTIONS

Preparation Techniques

FIB	Focused ion beam
IBAD	Ion beam assisted deposition
LPCVD	Low pressure chemical vapour deposition
MPIIID	Metal plasma immersion ion implantation deposition
PIII	Plasma immersion ion implantation

Analytical Methods

AES	Auger electron spectroscopy
AFM	Atomic force microscopy
EDX	Energy dispersive X-ray spectroscopy
ERDA	Elastic recoil detection analysis
EXAFS	Extended X-ray absorption fine structur
GRID	Gamma-ray induced Doppler-broadening
HRTEM	High resolution transmission electron microscopy
NRA	Nuclear reaction analysis
NMR	Nuclear magnetic resonance
PAS	Positron annihilation spectroscopy
PIGE	Proton induced Gamma-ray emission
PIRR	Polarized infrared reflection spectroscopy
PIXE	Proton induced X-ray emission
RBS	Rutherford backscattering spectroscopy
RBS/C	Rutherford backscattering spectroscopy under channeling conditions
SEIRA	Surface-enhanced infrared absorption
SEM	Scanning electron microscopy
SIMS	Secondary ion mass spectroscopy
SPIS	Slow positron implantation spectroscopy
SPR	Surface plasmon resonance
TEM	Transmission electron microscopy
XPS	X-ray excited photoelectron spectroscopy
XRF	X-ray fluorescence
XRD	X-ray diffraction
XRR	X-ray reflectometry
XTEM	Cross-section transmission electron microscopy

Hard Coatings

K. Albe

Molecular-Dynamics simulations on boron nitride thin film growth
The ion-assisted growth of boron nitride thin films has been studied by molecular-dynamics methods. A recently developed classical bond-order potential was used, which allows a fast and efficient calculation of interatomic forces and energies. The impact of energetic boron and nitrogen atoms on a small c-BN target was simulated for different ion energies at a fixed target temperature. Probably due to the unrealistically high ion flux and energy deposition only sp^2 bonded structures occur for all simulated energies (< 1 keV). In several cases textured, vertically oriented ring structures are found, which are also observed experimentally.

supported by SMWK

W. Fukarek
M.F. Plass
A. Kolitsch

Modelling of IR vibrational properties of layered h-BN/c-BN structures
Analysis of c-BN containing films requires the use of optical multilayer models with anisotropic optical properties taking into account the interfacial h-BN layer. Different models for oscillator broadening were employed and found to have only a minor influence on the fit to the measured reflectance data. The c-BN vibrational mode was found to be a considerably broadened Lorentzian ($\gamma \approx 140$ cm^{-1}) with an energy shift equivalent to compressive stress of about 10 GPa. The h-BN bending-mode is also a Lorentzian but less broadened ($\gamma \approx 50$ cm^{-1}). Deviating properties were found for the h-BN stretching mode. The broadening is comparable to that found for c-BN ($\gamma \approx 150$ cm^{-1}) but no satisfying fit of the oscillator shape (especially of the LO-mode) of calculated data to measured data could be obtained. This is assumed to be related to texture of optically anisotropic h-BN which is additionally under anisotropic stress (in film surface plane and normal to it) resulting in a very complex anisotropy.
Isotopically enriched ^{10}B was used to investigate the influence of the different isotopes present in natural boron on the position and shape of the IR vibrational modes. Oscillator shifts in ^{10}BN films perfectly fit to the theoretical prediction and the oscillator shape was found to be not significantly affected. It can be concluded that texture and anisotropic stress but not the different isotopes have a major influence on the shape of the h-BN stretching mode.

supported by SMWK

W. Fukarek
A. Kolitsch

Texture of h-BN nanocrystals and optical properties of h-BN films deposited using ion beam assisted deposition
Hexagonal boron nitride (h-BN) films and the interfacial h-BN layer between a silicon substrate and a cubic BN film deposited with ion beam assisted deposition (IBAD) were found to have a thin film biaxial anisotropy using Polarized Infrared Reflection Spectroscopy (PIRR). The c-axis of the h-BN nano-crystals is preferentially oriented parallel to the film surface plane as found in TEM some years ago. PIRR investigation showed an additional less pronounced preferred orientation of the c-axis normal to the plane formed by the direction of the ion beam (normal to sample surface) and the boron vapor stream from the e-beam evaporator. This anisotropy was found to be not related to the crystallographic orientation of the c-Si substrate and is also not influenced by electromagnetic fields from substrate heater or e-beam evaporator. Generalized ellipsometry (GE) investigation showed these films

to be biaxially anisotropic in the visible region apart from the anisotropy in the IR vibrational modes. Detailed GE-data analysis showed the h-BN films to be slightly absorbing in the visible region which is attributed to the films being slightly boron rich (1-3 at.%).

W. Fukarek
A. Kolitsch

In-situ spectroscopic ellipsometry investigation of BN film deposition with ion beam assisted deposition

In situ spectroscopic ellipsometry has been employed for investigations of the deposition process of BN thin films using ion beam assisted deposition. The change in substrate temperature and damage of the c-Si surface layer during Ar sputter cleaning process was monitored. The transition from the interfacial h-BN layer to c-BN growth during the deposition process was found to be only hardly detectable due to a gradual transition from one phase to the other in a nucleation-like process. Instabilities in the operation of the Kaufman ion source show up in abrupt changes in the optical properties of the growing film that are not detectable with other techniques. Comparison with in-situ ellipsometric data recorded during the deposition of c-BN films in a hollow cathode arc deposition system shows significant differences in the interfacial region being of major importance for film adherence.

supported by DFG

Collaboration: Universität Stuttgart

A. Kolitsch
*L. Sümmchen**
*V. Magula***

Synthesis of carbon nitride containing films by IBAD

A large number of carbon and carbonnitride films was investigated by Raman spectroscopy. The previous obtainment of the influence of the deposition temperature (ranging from RT to 1000°C) on the resulting film stoichiometry and the chemical C-N binding energies (ERDA, XPS) was compared with the Raman spectra of films prepared under the same conditions. A correlation of the analysed Raman peak structure to these results was successful. An unambiguous evidence of the predicted β-C_3N_4 did not succeed. Simultaneously TEM investigations with selected area diffraction and EELS anylysis confirm the rising graphitization and larger crystal size with increasing deposition temperature of 600 to 1000°C and a decreasing nitrogen content of the CN_x films.

supported by SMWK

Collaboration: *TU Dresden; **Welding Research Institute Bratislava, Slovakia

Semiconductor Materials

H. Wirth
M. Voelskow
D. Panknin
A. Mücklich
W. Skorupa
*A. Perez-Rodriguez**
*O. Gonzalez-Varona**

Ion-implantation induced damage in 6H-SiC: the influence of substrate temperature

The as-implanted state of a buried Al-implanted layer in n-type 6H-SiC was investigated by RBS/C, Raman Scattering Spectrometry and XTEM. The substrate was kept at temperatures between room temperature and 1300°C during implantation. For increasing substrate temperatures until 1000°C the crystal damage observed by RBS/C and Raman continously decreases. It is found a minimum of the damage at 1050°C. But for temperatures >1000°C there is a stronger dechanneling effect of the defects in RBS/C than for temperatures below 1000°C. According to XTEM investigations this phenomenon can be explained with an ion beam driven agglomeration of interstitial point defects forming platelets (dislocation loops) at temperatures >1000°C. In contrast to the damage minimum at 1050°C only the sample implanted at 1200°C shows p-type conduction in the as-implanted state (Hall effect measurements).

supported by Daimler-Benz AG, Frankfurt a.M.

Collaboration: *University of Barcelona, Spain

H. Weishart
M. Voelskow
W. Skorupa

Studies on high temperature annealing of 6H-silicon carbide

It is well known that during annealing at temperatures above 1000°C SiC suffers from degradation of its surface, mainly considered to be due to selective removal of silicon and graphitization. Our recent annealing experiments (1550 to 1950°C, 10 min) show that the degradation comprises of three parts: erosion, roughening and surface graphitization. In order to determine the exact amount of erosion, the SiC samples were implanted with buried In marker layers prior to annealing. The cause for the surface degradation is the removal of atoms from the SiC surface. This removal may occur via evaporation (Si, Si_2C and SiC_2) and/or via the formation of volatile compounds. The removal of atoms from the SiC surface usually occurs not regularly layer by layer, thus leading to roughening. In the presence of oxygen the main driving force for the removal of atoms is active oxidation. The rate of erosion may be as high as 100 nm/min. If no oxygen is present, the amount of residual hydrogen (from moisture or hydrocarbons) determines the rate of erosion. This rate is considerably lower and may reach values of 5 nm/min. Under our experimental conditions the silicon evaporation leading to graphitization gives only a minor contribution to the erosion process.

A. Höfgen
V. Heera
F. Eichhorn

Relaxation and crystallization of amorphous silicon carbide

SiC exhibits a strong volume swelling during amorphization by ion implantation. Step height measurements between irradiated and unirradiated surface regions were used to investigate the densification of thick (1.75 μm) as-amorphized SiC-layers during thermal annealing at temperatures between 250 and 1100°C. The amorphization was carried out by 2 MeV, 2×10^{16} Si^+/cm^2 implantation into single crystalline 6H-SiC at room temperature. The shrinking behaviour during annealing enables to identify the occurrence of two annealing regimes. (I) At temperatures below 800°C the relaxation of the as-amorphized state takes place. The relaxed amorphous states are stable for more than 10 h of annealing and are characterized by specific densities which

increase with annealing temperature. This tem-perature dependence is fitted quite well by an Arrhenius plot and provides an activation energy of E_a = (184 ± 15) meV for the relaxation process. XRD with grazing incidence has shown, that the densification at low temperatures is not caused by strong structural changes of the amorphous network. Instead a modell of densification due to defect recombination is prefered. (II) At 800°C the amorphous layer begins to recrystallize which was proved by XRD measurements. In contrast to thin amorphous layers, the recrystallisation of the thick amorphous layers is accompanied by stress induced suface patterning and spalling. This behaviour gives an useful advice for SiC-device production to avoid thermal annealing of amorphous layers thicker than 1µm.

supported by DFG

T. Henkel
V. Heera
R. Kögler
W. Skorupa

Comparative study on amorphization of SiC and Si by MeV ion implantation

The ion fluence and temperature dependence of the amorphization process in 6H-SiC and Si induced by 3 MeV I^{2+} has been investigated by in-situ laser reflectometry and ex-situ RBS/C analysis. There are strong differences in the amorphization kinetics between both materials. The damage accumulation in SiC proceeds more gradually in the preliminary stage of amorphization. In contrast to Si the critical energy density for amorphization of SiC by MeV ions is found to be very close to the values known from amorphization by keV ions. Below room temperature there is only a weak temperature dependence on the critical fluence for amorphization of SiC. The temperatures above that amorphization is no more possible have been found to be 626 K and 426 K for SiC and Si, respectively. Ion fluences necessary for amorphization of SiC are lower than those for Si at temperatures above room temperature. Below room temperature the opposite behaviour has been observed. The experimental results have been analysed in terms of several amorphization models.

V. Heera
*J. Stoemenos**
R. Kögler
W. Skorupa

Surface erosion during ion irradiation of SiC at elevated temperatures

A question of fundamental interest is whether surface erosion has to be considered during high temperature implantation of SiC. Unfortunately, erosion rates can not be measured by surface profiling between implanted and unimplanted regions because of the strong volume swelling of SiC during ion implantation. Therefore, experiments have been performed where the surface was partly protected by a thin, ion transparent Si layer (90 nm) that can be removed after ion irradiation. Preamorphized and crystalline 6H-SiC have been irradiated with 350 keV Al^+ ions at 500°C. Erosion rates of about 5 nm/10^{17} ions cm^{-2} and smaller than 2 nm/10^{17} ions cm^{-2} have been determined by RBS/C, XTEM and surface profiling for the preamorphized and the crystalline samples, respectively. These erosion rates are in the magnitude of order of calculated physical sputtering rates.However, a surface erosion of about 50 nm / 10^{17} ions cm^{-2} has been observed at an irradiation temperature of 1050°C. It can be assumed, that changes in the bonding structure of the surface are responsible for this enhanced erosion.

***Collaboration*:** *Aristotle University of Thessaloniki, Greece

G. Brauer
W. Anwand
W. Skorupa
*P.G. Coleman**
*W. Triftshäuser**[2]
*C.D. Beling**[3]
*A.H. Weiss**[4]
*F. Plazaola**[5]
*J. Kuriplach**[6]
*M. Puska**[7]

Characterization of vacancy-type defects in Ge^+ implanted and annealed SiC by SPIS

Implantations into 6H-SiC wafers were carried out by 200 keV Ge^+ ions at room temperature in a fluence range from 10^{12} cm^{-2} to 10^{15} cm^{-2}. Each wafer was separately heat treated at temperatures of 500, 900 and 1500°C, respectively. The characterization of vacancy-type defects has been performed by the established SPIS technique in order to determine the depth of damaged layers created by ion implantation and their annealing behaviour. It could be shown that the maximum depth of damage increases with the fluence up to 700 nm and extends beyond that predicted by TRIM (200 nm). As concluded from positron lifetime measurements the predominant defect type is the Si-C divacancy. Post-implantation annealing reduces the damage depth, but the damage can not be completely removed. The remaining damage is characterized mainly by agglomerates of about 13 divacancies. Theoretical calculations of positron lifetimes using the atomic superposition method are in good agreement with experiments and led to a scaling curve for interpretation of Doppler-broadening results. Characteristic bulk and surface positron properties of SiC were also measured, e.g. the positron work function could be determined to -3 eV. This value points to SiC as a prime candidate for development as a field-assisted positron moderator.

Collaboration: *University of East Anglia, UK; *[2]Universität der Bundeswehr München; *[3]University of Hong Kong, PR China; *[4]University of Texas at Arlington, USA; *[5]Euskal Herriko Universitatea, Bilbao, Spain; *[6]Charles University Prague, Czech Republic; *[7]Helsinki University of Technology, Finland

*R.A. Yankov**
W. Fukarek
U. Kreissig
A. Mücklich
G. Brauer
W. Anwand
M. Voelskow
W. Skorupa
*J. Pezoldt**
*P.G. Coleman***

The influence of substrate temperature and order of implantation on the formation of buried $(SiC)_{1-x}(AlN)_x$ layers in 6H-SiC by ion beam synthesis

Buried layers of $(SiC)_{1-x}(AlN)_x$ were synthesized in 6H-SiC wafers by multiple-energy, high-dose Al^+ and N^+ co-implantation at temperatures T_i in the range from 200 to1100°C. RBS/C, PIRR, PAS, ERDA and TEM were used to characterize the resulting structures in the as-implanted state and after 1200°C, 1 h annealing. Implanting at T_i = 200°C produced a buried amorphous layer extending to the surface. Elevated-T_i implants (> 400°C) were found to produce complex single-crystal structures and favour the process of Al-N bond formation. Dramatic improvement in the near-surface crystallinity accompanied with significant strain relief was achieved at T_i of 600°C and 800°C. Annealing at 1200°C for 1 h had relatively little effect on the SiC/AlN alloy formation, especially for T_i of 600°C and 800°C. From a viewpoint of maintaining layer crystallinity, introducing first Al^+ and then N^+ ions appeared to give better results.

supported in part by DFG

Collaboration: *Institut für Festkörperelektronik, TU Ilmenau; **School of Physics, University of East Anglia, Norwich, UK

F. Fontaine
J. von Borany
*F. Blum**

The project "Sensors for Extreme Environment" at the FZR

The project "Sensors for Extreme Environment" - started in April '97 - aims at fabricating pressure, temperature and radiation sensor prototypes based on diamond substrates suited to harsh environment and/or elevated temperatures up to 800°C. The task of the FZR is on the one hand to conduct research on the doping of diamond by ion-implantation, in particular for the n-type

conductivity, and on the other hand to perform the implantation doping of the diamond-based sensor prototypes designed by the partners. It has been chosen to investigate the so-called "hot implantation" doping route. For this purpose, a new high temperature target holder for ion-implantation has been designed, which can be operated up to 1400 °C. A special masking technique for hot ion implantation based on laser cut mechanical silicon masks has been developed. The accuracy of two different alignment levels is better than 20 μm. Ion implantations (boron for the p-type doping and lithium for the n-type doping) at temperatures up to 1300°C have been successfully performed. The electrical and structural characterization is under way. As a preliminary result, a temperature sensor consisting of boron implanted stripes has been realised. It exhibits an excellent temperature sensitivity of 0.1 °C up to 500°C.

supported by BMBF

Collaboration: *FernUniversität Hagen, Fachbereich Elektrotechnik

P.F.P. Fichtner[*a]*
J.R. Kaschny
*A. Kling***
*H. Trinkaus****
R.A. Yankov
A. Mücklich
W. Skorupa
F.C. Zawislak[*b]*
L. Amaral[*b]*
*M.F. da Silva*****
*J.C. Soares***

Nucleation and growth of platelet bubble structures in helium-implanted and annealed silicon

Cavities formed in Si by He ion implantation and annealing are known to be strong traps for transition-metal impurities. An understanding of the bubble nucleation and growth processes is crucial in determining the microstructure of the resulting cavity-containing layers. The samples used in this study were implanted with He^+ ions (40 keV, 1×10^{16} cm^{-2} or 30 + 60 + 120 keV, 5×10^{15} cm^{-2} for each energy) and rapid-thermally annealed between 300°C and 600°C for 10 min. Sample characterization was carried out by TEM and RBS/C. Contrary to what one would expect for light-ion-implanted and annealed single-crystal Si substrates, the dechannelling yield of the RBS/C spectra was found to increase with raising anneal temperature from 300°C to 470°C. This reverse-annealing behaviour is indicative of a thermally-activated growth process whose activation energy was calculated to be ≈ 0.33 eV. TEM data relates the above process to the nucleation and growth of platelet-like cavity structures exhibitting a specific strain contrast. At 500°C the TEM analysis reveals that the platelet-like morphology develops into a structure characterized by ring zones containing a large number of smaller, spherical-shaped cavities. The results obtained are interpreted on the basis of a nucleation model which accounts for the formation of overpressurized bubbles.

supported in part by CNPq -Brasil

Collaboration: *Departamento de Metalurgia (a)/Instituto de Física (b), Universidade Federal do Rio Grande do Sul, Porto Allegre, Brazil; **Centro de Física Nuclear, Universidade de Lisboa, Portugal; ***Institut für Festkörperforschung, Forschungszentrum Jülich; ****Instituto Technólogico e Nuclear, Sacavém, Portugal

*A. Antons**
K.-H. Heinig
*S. Mantl**

Process simulation of sub-µm pattern formation by local oxidation of $CoSi_2$/Si heterostructures

The excellent thermal and electrical properties of $CoSi_2$ are attractive for device applications. However, there are difficulties to form lateral $CoSi_2$ structures by wet chemical etching, reactive ion etching or sputtering. A possible solution of the problem is local oxidation of $CoSi_2$/Si hetero-structures, where SiO_2 forms on top of the stable $CoSi_2$ layer, i.e. the $CoSi_2$ layer is locally driven into the depth of the substate by oxidation.

Sufficiently thin (ca. 40 nm) $CoSi_2$ layers break into sublayers at the "bird's beak" of local oxidation, where 0.1 μm Si lengths of a $CoSi_2/Si/CoSi_2$ structure can be achieved by the control of the oxidation process, i.e. without advanced lithography. There are some obstacles for the application of this promising technique, e.g. the formation of $CoSi_2$ bridges across the $CoSi_2/Si/CoSi_2$ region. Our kinetic 3D kinetic lattice Monte Carlo (MC) simulation have been extended in order to achieve an understanding of the process and to predict process parameters for a reliable technology. It has been found that for a correct description of the process a multiconfigurational MC approach is necessary, which corresponds to interatomic interactions described by an embedded atom potential. Furthermore it has been predicted that for sufficiently thin $CoSi_2$ layers the strain field caused by the Si_3N_4 mask should separate the $CoSi_2$ layer even without the oxidation process. This theoretical prediction, which could be verified experimentally, provides now the most promising basis for the further development of this technology.

Collaboration: * Institut für Schicht- und Ionentechnik, Forschungszentrum Jülich

M. Posselt

Computer simulation of channeling profile analysis of implantation damage

Preexisting implantation damage causes enhanced dechanneling in a subsequent implantation step. This effect is employed to analyze the preexisting defects using low-dose channeling implants. The implantation into a channeling direction ensures a strong dependence of the profile shape on the predamage level. The low dose guarantees that the damage created by the analyzing implant is negligible. Compared to channeling RBS, this method is sensitive to lower defect concentrations. First systematic BC computer simulations were performed in order to reproduce experimental SIMS data obtained by boron channeling profile analysis of silicon targets predamaged by different ions with various energies. The data were provided by Intel Corporation, Hillsboro, OR. In the BC code Crystal-TRIM the damage accumulation during the preimplant is described by a phenomenological model which has been recently used in order to simulate the dose dependence of the shape of range profiles in ion implantation into virgin targets. The simulations yield an estimation of the distribution of such as-implanted defects which are relevant for the dechanneling process during the channeling profile analysis.

S. Hengst
H.-U. Jäger

Numerical aspects of modelling point defect-based dopant diffusion in silicon during oxidation

The 1D process simulator TESIM of IMS Dresden contains an advanced diffusion module designed to allow for the coupling of point defects (self-interstitials and vacancies) with the electrically active and inactive impurity species. Up to now this module was, however, not capable of modelling the effect of oxidation. The numerical key problem of including oxidation is to solve a two-phase Stefan problem with a moving boundary between oxide and silicon. Computer-time aspects make it attractive to keep the number of grid nodes fixed, but to allow them to move with the oxide boundary. For this purpose, an additional drift term describing the mobility of nodes was added to the diffusion-reaction equations of this TESIM diffusion module.

supported by SMWA

Collaboration: FhG-Institut für Mikroelektronische Schaltungen und Systeme (IMS) Dresden; Zentrum Mikroelektronik Dresden

M. Posselt
*H. Huber**
*W. Assmann**
*S.A. Karamian***

Computer simulation of blocking-to-channeling and random-to-channeling transition

Recent experimental investigations at the accelerator laboratory in Garching showed that directional distributions of recoiling silicon particles generated by a primary beam of swift heavy ions exhibit a blocking-to-channeling transition. The effect occurs only if the lengths of recoil trajectories are sufficiently large. Furthermore, it was demonstrated that energetic ions with initially random directional distributions have directional distributions with channeling patterns after transmission through a single-crystalline silicon foil if the thickness of the foil is large enough. Computer simulations using the BC code Crystal-TRIM were performed in order to obtain an understanding of the experimental results. Since the length of particle trajectories is usually in the order of 5-10 μm, some ten thousand binary collisions were simulated per particle, i.e. one had to take special care of the numeric precision. Particular attention was paid to check whether nuclear and electronic small-angle scattering are responsible for the observed phenomena. It was found that the transition to channeling cannot be completely understood by only considering these two effects.

Collaboration: *Beschleunigerlabor der Universität München; ** JINR Dubna, Russia

M. Dobler
H. Reuther
*S. Kruijer**

Phase formation of iron disilicides during ion beam synthesis

In the dose range from $2x10^{15}$ cm^{-2} to $1x10^{17}$ cm^{-2} ^{57}Fe atoms were implanted with 40 keV into Si at 350°C to form iron silicides. For phase analysis integral and depth selective conversion electron Mössbauer spectroscopy were used. With AES the iron concentration depth profiles were determined. Two regions of phase formation were found: For low doses (< $3x10^{16}$ cm^{-2}) the metastable γ-$FeSi_2$ is formed whereas at higher doses a mixture of α- and β-$FeSi_2$ exists. For the latter case the fraction of the β-phase increases with the implantation dose. The depth depending phase composition is correlated to the shape of the iron depth profiles. The largest fraction of the β-phase is found in the maximum of the iron distributions. Subsequent annealing of the as-implanted samples at 900°C and 1150°C induce the formation of the pure β- and α-phase, respectively. Based on these results and with respect to former investigations a model of phase formation in correlation with the development of the microstructure and the structural features of the phases has been developed.

supported by DFG

Collaboration: *Laboratorium für Angewandte Physik, Universität Duisburg

H. Reuther
*G. Behr**
M. Dobler
*A. Teresiak**

Angle dependent Mössbauer spectroscopy on ß-$FeSi_2$ single crystals

The semiconducting ß-$FeSi_2$ has been subject of Mössbauer spectroscopic investigations at powder and thin film samples since several years. The spectrum was decomposed into two doublets with equal spectrum areas and positive quadrupole splittings. However, recently it was shown that the sign of the two splittings must be different. Further, another coupling of the four lines to the two doublets was proposed. In the present study, for the first time high purity single crystals prepared with iron enriched with about 40% of the Mössbauer isotope ^{57}Fe were available. They were investigated by angle dependent conversion electron Mössbauer spectroscopy. It is shown that the coupling of lines 1 with 4 and 2 with 3 is the correct one and the sign of the

second quadrupole splitting is negative. The correct values for the isomer shift are 0.0766(25) mm/s and 0.0979(42) mm/s in reference to α-Fe and for the quadrupole splitting 0.5215(50) mm/s and -0.2974(73) mm/s for the two doublets, respectively. The site occupation for both iron places differs sligthly, 48 % for the first and 52 % for the second one.

supported by DFG

Collaboration: *FhG Institut für Festkörper- und Werkstofforschung Dresden

Nanoclusters

B. Schmidt
K.-H. Heinig
R. Grötzschel
A. Markwitz
W. Matz
M. Strobel
*S. Oswald**

Precipitation, ripening and chemical effects during annealing of Ge^+ implanted SiO_2 layers

Thermally grown 500 nm thick SiO_2 layers have been implanted with 350 keV Ge^+ ions (0.5 to $5x10^{16}$ cm^{-2}) and subsequently annealed at 600 to 1100°C for 15 to 1500 min in different ambients. The Ge redistribution and nanocrystal formation have been studied by RBS, TEM, EDX and XPS. The annealing in N_2 and Ar leads to a bimodal Ge depth distribution and a decoration of the Si/SiO_2 interface by Ge. As it has been proven by XPS measurements, the near-surface peak of that distribution is formed by Ge having Ge-O bonds, whereas in the second peak prevailing Ge-Ge bonds have been found. The Ge at the Si/SiO_2 interface can be attributed to Ge-Si bonds. XTEM images show Ge clusters in the second-peak region only, not in the near-surface peak region. A new kinetic 3D Monte-Carlo (MC) program has been developed to study this behaviour. Four species (Ge monomers, Ge in clusters, oxidant in SiO_2, GeO_2) and their chemical interactions are now taken into account by incorporation of additional MC lattices and atomic hopping probabilities. Assuming a tiny concentration of moisture (oxidant) in the "inert" Ar or N_2 annealing atmosphere, the MC simulations reproduce even details of the RBS spectra of Ge and the TEM images of Ge nanoclusters. Completely different results have been obtained by annealing in a hydrogen containing ambient (Ar+7%H_2). The Ge redistribution is strongly accelerated and/or occurs at lower temperatures. For instance, very large Ge nanocrystals (20...40 nm) forming a band of 40...60 nm thickness, which is much narrower than the as-implanted Ge profile (ΔRp= 180 nm), have been found after annealing at 950°C for 1h.

Collaboration: * Institut für Festkörperanalytik und Strukturforschung, IfW Dresden

K.-H. Heinig
B. Schmidt
*V. Borodin**
A. Markwitz
R. Grötzschel

Ge redistribution and precipitation in Ge^+ implanted SiO_2 layers during annealing in oxidizing ambient

In former experiments a substantial redistribution of Ge had been found in Ge^+ implanted SiO_2 layers after annealing in "inert" atmospheres like Ar and N_2. The most striking feature was the transformation of the as-implanted Gaussian Ge depth profile into a bimodal depth distribution. The oxidation of Ge by the residual moisture of a few ppm in the annealing gas had been considered as a possible origin for this redistribution. A specific experiment using pure O_2 annealing (950°C, 15 to 45 min) was performed to prove this assumption. In comparison with annealing in "inert" ambients two differences have been found: (i) The formation of the bimodal Ge distribution as measured by RBS is considerably accelerated and (ii) the region of the near-surface peak of the Ge distribution contains now noncrystalline clusters of GeO_2. Theoretically we extended the continuum theory of Ostwald ripening by the chemical reaction kinetics with impurities (oxidizing species). An excellent reproduction of the evolution of the Ge profile has been achieved, which allows to determine the diffusion coefficient and solubility of Ge in SiO_2.

Collaboration: * Kurchatov Institute, Moscow, Russia

A. Markwitz
L. Rebohle
W. Skorupa

Homogeneously size distributed Ge nanoclusters in SiO_2 layers

500 nm amorphous SiO_2 layers were implanted with 450 and 230 keV Ge ions at room temperature to a total dose of $4.8x10^{16}$ cm^{-2} in order to achieve a Ge concentration of about 4 at.% in the oxide film. Afterwards, the specimens

were annealed between 500 and 1200 °C for 30 min in dry N_2 atmosphere. XTEM analysis shows homogeneously distributed Ge nanocrystallites of nearly uniform size arranged in a broad band (about 350 nm) in the SiO_2 layer. The typical mean cluster diameter ranges between 2 and 5 nm increases with the annealing temperature. Close to the surface of the specimens, always cluster-free regions are observed. In addition, a narrow Ge nanocluster band (thickness <10 nm) appears at the SiO_2/Si interface in a distance of ≈10 nm for annealing temperatures > 800 °C. EDX analysis performed in the scanning TEM mode shows that the nanoclusters in the broad band are related to peaks in the Ge depth distributions as measured also with RBS. Such Ge rich SiO_2 layers are of major interest for luminescence applications.

A. Mücklich
H. Tyrroff
*C. Allen**
W. Skorupa
B. Schmidt

In-situ study of implantation of Ge in SiO_2

Nanocluster formation was studied by TEM in-situ during the implantation of Ge into amorphous SiO_2. The experiments were performed at the dedicated user facility at ANL. Beside the scientific aspect the experiments are part of the preparation for prospective introduction of an ion beam from a 500 keV implanter into the CM300 TEM at Rossendorf.

At temperatures below (850°C) and above (960°C) of the Ge melting point (937°C) 55 keV Ge ions were implanted into a fee standing 80 nm SiO_2 film produced by thermal oxidation. The kinetics of precipitation of Ge clusters was recorded on a video tape. The analysis reveals the onset of observable cluster formation at a dose of $4x10^{15}$ cm^{-2}. The maximum diameter of clusters (6 nm) is reached at $1.6x10^{16}$ cm^{-2} for 850°C sample temperature whereas for 960°C half of the dose already leads to the same effect. These are lower doses than for ex-situ experiments.

Collaboration: * HVEM Tandem Facility, Argonne National Laboratory, USA

L. Rebohle
J. von Borany
W. Skorupa
*I.E. Tyschenko**
*H. Fröb***
*K. Leo***

Concentration and annealing dependence of the blue photoluminescence in Ge-rich SiO_2-layers produced by ion beam synthesis

The photoluminescence (PL) properties of Ge-implanted SiO_2 layers thermally grown on Si substrates have been investigated as a function of implantation dose and annealing temperature for two different oxide layer thicknesses. Thick (500 nm) Ge-rich layers were produced by double implantation (450 + 230 keV), whereas for thin (100 nm) layers single step implantation was applied. All implantations were performed at LN_2 temperature.

Depending on the Ge concentration and on the oxide thickness, maximum PL intensities (around 400 nm) are obtained after annealing between 400 °C and 700 °C. The optimized paramters result in an intense blue PL with an external quantum efficiency in the range $10^{-3}...10^{-4}$. The specific nature of the luminescence centers and the correlation to the observed PL dependencies are still under investigation.

Collaboration: *Institute of Semiconductor Physics, Novosibirsk, Russia; **Institut für Angewandte Photophysik, TU Dresden

M. Goldberg
J. von Borany
R. Grötzschel
A. Markwitz
B. Schmidt

Cathodoluminescence investigations on germanium implanted SiO_2-films

Cathodoluminescence (CL) spectra of Ge implanted (350 keV, $5x10^{16}$ cm^{-2}, room temperature implantation) into 500 nm amorphous SiO_2 layers are dominated by two bands at 395 nm and 290 nm. These bands are clearly related to defects involving germanium and oxygen. The peak position and

peak width are nearly independent of the annealing temperature (500-1100°C), whereas the intensity of the blue luminescence peak reaches a maximum at around 900°C. Information on the depth distributions of the CL was obtained varying the electron beam energy. Including additional results from TEM and RBS analysis these experiments show that: (i) significant luminescence contribution originates from the germanium existing inside the oxide near the Si/SiO_2 interface, (ii) only Ge atoms at the cluster surface contribute to the CL signal from the Ge nanocluster band, (iii) Ge bonded into stoichiometric Ge oxides gives probably minor contribution to the luminescence yield. Due to similar excitation mechanism CL is a well-suited method to predict the electroluminescence intensity with low preparation effort.
Collaboration: Sektion Physik, Universität Rostock

H.Seifarth
R.Grötzschel
A.Markwitz
W.Matz
P.Nitzsche
L.Rebohle

Investigation of Si nanocrystal formation in sputtered SiO_x films
SiO_x films with $1 < x < 2$ were deposited on silicon wafers by reactive rf-magnetron sputtering at substrate temperatures of $T_s = 20°C$ and $T_s = 500°C$, respectively, and have been investigated by RBS, XRD and HRTEM. The as-deposited layers show an XRD pattern typical for amorphous structures. During annealing at T = 1000°C for 1h in N_2 atmosphere, the exceeding Si forms nanocrystals in a surrounding SiO_2 network. The annealed samples with a high Si concentration corresponding to x = 1 show distinct XRD peaks of crystalline silicon. The mean size of the Si nanocrystals with nearly spherical shape was estimated by XRD and HRTEM to about 5 nm. The results indicate that the number of Si nanocrystals is a function of the Si concentration of the SiO_x film. Furthermore, the low temperature deposition is favourable for the formation of Si nanocrystals because of quenched defects and/or stress which relaxes during annealing. The as-deposited SiO_x films show only a weak PL in the visible region, whereas after nucleation of Si nanocrystals due to annealing, a significant PL was measured. The PL intensity and wavelength depend on the initial Si concentration in the SiO_x film and the annealing conditions.

M. Strobel
K.-H. Heinig
*C.W.White**
*R.A. Zuhr**
*J.D. Budai**
*S.P.Withrow**

Dependence of the ion beam synthesized nanocluster size distribution on implantation parameters
The high-dose ion implantation of metals (e.g. Au, Ag, Cu) into SiO_2 leads to the formation of metallic nanoclusters (NCs) even without post-implantation annealing. The nucleation of NCs from a temporally and spatially inhomogeneous supersaturated solid solution as well as their subsequent growth have been studied by comprehensive kinetic Monte Carlo (KMC) simulations. The modelled size and depth dependencies of the evolution of Au NC distributions in SiO_2 on implantation fluence, time and temperature are qualitatively in very good agreement with the experimental results. Additionally, the KMC studies predict, that bimodal size distributions can be obtained by a controlled variation of the implantation parameters during ion implantation. For instance, by lowering the implantation temperature, a second nucleation stage can be initiated.
supported by DAAD
Collaboration: *Solid State Division, Oak Ridge National Laboratory, Oak Ridge, TN, USA

M. Strobel
K.-H. Heinig

Simulation of late processes of nanoclusters formation by combining atomistic and mesoscopic models

By means of ion beam synthesis, nanoclusters are formed by rather fast processes (nucleation, growth) and evolve later on by very slow processes (Ostwald ripening, coalescence). Atomic-scale kinetic Monte Carlo simulation is the appropriate approach to describe the nucleation caused by ion implantation induced time-dependent and spatially inhomogeneous supersaturation. However, due to the restricted computer resources, this method is inefficient for the simulation of Ostwald ripening. Here, on a mesoscopic scale, the direct integration of rate-equations of a huge ensemble of nanoclusters is much more efficient. As the evolution of a nanocluster system by means of Ostwald ripening depends strongly on the initial nanocluster distribution, the computer simulations using the mesoscopic model has been combined with atomic-scale MC simulations which deliver the initial distributions. Combining atomistic and mesoscopic models provides for the first time an efficient simulation tool for studies of the whole process of ion beam synthesis.The method has been successfully applied to the study of ion beam synthesis of semiconductor and metal nanocrystals.

M. T. Pham
D. Möller
W. Matz
A. Mücklich
*S. Oswald**

CdS nanocrystals entrapped in thin SiO_2 films

The synthetic route relies on implanting Cd^+ and S^+ ions into a 100 nm-thin SiO_2 film structure subjected then to an annealing at 500°C in N_2. CdS nanocrystals formed, nearly spherical in shape and of hexagonal structure with an average size of 7 nm, are confined completely within the SiO_2 films. The formation of CdS is the result of energetic S^+ ions reacting with preformed Cd nanoparticles. The reaction toward CdS is induced during implantation and completed by a subsequent annealing. Byproducts identified in the implanted layer are CdO and unreacted Cd and S. The thermal annealing leads to loss of Cd and S from the film and coarsening the CdS particles. There is an optimal temperature regime for removing the unreacted components Cd and S, which are less mobile relative to CdS, from the film. The film-immobilized nanocrystals are readily accessible to surface characterizing techniques.

Collaboration: *Institut für Festkörperphysik und Werkstofforschung, Dresden

M. T. Pham
*G. Steiner**
*C. Kuhne**
*R. Salzer**

Ion-implantation generated Ag nanoclusters for sensors using optical resonance

Sapphire and glass were implanted with Ag^+ ions at energy of 20-58 keV to doses of 10^{16}-10^{17} ions/cm². The resulting surfaces were characterized by UV-vis spectroscopy. Their application was tested for surface plasmon resonance (SPR) and surface-enhanced infrared absorption (SEIRA). The results show that collective particle surface plasmon modes are present in the 350-500 nm spectral region. The resonance wave length remains stable over a tested period of 7 weeks in water. SPR measurements with glucose solution confirmes the plasmon - analyte concentration correlation. SEIRA measurements with a biomembrane demonstrate a resonance enhancement factor of ca. 10.

Collaboration: *Institut für Analytische Chemie, TU Dresden

Focused Ion Beam

L. Bischoff
J. Teichert
D. Panknin
*T. Ganetsos**
*D. Tsamakis***
*G.L.R. Mair**
*C. Aidinis**

FIB fabrication and electrical characterization of Si_{1-x} Ge_x micro structures

The Rossendorf FIB system IMSA-100 was used for writing implantation of singly and doubly charged Ge ions (35 or 70 keV, $9x10^{15}$ to $7x10^{16}$ cm^{-2}) from an $Au_{73}Ge_{27}$ liquid alloy ion source into silicon to form $Si_{1-x}Ge_x$ micro structures. The spreading resistance was measured as a function of the annealing temperature (700-1000°C) where at 800°C, 1h in N_2 atmosphere a minimum was found with 10 kΩ for a dose of $7x10^{16}cm^{-2}$ and 30 kΩ for the lowest implantation dose. The drift carrier mobility was determined to1000-1300 cm^2/Vs which corresponds with the predicted values using the Bufler-Rieger theory. The results for the FIB fabricated structures are in a good agreement with that samples formed by LPCVD.

Collaboration: * University of Athens, Physics Department, Greece; ** University of Athens, Department of Electrical Engineering, Greece

L. Bischoff
J. Teichert
*S. Howitz**
*R. Ameling***

Nanolithography for optical investigations by means of a focused ion beam

Investigations of an optical nano-aperture system with dimensions of the optical wave length require precisely located and well defined apertures with a diameter of 200 - 400 nm. Therefore, aluminum was deposited on borofloate glass with a film thickness of 100 nm and 150 nm. For focused ion beam sputtering using 35 keV Co^+ ions the beam parameters such as number of pixels and dose were optimized in combination with SEM analysis. 256 holes per wafer with a diameter of 200 to 400 nm were milled into the Al film with a position accuracy better than 1 µm.

Collaboration: * GeSiM - Gesellschaft für Silizium-Mikrosysteme mbH, Rossendorf; ** Carl Zeiss Oberkochen, Abt. Forschung Bildtechnik

L. Bischoff
J. Teichert
V. Heera

Focused ion beam sputtering of 6H:SiC

Only a few experimental erosion data are available for heavy ion bombardment of SiC in the energy range from 30 to 100 keV. The focused ion beam is a very useful tool to create holes with well defined dimensions which can be easily analyzed by surface profiling measurements. Applying this volume loss method the milling rates of 6H:SiC were measured for 35 and 70 keV Co, Ge, Nd and Au ions obtained from the mass separated focused ion beam system IMSA-100. For gold ions the milling rates were determined as a function of incident angle and processing temperature in the range of 25 to 400°C. The swelling of the SiC due to ion implantation was investigated as a function of ion species and dose. A simple model was applied to extract the sputtering yields from the milling rates. The experimental results are in good agreement with sputtering yield calculations using the Bohdansky formalism.

L. Bischoff
J. Teichert
*R. Wannemacher**
*H.E. Wilhelm**

FIB generation and spectroscopic characterization of color centers in bulk and nanocrystalline synthetic diamond and CVD diamond layers

Due to their photophysical properties color (luminescence) centers in diamond are promising candidates for use as light sources in near-field optical microscopy. The application of a focused ion beam allows to implant structu-

res with micron and submicron dimensions and to create color centers in the near surface region due to the low penetration depth of the ions compared with that of electrons. This may result in a good resolution of the light source for the near-field optical microscopy. Color centers have been generated by electron irradiation and by focused ion beam implantation of 70 keV Ge^{2+} and Co^{2+} ions in bulk synthetic diamond crystals, nanocrystalline diamonds, and CVD-diamond layers using the Rossendorf FIB system IMSA-100 followed by thermal annealing. Different spectral characteristics have been found for various samples and are attributed to color centers reported in the literature, as well as to contributions from graphitic carbon. Emission profiles of color center structures generated by focussed ion beam irradiation have been obtained for various excitation wavelengths using a confocal microscope.
Collaboration: * Technische Universität Chemnitz, Institut für Physik

J. Teichert
L. Bischoff
G. Hofmann
W. Probst
*E. Hesse**

Energy distribution measuring system for ions and ionized cluster beams from liquid metal ion soures

An experimental equipment has been developed and constructed which allows the measurement of mass-resolved energy distributions of ion beams and ionized cluster beams emitted from liquid metal ion sources (LMIS). Hairpin type and capillary type LMIS with pure metals or alloys as source materials can be investigated. The ion optical column consists of an electrostatic einzel lens, an ExB mass separator, an octopole deflection system, and a retarding field energy analyser. The ExB filter has a magnetic field strength of 0.6 T and provides a mass resolution between 80 (400 AMU) and 300 (20 AMU). Behind the lens the ion beam is collimated with an angle deviation of less than 1 mrad. The retarding lens in the energy analyser contains a double mesh and properly designed electrodes which gives an energy resolution of about 1 eV. The system operates at an acceleration voltage of 10 kV.
Collaboration: *Central Microstructure Facilitiy, Rutherford Appleton Laboratory, Chilton, Didcot, UK

Plasma Immersion Ion Implantation

S. Mändl
R. Günzel

Sheath and presheath dynamics in plasma immersion ion implantation

For plasma immersion ion implantation (PIII) the ion flux onto the target is determined by the expansion of the plasma sheath during the voltage pulses. After applying a potential very large compared to the electron temperature the sheath expands as the space charge region must be enlarged to accommodate the higher potential. The presheath is temporarily reduced in its width and reaches its original extension L only after a sufficiently long time, due to the longer time constant governing the presheath relaxation. An empirical model, verified by Langmuir probe measurements, was elaborated to describe the delayed reaction of the original presheath to the moving sheath edge and the formation of a new presheath. In the case of a spherical electrode pulsed with 5 kV after 10 μs the sheath is stationary whereas the presheath has started to react and is moving into the bulk plasma. After 50 μs, at the end of the pulse a new fully developed presheath, displaced by 18 mm into the plasma is obtained. Finally, after the sheath edge is stationary, the full presheath width is recovered with the time constant $T_{pre} = L/u_B$.

R. Günzel
M. Betzl
*I. Alphonsa**
*B. Gangul**
*P.I. John**
*S. Mukherjee**

Comparison of plasma immersion ion implantation and glow discharge plasma nitriding of stainless steel

For nitriding of stainless steel, plasma immersion ion implantation (PII) and glow discharge plasma nitriding (GDPN) were performed for the same treatment time of two hours, using the same treatment voltage (700V) and duty ratio (50%) during the nitridation process of stainless steel samples. The temperature during treatment was fixed at 380°C and controlled by an isolated thermocouple. The only difference in the experimental conditions was the pressure during treatment of 0.1 Pa in the case of PII and 500 Pa in the case of GDPN. Pure nitrogen as well as a nitrogen-hydrogen mixture was used as feed gas. The resulting concentration profiles were determined by glow discharge optical spectroscopy depth profiling to determine the nitrogen incorporation rate of both nitriding techniques. The surface properties were investigated by wear and hardness measurements. Both technologies yield a nitrided layer with an increased hardness. The highest nitrogen concentration and widest hardened layer was found in case of PII using a nitrogen-hydrogen plasma.

Collaboration: *Institute for Plasma Research Bhat, Gandhinagar, India

J. Brückner

Vacuum arc plasma source with magnetic particle filter

The properties of a filtered vacuum arc plasma source have been improved using a special magnetic field structure in the anode region. The magnetic field produced by the curved magnetic filter at the cathode surface is compensated by a coil located inside the anode. This configuration results in a considerable reduction of the arc voltage and very stable arc operation without the need of a working gas. The inner tube of the filter was equipped with a series of baffles to suppress the reflection of particles. For a filter with 90° deflection a maximum transmission of 23% has been achieved. The motion of the arc spots is controlled by 2 concentric magnetic coils located behind the cathode surface. This allows to switch between different areas of the cathode which may consist of different materials (inner part and outer ring). This procedure has been demonstrated for the combination aluminium/copper and switching frequencies up to 10Hz.

J. Brückner
R. Günzel

Metal plasma immersion ion implantation: chromium on magnesium

Chromium films have been deposited on magnesium by MPIIID using a filtered vacuum arc plasma source. The corrosion potential measured in a corrosion test becomes more positive by reducing the particle content of the film indicating a better passivation of the specimen. This can be attributed to the reduced number of defects in the film. By applying an implantation step before film deposition a further strong improvement has been observed, which is attributed to the removal of surface oxide and the formation of an intermixed layer.

J. Brückner
*T. Witke**

Ion implantation using a pulsed high current vacuum arc

A metal plasma immersion ion implantation system with a pulsed high current vacuum arc plasma source has been used for the implantation of carbon into silicon and niobium into Ti6Al4V alloy. The arc source was operated at duty cycles in the order of 1%, and during the plasma pulse a pulsed high voltage was applied to the substrates. Implantation voltages between 5 and 20 kV and duty cycles between 20 and 65% have been used. The shape of the implantation profile depends on the high voltage duty cycle. At sufficiently high duty cycles all material deposited in the pulse pauses is removed by sputtering and pure implantation profiles can be obtained.

supported by SMWK

Collaboration: *Institut für Werkstoffphysik und Schichttechnologie Dresden

Ion Beam Analysis

C. Neelmeijer
M. Mäder
J. Hüller
*B. Borchers**
*J. Jarjis***

A simple paper-based secondary standard for energy dispersive X-ray analysis

For the purpose of routine checking of the spectral efficiency $\varepsilon(E_X)$ of Si(Li) detectors a comfortable multi-elemental secondary standard has been developed which will allow easy checks of detector stability and inter-laboratory comparisons of X-ray facilities. The standard consists of a non-glued chromatography paper matrix which is doped from the solution of well defined metallic salts. It fulfils the following criteria: (i) generation of a large number of non-interfering X-ray lines, (ii) minimum matrix-based background, (iii) reasonable X-ray counting rate, (iv) elemental homogeneity plus stability, and (v) simple fabrication.

Collaboration: * Papiertechnische Stiftung Institut für Zellstoff und Papier, Heidenau; ** Materials SPM, Nuclear Physics Laboratory, University of Oxford, UK

C. Neelmeijer
M. Mäder
*M. Schreiner**

COST-G1: "Paint layer indications by XRF"

XRF measurements shall be utilised in museums to preselect art objects of interest for detailed studies at accelerators using external IBA methods. For this purpose a mobile XRF facility should detect chemical elements down to Al and possibly indicate a layered or admixed arrangement of painting materials. The "TRACOR 2000" stationary XRF facility of the Academy of Fine Arts Vienna was successfully used for initial tests: Following the Rossendorf external proton beam set-up, the TRACOR in-air version was upgraded by a He gas jet to ensure light element detection with sufficient efficiency. For special pigment combinations and layer thicknesses d>30 µm it was shown that paint layer arrangements can be distinguished from the corresponding pigment admixtures via changes of the K_α/K_β or L_α/L_β X-ray yield ratios induced by selective absorption and secondary excitation effects.

Collaboration: *Akademie der Bildenden Künste Wien, Österreich

M. Mäder
C. Neelmeijer
*M. Schreiner**
*G. Woisetschläger**
D. Grambole
F. Herrmann

Study of glass corrosion state using external PIXE/PIGE

Knowledge on the chemical composition of historic silicate materials represents one of the fundamentals for proper classification, storage and conservation of art objects made from glass. However, composition analysis of the bulk material may be impossible or becomes at least modified by the presence of altered surface layers generated by natural glass corrosion. This alteration process includes leaching of the glass network modifiers, i.e. K and Ca, and replacing of them by H^+ or H_3O^+ from the humid atmosphere.

Corrosion layers of different thicknesses were produced on the model glass M3 by the aid of treating in HCl. Combining the external PIXE and PIGE techniques both the characteristic X- and γ-radiation of the element Si were detected simultaneously. The yield ratios of both lines were measured as a function of the surface layer thickness. Different PIXE/PIGE yield ratios reflect different thicknesses of the leached layer. The method proves suitable to distinguish thin altered layers from deep corrosion destruction.

supported by BMBF

Collaboration: *Institut für Farbenchemie, Akademie der Bildenden Künste Wien, Österreich; Bundesanstalt für Materialforschung und -prüfung Berlin

D. Grambole
F. Herrmann
*T. Arnold**

Characterization of phyllite with micro-PIXE

Micro-PIXE was used together with SEM/EDX and thin section microscopy to characterize the phyllite, which is a low grade metamorphic rock. Phyllite is common in the Western "Erzgebirge" in Saxony, Germany. Its importance in connection with residual contaminations from the former uranium mining requires a detailed characterization.

A polished sample of a phyllite rock was studied by measuring maps and line scans using a 3 µm proton beam of the nuclear microprobe at the 3 MV tandetron accelerator. The elements Si, K, Fe, Ti, and Ca were detected with PIXE. Based on their distributions it was possible to distinguish various mineral layers within the phyllite. Layers enriched in Si and without K, Fe, or Ti were attributed to quartz layers. Potassium enriched layers indicated the presence of muscovite, and layers enriched in Si and Fe were attributed to chlorite. In addition, it was possible to identify iron oxides and titanium oxides. Iron oxides were found either as locally enriched spot-like zones, or accumulated in fissures and cracks, indicating the formation of secondarily formed iron oxide minerals, e.g. ferrihydrite. Ti usually occurred as locally enriched zones, very likely representing small rutile minerals (TiO_2). Moreover, monazite (Ce, Th, Nd, La)PO_4, apatite $CaPO_4$, and zircon $ZrSiO_4$ were detected as accessory minerals. In particular monazite was identified because of its ion luminescence behaviour.

Collaboration: *Institut für Radiochemie des FZR

D. Grambole
R. Grötzschel
F. Herrmann
*K. Maser**
*J. Krauser***

Hydrogen depth profiling in thermally grown SiO_2 layers

Hydrogen depth distributions in 90 nm thick SiO_2-layers on silicon substrates prepared at the TU Berlin were studied by resonance depth profiling using the narrow 6.385 MeV resonance of the nuclear reaction $^{1}H(^{15}N,\alpha,\gamma)^{12}C$. The oxide was thermally grown at 700°C in water steam atmosphere. The hydrogen depth profiles of identical samples were measured both at the 6 MV VdG accelerator of the HMI Berlin at LN_2 temperature, with typical beam current densities of 2 µA/cm² and 50 µC collected charge per data point, and at the 5 MV tandem accelerator of the FZR, with typically 30 nA/cm² and 5 µC at room temperature. The results differ strongly as a consequence beam-induced H outdiffusion. The measurements at the HMI show a strong hydrogen depletion except for the SiO2/Si interface. This indicates a strong binding of hydrogen to the interface, whereas the hydrogen in the bulk of the SiO_2 gets mobile and an hydrogen outdiffusion occurs at high beam current densities even at low temperatures.

Collaboration: *Institut für Mikroelektronik und Festkörperelektronik, TU Berlin; **Hahn-Meitner-Institut Berlin

D. Grambole
F. Herrmann
*K. Noll**
*U. Krähenbühl**

Investigation of the terrestrial fluorine enrichment of Martian meteorite ALH84001 and other Antarctic meteorites by micro-NRA

Meteorites found in Antarctica were embedded and conserved by the ice during a long part of their history on our planet. The contamination by terrestrial compounds begins just after a meteorite has emerged from the ice and is exposed to the atmosphere. The duration of this exposure can be estimated by measuring the enrichment of fluorine on the meteorite's surface. The fluorine concentrations of some Antarctic meteorites were determined by measuring the 110 keV γ-rays of the nuclear reaction $^{19}F(p,p'\gamma)^{19}F$ at a proton energy of 3.4 MeV using the nuclear microprobe installed at the 3 MV tandetron accelerator. The lateral distributions and the depth profiles of

fluorine were obtained by mapping and line scans over cross sections of the meteorites, respectively. The detection limit of fluorine was estimated to 3.5 wt.-ppm. The surface of Martian meteorite ALH 84001 revealed a fluorine concentration of about 6 wt.-ppm. Compared with the F-enrichment of other Antarctic meteorites, an upper limit of 500 years of exposure on the ice surface was evaluated. Consequently, the Martian meteorite ALH84001 was enclosed and protected by ice for more than 96% of its terrestrial residence of about 13000 years.

Collaboration: *Labor für Radio- und Umweltchemie, Universität Bern, Schweiz

D. Grambole
F. Herrmann
*B. Groß**
*R. Hempelmann**

Characterization of thin proton conducting films by means of the ^{15}N nuclear resonance reaction analysis

Ceramic high temperature proton conductors of the perovskite type are applied actually or potentially for widely different purposes such as hydrogen sensors, steam electrolysers and, particularly, in solid oxide fuel cells. For the investigation of the dissociative water vapour absorption in these materials and its thermodynamic description the absolute hydrogen concentrations have to be known. Thin $Ba_3Ca_{1.18}Nb_{1.82}O_{8.73}$ films were prepared by the sol-gel method on silicon substrates. To determine the thermodynamic quantities ΔS and ΔH the samples were charged with water vapour at partial pressures between 5 and 845 mbar and temperatures between 823 K and 973 K. Analysis by the $^{1}H(^{15}N,\alpha\gamma)^{12}C$ resonance reaction revealed a hydrogen concentration of 0.5 to 2.5 at.%.

supported by BMBF

Collaboration: *Institut für Physikalische Chemie, Universität des Saarlandes, Saarbrücken

D. Grambole
F. Herrmann
*D. Gehre**
*W. Hauffe**
*R. Behrisch***

Hydrogen and deuterium depth profiling of divertor tiles by micro-ERDA

Depth profiling by means of conventional ERDA is limited to a depth smaller than 1 µm. To investigate distributions of the hydrogen isotopes in larger depth regions of divertor samples from the ASDEX UPGRADE tokamak of the Max-Planck-Institut für Plasmaphysik the samples (0.5 mm tungsten on carbon) were bevelled at an angle of 60° with respect to the surface normal by mechanical cutting and polishing. For polishing hydrogen a free suspension ($Al_2O_3 + CCl_4$) was used. One sample was additionally polished by ion beam sputtering with target rotation to avoid anisotropic etching. For profiling using the Rossendorf nuclear microprobe a 10 MeV Si beam was focused to about 3.5 µm and scanned linearly across the slope from the surface to a depth of about 750 µm. In the absence of the additional polish, hydrogen analysis is obscured by water adsorption on the slope surface. Deuterium and hydrogen were found at depths < 10 µm. The deuterium concentration was about 5 at%.

supported by BMBF

Collaboration: *Institut für Oberflächenphysik und Mikrostrukturphysik, TU Dresden; **Max-Planck-Institut für Plasmaphysik, Garching

Equipment

M. Friedrich
S. Turuc
W. Bürger

Operation and development of the electrostatic accelerators

The *2 MV VdG* has been applied exclusively for RBS measurements. The power supplies for the analysing and switching magnets have been modernised and the NMR device for stabilisation of the analysing magnet field was replaced by a Hall probe system, resulting in an improved beam stability.

The ***5 MV Tandem*** has now been 25 years in operation. It has been applied to ion beam analysis, high energy implantation, basic ion-solid interaction research and detector development. The injector was completely reconstructed. Due to the installation of a stigmatically focusing 90° injector magnet and a 5 port switching magnet, an increase of about 20 – 30 % for heavy ion transmission through the accelerator has been obtained, and the possibility for the installation of additional ion sources has been created. Both magnets are controlled by Hall probes. On the basis of a modular programmable logic controller SIMATIC S5 (Siemens) a remote control of all parameters at the duoplasmatron injector is now available as for the sputter injector. The complete control panel of the accelerator and the power supplies of the analysing and switching magnets have been modernised. The NMR probe for stabilisation of the analysing magnet field was replaced by a Hall probe system.

The ***3 MV Tandetron*** has been used for high energy ion implantation, ion beam synthesis and ion beam analysis. Only one maintenance due to a failure at the high voltage power amplifier was necessary. In preparing the Tandetron beamline system to be installed in the new accelerator building, an analysing magnet with higher magnetic rigidity (100 MeV*amu/n^2 at 30^0 deflection) has been installed. The magnetic fields of this magnet as well as the low-energy magnet have been equipped with Hall probes. An additional chamber in the implantation beam line has increased the efficiency and purity for silicon wafer implantation up to 5" wafer diameter.

Other Activities

K.-H. Heinig
*M. Jentschel**
T. Koch
*H. Börner**

supported by SMWK

Crystal-GRID measurements with iron samples

At ILL Grenoble, Crystal-GRID experiments were performed with the aim to study the reliability of the interatomic universal and embedded atom potentials of iron in the region of a few hundert electron volts. First results of the still ongoing data analysis indicate that in the medium-energy region for metallic crystals the deviation between the low-energy many-body potential and the high-energy binary potential is not so pronounced as in the formerly studied ionic crystals.

Collaboration: * ILL Grenoble, France

E. Wieser
*I. Zyganov**
W. Matz
H. Reuther
*S. Oswald***
T. Pham
E. Richter

Modification of titanium by ion implantation of calcium and/or phosphorus

Pretreatment of titanium by implantation of P and Ca is of interest in order to improve the quality of hydroxyapatite coatings used to enhance its biocompatibility. A near surface implantation of high doses of calcium results in an oxidation of the modified layer and the formation of CaO. As a very interesting effect, for deeper calcium implantations precipitation of the metastable hexagonal modification of calcium has been observed instead of the cubic equilibrium phase. By high dose implantation of phosphorus the implanted layer becomes amorphized, which hinders the reaction with oxygen. The thickness of the surface oxide corresponds to the native oxide layer. For high dose double implantation with both elements, due to the strong swelling effect and the incorporation of oxygen, an enrichment closer the surface is observed for the second implant, if the energies are chosen so that the profiles should be overlapping into pure titanium. No indication for compound formation beside calciumoxide has been found.

Collaboration: *Lipetsk State Technical University, Russia; **Institut für Festkörper- und Werkstofforschung, Dresden

J. Noetzel
H. Reuther
E. Wieser
*A. Gorbunov**
*W. Pompe**
*R. Dietsch***
*H. Mai***

Interface Structure of Fe-Al Multilayers

This work is part of a program concerned with structural transformations and phase formation in binary metallic systems with limited miscibility starting with structures far away from thermodynamic equilibrium. Such non-equilibrium systems are nanoscale multilayers with a high contribution of interface energy. Fe-Al multilayers were prepared by pulsed laser deposition. Some intermixing of Fe and Al atoms in the interface region should occur by ballistic collisions of the arriving particels which has been estimated by computer simulation. On the iron side of the interface iron atoms will have a certain probability for Al neighbours. Fe on the Al side is characterized by a high number of Al neighbours. The probability to find Fe atoms with n Al neighbours has been evaluated experimentally from the magnetic hyperfinefield distribution determined by ^{57}Fe conversion electron Mössbauer spectroscopy (CEMS). The probability for $n = 1$ is higher and for $n \geq 5$ lower as expected for pure ballistic mixing. Ion beam mixing of the multilayer structure by 1×10^{15} Fe^{+}/cm^{2} (150 keV) increases the probability for $n = 1$-3 while the contribution of $n \geq 5$ remains nearly unchanged. These effects are

supported by DFG (SFB "Strukturbildung und Eigenschaften in Grenzschichten")

explained by chemical driving forces which favour the formation of Fe-Al pairs on the Fe-rich side and counterbalance the ballistic effect by demixing on the Al-rich side.

Collaboration: *Technische Universität Dresden, Institut für Werkstoffwissenschaft; **FhG-Institut für Werkstoffphysik und Schichttechnologie

H. Reuther
M. Betzl
W. Matz
E. Richter

Alloying by high dose ion implantation of iron into magnesium and aluminium

Alloys of the systems Fe-Al (miscible over the whole concentration range) and Fe-Mg (insoluble with each other) were produced by implantation of Fe ions into Al and Mg, respectively. The implantation energy was 200 keV and the ion doses ranged from $1x10^{14}$ to $9x10^{17}$ cm^{-2}. The implantation profiles determined by AES depth profiling indicate maximum iron concentrations up to 60 at.% for implantation into Al and up to 94 at.% for implantation into Mg. Phase analysis of the implanted layers was performed by conversion electron Mössbauer spectroscopy and XRD analysis. For implantation into Mg, two different kinds of Mössbauer spectra were obtained: at low doses paramagnetic doublets indicating at least two different iron sites and at high doses a dominant ferromagnetic six-line-pattern with a small paramagnetic fraction. The XRD pattern let conclude that in the latter case a dilated α-iron lattice is formed.

For implantation into Al, the Mössbauer spectra were doublet structures very similar to those obtained at amorphous Fe-Al alloys produced by rapid quenching methods. They indicate also at least two different main iron environments. For the highest implanted sample a ferromagnetic six-line-pattern with magnetic field values close to those of Fe_3Al appeared.

W. Matz
F. Prokert
H. Reuther

X-ray diffraction and Mössbauer studies of geological samples and complex compounds

Different samples from natural rocks chlorite type have been analysed for phase composition by X-ray diffraction. The materials were used for solubility or chemical enrichment studies in order to get insight into transport processes of heavy metal compounds in geological formations. The XRD analysis is used to detect structural changes after different treatments. Mössbauer spectroscopy was used for the investigation of iron reduction in the minerals. Crystal structure investigations by XRD was performed to support the development of preparation technology of sodium arsenate hydrate, uranyl arsenate hydrate, barium uranyle phosphate, and calcium uranyl carbonate (Liebigite) in the Institute of Radiochemistry. The X-ray data were used to judge the phase purity of samples. The confirmation of crystallographic data is essential for EXAFS studies to be performed at the compounds.

Collaboration: Institut für Radiochemie, FZ Rossendorf

F.Eichhorn
F. Prokert
*K. Mazur**
*J. Sass**

Roughness studies of wafer materials by X-ray reflectometry

In direct collaboration with industrially oriented research groups X-ray reflectometry (XRR) investigations were performed mainly on Si and $A_{III}B_V$-type semiconductor materials. The studies on unmodified wafers (e.g.Si, GaAs, GaP, $NdGaO_3$, $SrLaAlO_3$), simple layer structures (e.g. Si/SiO_2,Si/SiC)

and multilayers (e.g. Si/nx[W/C]) were aimed to characterize especially the roughness of the surface and interfaces.

The surface roughness of the substrate materials is of special technical interest because it influences the quality of epitaxial layers. XRR measures the roughness contact free and averages over a macroscopic region which is not the case in other methods (e.g. AFM or STM). Significant influence of polishing procedures and type of material on the surface roughness could be observed. The rms-roughness is detectable down to 0.1 nm. It was found, that on wafers the roughness is direction dependent rather than uniform.

Gradient multilayers designed for X-ray optics were studied in respect to the linearity if the lateral gradient of layer thicknesses and homogenity in perpendicular direction. The total reflectivity and the sharpness of the first-order Bragg peak of the superlattice is significantly influenced by the interface roughness.

Collaboration: *Inst.of Electronic Materials Technology, Warsaw; FhG Institut für Werkstoffphysik und Schichttechnologie Dresden; Advanced Micro Devices, Dresden

E.-M. Nicht
G. Brauer
*M. Cieslar**
*P. Vostry**

PAS, electrical resistivity, and microstructural TEM studies of the CuMn system

The annealing behaviour of cold deformed Cu-17at%Mn and Cu-25at%Mn alloys has been investigated by PAS (lifetime, Doppler broadening) and electrical resistivity measurements. Ordering processes and the recovery of crystal lattice defects were revealed. To characterize details of microstruc-tural changes during annealing and to verify the interpretation of PAS and resisti-vity measurements, TEM observations were carried out.

It is shown that resistivity changes in the region between 100 and 250°C annealing are due to the atomic short range ordering (SRO) process, whereas the changes between 250 and 400°C are caused by the destruction of this order. Both the average positron lifetime and S-parameter changes reflect the recovery of deformation-induced vacancies between 100 and 220°C. The decrease in the dislocation density from $3x10^{13}$ m^{-2} (initial state) to $3x10^{12}$ m^{-2} (550°C) was proven by TEM studies and supports the explanation of the second annealing stage of the mean positron lifetime (>400°C) by recovery of dislocations. The increase in S-parameter values in the temperature region >220°C is probably due to the developing of vacancy-like defects connected with the formation of Mn precipitates (misfits) due to the destruction of the atomic SRO.

supported by SMWK

Collaboration: *Charles University, Prague, Czech Republic

T. Gehring,
J. von Borany,
*S. Howitz**

New flow sensor for microfluidic systems

For the detection of flow rates in microfluidic systems a new flow sensor has been developed. The sensor is based on a thin film heater on a SiN bridge surrounded by thin film thermistors. The flow rate can be determined from the fluid temperature difference measured at two ther-mistors, which are arranged at opposite sides of the heater parallel to the flow direction. The new sensor is able to determine continuous flow rates from less than 1 µl/min to 100µl/min as well as single fluid drops (1 nl) with a fast response time below 1 s. The high sensitivity and fast response time is due to the fact, that heater and thermistors are arranged on a free standing SiN membrane on structured silicon, which is incorporated into the microfluidic channel. Therefore a very

low heat capacitance and a direct thermal coupling between the flow sensor and the fluid is realized. The sensor is designed for failure diagnostics of silicon micropumps and the measurement of flow rates in a miniature chemical analysis system based on flow injection analysis.

supported by SMWA

Collaboration: *GeSiM mbH, Technologiezentrum Rossendorf; Institut für Physikalische Hochtechnologien, Jena

Statistics

Publications

Albe, K.,
Theoretical study of boron nitride modifications at hydrostatic pressures,
Phys. Rev. B55 (1997) 6203

Albe, K., Möller, W.,
Modelling of boron nitride: Atomic scale simulations on thin film growth,
Comput. Mat. Sci. 557 (1997) 1

Albe, K., Möller, W., Heinig, K.-H.,
Computer simulation and boron nitride,
Rad. Eff. Def. Sol. 141 (1997) 85

Anwand, W., Brauer, G., Coleman, P.G., Goodyear, A., Reuther, H., Maser, K.,
Investigations of the transition region between Si and thermally grown SiO_2 layers,
J. Phys.: Condens. Matter 9 (1997) 2947

Assmann, W., Huber, H., Mieskes, H.D., Nolte, H., Gazis, E., Kokkoris, M., Kossionidis, S., Vlastou, R., Grötzschel, R., Mücklich, A., Prusseit, W., Karamian, S.A.
Heavy-Ion induced effects in Ge crystal damage at the 100 MeV energy range
Nucl. Instr. Meth. B 122 (1997) 250

Barklie, R.C., Collins, M., Holm, B., Pacaud, Y., Skorupa, W.,
An EPR study of defects induced in 6H-SiC by ion implantation,
J. Electronic Materials 26 (1997) 137

Barradas, N.P., Maas, A.J.H., Mändl, S.,
Comparison of computer generated and ERDA depth profile of oxygen implanted into silicon with plasma immersion ion implantation,
Nucl. Instr. Meth. B124 (1997) 63

Barradas, N.P., Maas, A.J.H., Mändl, S., Günzel, R.,
Alpha-ERDA analysis of the energy distribution of oxygen ions implanted into silicon with plasma immersion ion implantation,
J. Appl. Phys. 81 (1997) 6642

Barradas, N.P., Maas, A.J.H., Mändl, S., Günzel, R.,
Short pulse plasma immersion ion implantation of oxygen into silicon: Determination of the energy distribution,
Surf. Coat. Technol. 93 (1997) 238

Barradas, N.P., Panknin, D., Wieser, E., Schmidt, B., Betzl, M., Mücklich, A., Skorupa, W.,
Influence of the ion irradiation on the properties of β-$FeSi_2$ layers prepared by ion beam assisted deposition,
Nucl. Instr. Meth. B 127 (1997) 316

Beling, C.D., Fung, S., Cheung, S.H., Gong, M., Ling, C.C., Hu, Y.F., Brauer, G.,
Positron mobility in semi-insulating 4H-SiC,
Mat. Sci. Forum 255-257 (1997) 260

Bischoff, L., Teichert, J.,
Application of highly focused ion beams,
Mat. Sci. Forum 248-249 (1997) 445

Bischoff, L., Teichert, J.,
Application of highly focused ion beams,
Proc. 14th Int. Conf. Application of Accelerators in Research and Industry, vol. 392, ed. J.L. Duggan and I. L. Morgan, AIP Press, New York (1997) 1175

Borany, J. von , Grötzschel, R., Heinig, K.-H., Markwitz, A., Matz, W., Schmidt, B., Skorupa, W.,
Multimodal impurity redistribution and nanocluster formation in Ge implanted silicon dioxide films,
Appl. Phys. Lett. 71 (1997) 3215

Borodin, V., Heinig, K.-H., Reiss, S.,
Self-organization in finite precipitate ensembles during coarsening,
Phys. Rev. B56 (1997) 5332

Brauer, G., Anwand, W., Nicht, E.-M., Coleman, P.G., Wagner, N., Wirth, H., Skorupa, W.,
Experimental determination of positronic and electronic characteristics of 3C-SiC,
Appl. Surf. Sci. 116 (1997) 19

Brauer, G., Wendler, W., Büttig, H., Gabriel, F., Gippner, P., Gläser, W., Grosse, E., Guratzsch, H., Dönau, F., Höhnel, G., Janssen, D., Nething, U., Pobell, F., Prade, H., Pröhl, D., Schilling, K.D., Schlenk, R., Seidel, W., Stephan, J., vom Stein, P., Wenzel, M., Wustmann, B., Zahn, R.,
The ELBE radiation source project at the Research Center Rossendorf,
Mat. Sci. Forum 255-257 (1997) 732

Brenscheidt, F., Wieser, E., Matz, W., Mücklich, A., Möller, W.,
Tribological properties of chromium implanted silicon nitride ceramics correlated with microstructure,
Appl. Phys. A65 (1997) 281

Brenscheidt, F., Matz, W., Wieser, E., Möller, W.,
Annealing studies of chromium-implanted silicon nitride ceramics,
Nucl. Instr. Meth. B127/128 (1997) 677

Brenscheidt, F., Oswald, S., Mücklich, A., Wieser, E., Möller, W.,
Wear mechanisms in titanium implanted silicon nitride ceramics,
Nucl. Instr. Meth. B129 (1997) 483

Brenscheidt, F., Mändl, S., Günzel, R., Wieser, E., Möller, W., Fischer, W., Herrmann, M., Tribological Properties of Silicon Nitride Ceramics Modified by Titanium and Subsequent Oxygen Implantation,
Surf. Coat. Technol. 97 (1997) 675

Brutscher, J., Günzel, R., Möller, W.,
Plasma immersion ion implantation using pulsed plasma with D.C. and pulsed high voltages,
Surf. Coat. Technol. 93 (1997) 197

Chudoba, T., Zschiesche, R., Uhlmann, K.,
Modifizierung von Polymeroberflächen durch Ionenimplantation,
JOT 37 (1997) VI-VIII

Deshkovskaya, A.A., Richter, E.,
Wear improvement of silicate glass surfaces by ion implantation,
Surf. Coat. Technol. 93 (1997) 150

Dvurechenskii, A., Zinovyev, Markov, V., Grötzschel, R., Heinig, K.-H.,
Effects of pulse-irradiation by low-energy ions during homoepitaxy of silicon from a molecular beam,
JETP Letter 64 (1996) 242

Eichhorn, F., Podurets, K.M., Shilstein, S.S.,
Diffuse scattering of neutrons in thermally oxidized silicon,
Physica B 229 (1997) 128

Eremin, V., Ivanov, A., Verbitskaya, E., Li, Z., Schmidt, B.,
Long term instabilities in the defect assembly in irradiated high resistivity silicon detectors,
IEEE Trans. Nucl. Sci. 44 (1997) 819

Fichtner, P.F.P., Kaschny, J. R., Yankov, R.A., Mücklich, A., Kreißig, U., Skorupa, W.,
Overpressurized bubbles versus voids in helium implanted and annealed silicon,
Appl.Phys.Lett. 70 (1997) 732

Friedrich, M., Sun, G., Grötzschel, R., Behrisch, R., Garcia-Rosales, C., Roberts, M. L.,
Tritium depth profiling in carbon by accelerator mass spectrometry,
Nucl. Instr. Meth. B123 (1997) 410

Fukarek, W., Kruse, O., Kolitsch, A., Möller, W.,
Investigations on the structure of boron nitride films,
Thin Solid Films 308-309 (1997) 38

Fukarek, W., Möller, W., Hatzopoulos, N., Armour, D.G., van den Berg, J.A.,
Ellipsometric investigation of damage distribution in low energy boron implantation of silicon,
Nucl. Instr. Meth. B127/128 (1997) 879

Grigull, S., Jacob, W., Henke, D., Mücklich, A., Spaeth, Ch., Sümmchen, L.,
On the presence of molecular nitrogen in nitrogen-implanted amorphous carbon,
Appl. Phys. Lett. 70 (1997) 1387

Günzel, R., Brutscher, J., Mändl, S., Möller, W.,
The use of plasma source ion implantation for wear protection,
in: Protective Coatings and Thin Films, eds. Y. Pauleau and P.B. Barna (Kluwer, Dordrecht, 1997), p. 635

Günzel, R., Brutscher, J., Mändl, S., Möller, W.,
Utilization of plasma source ion implantation for tribological applications,
Surf. Coat. Technol. 96 (1997) 16

Hatzopoulos, N., Siapkas, D.I., Hemment, P.L.F.,Skorupa, W.,
Formation and characterisation of Si/SiO_2 multilayer structures by oxygen implantation into silicon,
J. Appl. Phys. 80 (1997) 4960

Hatzopoulos, N., Suder, S., van den Berg, J., Donelly, S.E., Armour, D.G., Panknin, D., Fukarek, W., Frey, L., Foad, M.A., Moffat, S., Bailey, P., Naakes, C.T.Q.,
Range and damage distribution in ultra low energy boron ion implantation,
Proc. 11th Int. Conf. Ion Implantation Techology, eds.: E.Ishidida, S.Banerjee, S.Mehta, T.C.Smith, M.I.Current, L.Larson, A.Tasch, T.Romig; The Institute of Electrical and Electronics Engineers, Piscataway, USA, 1997, IEEE Publications 96TH8182 p.527

Heera, V., Prokert, F., Schell, N., Seifarth, H., Fukarek, W., Voelskow, M., Skorupa, W.,
Density and structural changes in SiC after amorphization and annealing,
Appl. Phys. Lett. 70 (1997) 3531

Heera,V.,Skorupa, W.,
Ion implantation and annealing effects in silicon carbide,
MRS Symp. Proc. 438 (1997) 241

Hempelmann, R., Eschenbaum, J., Altmayer, M., Groß, B., Grambole, D., Herrmann, F., Nagengast, D., Krauser, J., Weidinger, A.,
Pressure/composition isotherms of prodon conducting $SrYb_{0.05}Zr_{0.95}O_{2.975}/H_2O$ by means of nuclear resonance reaction analysis,
Ber. Bunsenges. Phys. Chemie 101 (1997) 985

Henkel, T., Heera, V., Kögler, R., Skorupa, W., Seibt, M.,
The kinetics of the ion-beam-induced interfacial amorphization in silicon,
J. Appl. Phys. 82 (1997) 5360

Huber, H., Assmann, W., Grötzschel, R., Mieskes, H.D., Mücklich, A., Nolte, H., Prusseit, W.,
Void formation and surface rippling in Ge induced by high energetic Au irradiation,
Mat. Sci. Forum 248/249 (1997) 301

Huber, H., Assmann, W., Karamian, S.A., Mücklich, A., Prusseit, W., Gazis, E., Grötzschel, R., Kokkoris, M., Kossiomidis, E., Mieskes, H.D., Vlaston, R.,
Void formation in Ge induced by high energy heavy ion irradiation,
Nucl. Instr. Meth. B122 (1997) 542

Jentschel, M., Heinig, K.-H., Börner, H., Doll, C.,
Crystal-GRID investigations of atomic collision cascades in ionic compounds,
Mat. Sci. Forum 248-249 (1997) 49

Kachurin, G.A. , Tyschenko, I.E., Skorupa, W., Yankov, R.A., Zhuravlev, K.S., Pazdnikov, N.A., Volodin, V.A., Gutakovskii, A.G., Leier, A.F.,
Photo-luminescence from SiO_2 layers implanted with Si^+ and annealed in a pulse regime,
Phys. Techn. Semicond. 31/No 6 (1997) 730 (in Russian)
(English version - G.A. Kachurin et al., Semicond. 31/No 6 (1997) 626)

Kachurin, G. A., Tyschenko, I.E., Zhuravlev, K.S., Pazdnikov, N.A., Volodin, V.A., Gutakovsky, A.K., Leier, A.F., Skorupa, W., Yankov, R. A.,
Visible and near-infrared luminescence from Si nanostructures formed by ion implantation and pulse annealing,
Nucl. Instr. Meth. B122 (1997) 571

Kachurin, G.A., Zhuravlev, K.S., Pazdnikov, N.A., Leyer, A.F., Tyschenko, I.E., Volodin, V.A., Skorupa, W., Yankov, R.A.,
Annealing effects in light emitting Si nanostructures formed in SiO_2 by ion implantation and transient preheating,
Nucl. Instr. Meth. B127/128 (1997) 583

Kalitzova, M., Simov, S., Yankov, R. A., Angelov, C., Vitali, G., Rossi, M., Pizzuto, C., Zollo, G., Fauré, J., Killian, K., Bonhomme, P., Voelskow, M.,
Amorphization and crystallization effects in high-dose zinc-implanted silicon,
J. Appl. Phys. 81 (1997) 1143

Kaschny, J.R., Mücklich, A., Kreißig, U., Yankov, R.A., Kögler, R., Skorupa, W., Fichtner, P.F.P., Danilin, A.B.,
Helium induced cavities in silicon: their formation, microstructure and gettering ability,
MRS Conf. Proc. 469 (1997) 321

Kögler, R., Kaschny, J.R., Yankov, R.A., Werner, P., Danilin, A.B., Skorupa, W.,
Metal gettering by defective regions in carbon-implanted silicon,
Solid State Phenomena 57/58 (1997) 63

Kögler, R., Panknin, D., Werner, P., Danilin, A.B., Skorupa, W.,
Impurity gettering in damaged regions of Si produced by high energy ion implantation,
Proc. 11th Int. Conf. Ion Implantation Techology, eds.: E.Ishidida, S.Banerjee, S.Mehta, T.C.Smith, M.I.Current, L.Larson, A.Tasch, T.Romig; The Institute of Electrical and Electronics Engineers, Piscataway, USA, 1997, IEEE Publications 96TH8182 p. 679

Kögler, R., Posselt, M., Yankov, R.A., Kaschny, J.R., Werner, P., Danilin, A.B., Skorupa, W.,
Detection of metastable defective regions in ion-implanted Si by means of metal gettering,
MRS Conf. Proc. 469 (1997) 224

Kögler, R., Reuther, H., Voelskow, M., Skorupa, W., Romano-Rodriguez, A., Perez-Rodriguez, A., Serre, C., Calvo-Barrio, L., Morante, J.R.,
Ion beam synthesis of SiC in silicon-on-insulator,
Proc. 11th Int. Conf. Ion Implantation Techology, eds.: E.Ishidida, S.Banerjee, S.Mehta, T.C.Smith, M.I.Current, L.Larson, A.Tasch, T.Romig; The Institute of Electrical and Electronics Engineers, Piscataway, USA, 1997,IEEE Publications 96TH8182 p. 709

Korzec, D., Raiko, V., Engemann, J., Günzel, R., Brutscher, J., Möller, W.,
Application of the ECR slot antenna plasma source for ion implantation,
Surf. Coat. Technol. 93 (1997) 217

Kruijer, S., Keune, W., Dobler, M., Reuther, H.,
Depth analysis of phase formation in Si after high-dose Fe ion implantation by depth-selective conversion-electron Mössbauer spectroscopy,
Appl. Phys. Lett. 70 (1997) 2696

Lossy, R., Reichert, W., Obermeier, E., Skorupa, W.,
Doping of 3C-SiC by implantation of nitrogen at high temperatures,
J. Electronic Materials 26 (1997) 123

Mändl, S., Barradas, N.P., Brutscher, J., Günzel, R., Möller, W.,
Comparison of measured and calculated dose for plasma source ion implantation in 3-D objects,
Nucl. Instr. Meth. B127/128 (1997) 996

Mändl, S., Reuther, H., Brutscher, J., Günzel, R., Möller, W.,
Measured and calculated dose distribution for 2D-plasma immersion ion implantation,
Surf. Coat. Technol. 93 (1997) 229

Mändl, S., Brutscher, J., Günzel, R., Möller, W.,
Ion energy distribution in plasma immersion ion implantation,
Surf. Coat. Technol. 93 (1997) 234

Mazur, K., Fink-Finowicki, J., Berkowski, M., Schell, N.,
Defects in detwinned $LaGaO_3$ substrates,
Acta Physica Polonica A92 (1997) 205

Mazur, K., Sass, J., Giersz, W., Schell, N.,
X-ray diffraction investigations of $NdGaO_3$ single crystals,
Acta Physica Polonica A92 (1997) 226

Möller, D., Pham, M.T., Hüller, J.,
Sensitization of silicon nitride surfaces for Ag^+ ions by ion implantation,
Sensors and Actuators B43 (1997) 110

Möller, W.,
Computer simulation of ion-assisted thin film deposition,
Radiat. Eff. Def. Sol. 141 (1997) 73

Möller, W., Günzel, R., Mändl, S., Richter, E.,
Plasma-Immersions-Ionenimplantation für große Oberflächen,
JOT 37 (1997) II-IV

Murthy, C.S., Posselt, M., Feudel, T.,
Physically-based modeling of 2d and 3d implantation profiles: influence of damage accumulation,
Proc. of the 4th International Workshop on the Measurement, Characterization and Modeling of Ultra-Shallow Doping Profiles in Semiconductors,
M. Current, M. Kump, G. McGuire (eds.), Research Triangle Park, USA, April 1997, p.48.1

Nakamura, K., Mändl, S., Brutscher, J., Günzel, R., Möller, W.,
Development of a new technique for high-energy secondary-electron measurements in plasma immersion ion implantation,
Plasma Sources Sci. Technol. 6 (1997) 86

Nakamura, K., Mändl, S., Brutscher, J., Günzel, R., Möller, W.,
Incident ion monitoring during plasma immersion ion implantation by direct measurements of high-energy secondary electrons,
Surf. Coat. Technol. 93 (1997) 242

Nangia, A., Kim, J.H., Weiss, A.H., Brauer, G.,
Experimental determination of positron related surface characteristics of 6H-SiC,
Mat. Sci. Forum 255-257 (1997) 711

Neelmeijer, C., Mäder, M., Wagner, W., Schramm, H.-P.,
Layered artefacts: Non-destructive characterization by PIXE and RBS,
in: Optical Technologies in the Humanities, OWLS IV, ed. by D. Dirksen, G. von Bally, Springer, (1997) 105

Nicht, E.-M., Brauer, G., Cieslar, M., Vostry, P.,
Positron annihilation spectroscopy, electrical resistivity, and microstructural transmission electron microscopy studies of the CuMn system,
Mat. Sci. Forum 255-257 (1997) 572

Nicht, E.-M., Brauer, G., Vostry, P., Cieslar, M., Blazek, P.,
Electrical resistivity and positron lifetime studies of the Cu-Mn system,
Nukleonika 42 (1997) 175

Noll, K., Döbeli, M., Tobler, L., Grambole, D., Krähenbühl, U.,
Fluorine profiles in achondrites and chondrites from antarctica by nuclear reaction analysis (NRA),
Meteorites and Planet Sci. 32 (1997) A101

Nomura, N., Shiozawa, H., Takada, T., Reuther, H., Richter, E.,
Gas-sensor properties of SnO_2 films implanted with gold and iron ions,
J. Mat. Sci.: Materials in Electronics 8 (1997) 301

Pacaud, Y., Heera, V., Yankov, R.A., Kögler, R., Brauer, G., Voelskow, M., Skorupa, W.,
Damage behaviour and annealing of germanium implanted 6H-SiC,
Proc. 11th Int. Conf. Ion Implantation Techology, eds.: E.Ishidida, S.Banerjee, S.Mehta, T.C.Smith, M.I.Current, L.Larson, A.Tasch, T.Romig; The Institute of Electrical and Electronics Engineers, Piscataway, USA, 1997, IEEE Publications 96TH8182 p. 713

Palard, M., Ruault, M.-O., Bernas, H., Strobel, M., Heinig, K.-H.,
In-situ TEM study of the evolution of $CoSi_2$ precipitates during annealing and ion irradiation,
Proc. of the Royal Microscopical Society Conference "Microscopy of Semiconducting Materials 1997", A.G. Cullis and J.L. Hutchison (eds.), Inst. Phys. Conf. Ser. 157 (1997) 501

Pham, M.T., Matz, W., Seifarth, H.,
Surface roughness with nanometer-scale Ag particles generated by ion implantation,
Analytica Chemica Acta 350 (1997) 209

Plass, M.F., Fukarek, W., Kolitsch, A., Möller, W.,
Growth and characterization of boron nitride films: layer sequence and phase identification,
Diam. Relat. Mater. 6 (1997) 594

Plass, M.F., Fukarek, W., Kolitsch, A., Möller, W.,
Layered structure diagnostic and optical modelling of c-BN films,
Nucl. Instr. Meth. B127/128 (1997) 857

Plass, M.F., Fukarek, W., Kolitsch, A., Schell, N., Möller, W.,
Layered growth of boron nitride films,
Thin Solid Films 305 (1997) 172

Posselt, M., Schmidt, B., Murthy, C.S., Feudel, T., Suzuki, K.,
Modeling of damage accumulation during ion implantation into single-crystalline silicon,
J. Electrochem. Soc. 144 (1997) 1495

Rebohle, L., von Borany, J., Yankov, R.A., Skorupa, W., Tyschenko, I.E., Fröb, H., Leo, K.,
Strong blue and violet photoluminescence and electro-luminescence from germanium-implanted and silicon-implanted silicon-dioxide films,
Appl. Phys. Lett. 71 (1997) 2809

Rebohle, L., Tyschenko, I.E., Fröb, H., Leo, K., Yankov, R.A., von Borany, J., Kachurin, G.A., Skorupa, W.,
Blue and violet photoluminescence from high-dose Si^+- and Ge^+-implanted silicon dioxide layers,
Microelectr. Eng. 36 (1997) 107

Reichert, W., Lossy, R., Gonzalez Sirgo, M., Obermeier, E., Skorupa, W.,
Investigation of the effects of high temperature implantation and post implantation annealing on the electrical behaviour of nitrogen implanted β-SiC films,
Diam. Relat. Mater. 6 (1997) 1445

Richter, E., Günzel, R.,
Härten von Edelstahl durch Stickstoff-Plasma-Immersions-Ionenimplantation,
Ingenieur-Werkstoffe 6 (1997) 44

Romano-Rodriguez, A., Perez-Rodriguez, A., Serre, C., Calvo-Barrio, L., Bachrouri, A., Gonzales-Varona, O., Morante, J.R., Kögler, R., Skorupa, W.,
TEM characterisation of carbon ion implantation into epitaxial $Si_{1-x}Ge_x$,
Inst. Phys. Conf. Ser. 157 (1997) 419

Šaroun, J., Eichhorn, F., Hempel, A., Lukas, P., Kolman, B., Neufuss, K., Mikula, P., Strunz, P.,
SANS investigation of plasma-sprayed materials using double-crystal diffractometer,
Physica B234-236 (1997) 1011

Schmidt, B., Bischoff, L., Teichert, J.,
Writing FIB implantation and subsequent anisotropic wet chemical etching for fabrication of 3D structures in silicon,
Sensors and Actuators A61 (1997) 369

Schmidt, B., Nitzsche, P., Lange, K., Grigull, S., Kreissig, U.,
In-situ investigation of ion drift processes in glass during anodic bonding,
Proc. of EUROSENSORS XI, The 11th European Conference on Solid-State Transducers, September 21-24, 1997, Warsaw, Poland (Ed. R. S. Jachowicz), vol. 3, 1365

Schroer, E., Hopfe, S., Tong, Q.-Y., Gösele, U., Skorupa, W.,
Growth of buried oxide layers of SOI-structures by thermal oxidation of the top silicon layer,
J. Electrochem. Soc. 144 (1997) 2205

Serre, C., Perez-Rodriguez, A., Romano-Rodriguez, A., Calvo-Barrio, L., Morante, J.R., Esteve, J., Acero, M.C., Skorupa, W., Kögler, R.,
Synthesis of SiC microstructures in Si technology by high dose carbon implantation: Etch stop properties,
J. Electrochem. Soc. 144 (1997) 2211

Simoen, E., Vanhellemont, J., Alaerts, A., Claeys, C., Gaubas, E., Kaniava, A., Ohyama, H., Sunaga, H., Nashiyama, I., Skorupa, W.,
Proton irradiation effects in silicon devices,
Proc. of the 7.Int.Symp. on "Recent progress in Accelerator Beam Applications", Takasaki, Japan, JAERI-Conf.97-003, p.224

Simoen, E., Vanhellemont, J., Alaerts, A., Claeys, C., Gaubas, E., Kaniava, A., Ohyama, H., Sunaga, H., Nashiyama, I., Skorupa, W.,
Proton irradiation effects in silicon junction diodes and charge-coupled devices,
Radiation Phys.Chem. 50 (1997) 417

Skorupa, W., Yankov, R.A., Hatzopoulos, N., Danilin, A.B.,
Proximity gettering of iron in SIMOX wafers,
Proc. 11th Int. Conf. Ion Implantation Techology, eds.: E.Ishidida, S.Banerjee, S.Mehta, T.C.Smith, M.I.Current, L.Larson, A.Tasch, T.Romig; The Institute of Electrical and Electronics Engineers, Piscataway, USA, 1997,IEEE Publications 96TH8182 p.737

Spaeth, M., Kühn, M., Kreissig, U., Richter, F.,
Preparation of CNx films by ion beam assisted filtered cathodic arc deposition,
Diamond and Rel. Mat. 6 (1997) 626

Spieß, L., Nennewitz, O., Weishart, H., Lindner, J., Skorupa, W., Romanus, H., Erler, F., Petzoldt, J.,
Aluminium implantation of p-SiC for ohmic contacts,
Diamond and Rel. Mat. 6 (1997) 1414

Strobel, M., Reiss, S., Heinig, K.-H., Möller, W.,
Computer simulation of precipitate coarsening: a unified treatment of diffusion and reaction controlled Ostwald ripening,
Rad. Eff. Def. Sol. 142 (1997) 99

Sun, G., Friedrich, M., Grötzschel, R., Bürger, W., Behrisch, R., Garcia-Rosales, C.,
Quantitative AMS depth profiling of the hydrogen isotopes collected in divertor and wall tiles of the tokamak ASDEX upgrade,
J. Nucl. Mat. 246 (1997) 9

Teichert, J., Bischoff, L., Hausmann, S.,
Fabrication of MSM detector structures on silicon by focused ion beam implantation,
Microelectronic Engineering 35 (1997) 455

Teichert, J., Bischoff, L., Köhler, B.,
Study of the ion-acoustic effect using focused ion beams,
MRS Symp. Proc. 438 (1997) 555

Tyschenko, I.E., Kachurin, G.A., Zhuravliov, K.S., Pazdnikov, N.A., Volodin, V.A., Gutakovsky, A.K., Leier, A.F., Fröb, H., Leo, K., Böhme, T., Rebohle, L., Yankov, R.A., Skorupa, W.,
Quantum-sized silicon precipitates in silicon-implanted and pulse-annealed silicon-dioxide films: photo-luminescence and structural transformations,
MRS Symp. Proc. 438 (1997) 453

Verbitskaya, E. M., Eremin, V. K., Ivanov, A. M., Li, Z., Schmidt, B.,
Formation of radiation defects in high-resistivity silicon as a result of cyclic irradiation and annealing,
Semiconductors 31 (1997) 189

Verbitskaya, E. M., Eremin, V. K., Ivanov, A. M., Li, Z., Schmidt, B.,
Generation of radiation defects in high resistivity silicon at cyclic irradiation and annealing,
Fisika i Tekhnika Poluprovodnikov 31 (1997) 235

Wang, X., Kolitsch, A., Möller, W.,
Roughness improvement and hardness enhancement in nanoscale Al/AlN multilayered thin films,
Appl. Phys. Lett. 71 (1997) 1951

Weise, G., Mattern, N., Hermann, H., Teresiak, A., Bächer, I. Brückner, W., Bauer, H.-D., Vinzelberg, H., Reiss, G., Kreissig, U., Mäder, M., Markschläger, P.,
Preparation, structure and properties of MoS_x films,
Thin Solid Films 298 (1997) 98

Weishart, H., Heera, V., Matz, W., Skorupa, W.,
Ion beam assisted deposition of a tungsten compound layer on 6H-silicon carbide,
Diam. Relat. Mater. 6 (1997) 1432

Weishart, H., Schöneich, J., Voelskow, M., Skorupa, W.,
Ion beam synthesis by high dose tungsten implantation into 6H-SiC,
MRS Symp. Proc. 438 (1997) 283

Werner, P., Eichler, S., Mariani, G., Kögler, R., Skorupa, W.,
TEM investigation of CxSi defects in C implanted silicon,
Appl. Phys. Lett. 70 (1997) 252

Werner, P., Kögler, R., Eichler, D., Skorupa, W.,
TEM investigation of C-Si defects in Carbon-implanted Silicon,
Proc. 11th Int. Conf. Ion Implantation Techology, eds.: E.Ishidida, S.Banerjee, S.Mehta, T.C.Smith, M.I.Current, L.Larson, A.Tasch, T.Romig; The Institute of Electrical and Electronics Engineers, Piscataway, USA, 1997, IEEE Publications 96TH8182 p. 675

Wieser, E., Panknin, D., Barradas, N. P., Betzl, M., Reuther, H., Henrion, W., Lange, H.,
Formation of ternary $(Fe_{1-x}Co_x)Fe_2$ structures by ion beam assisted deposition and ion implantation,
Nucl. Instr. Meth. B124 (1997) 533

Yankov, R.A., Hatzopoulos, N., Fukarek, W., Heera, V., Voelskov, M., Pezoldt, J., Skorupa, W.,
Formation of $(SiC)_{1-x}(AlN)_x$ layers in 6H-SiC using ion-beam synthesis,
MRS Symp. Proc. 438 (1997) 271

Yankov, R.A., Kaschny, J.R., Fichtner, P.F.P., Mücklich, A., Kreißig, U., Skorupa, W.,
Impurity gettering effects in separation-by-implanted-oxygen (SIMOX) wafers: what getters what, where and how?
Microelectr. Eng. 36 (1997) 129

Yankov, R.A., Voelskow, M., Kreißig, U., Kulikov, D.V., Pezoldt, J., Skorupa, W., Truschin, Y.V., Kharlamov, V.S., Tsigankov, D.N.,
Computer-simulation and RBS/C studies of high-dose N^+ and Al^+ co-implantation in 6H-SiC,
Techn. Phys. Lett. 23 (1997) 617
(Russian version - Pis'ma v ZhTF 23(No 16) (1997) 6)

Conference Contributions

Albe, K., Möller, W. ,
Computersimulationen zur Schichtabscheidung von Bornitrid,
Frühjahrstagung der DPG, AK: Festkörperphysik, FB: Dünne Schichten,
Münster, Germany, March 17-21, 1997

Albe, K., Möller, W.,
Modelling of boron nitride: atomic scale simulations on thin film growth,
E-MRS Spring Meeting, Symp. D: Computational Modeling of Issues in Materials Science,
Strasbourg, France, June 16-20, 1997

Albe, K., Möller, W., (invited)
Molecular-dynamics simulations on boron nitride thin film deposition,
10th Int. Conference on Surface Modification of Metals by Ion Beams,
Gatlinburg, USA, September 22-26, 1997

Albe, K., Posselt, M., Möller, W.,
Atomic scale simulations based on classical molecular-dynamics and ab initio-methods: advantageous tools for understanding growth and properties of boron nitride,
Int. Workshop on Challenges in Predictive Process Simulation (ChiPPS '97), Wandlitz, Germany,
Aug. 17-20, 1997

Antons, A., Heinig, K.-H., Mantl, S.,
Process simulation of sub-μm pattern formation by local oxidation of $CoSi_2$/Si heterostructures,
Int. Workshop on Challenges in Predictive Process Simulation (ChiPPS '97), Wandlitz, Germany,
Aug. 17-20, 1997

Anwand, W., Brauer, G., Skorupa, W., Coleman, P.G.,
Characterization of vacancy-type defects in ion implanted and annealed SiC by positron annihilation spectroscopy,
MRS Fall Meeting, Boston, MA, USA, Dec. 1 - 5, 1997

Anwand, W., Parascandola, S., Richter, E., Brauer, G., Coleman, P.G., Möller, W.,
Positron implanatation spectroscopy of high-current, low-energy nitrogen implanted austenitic stainless steel,
13th Int. Conf. on Ion Beam Analysis (IBA-13), Lisboa, Portugal, July 1997

Anwand, W., Parascandola, S., Richter, E., Brauer, G., Coleman, P.G., Möller, W.,
Analysis of deuterium induced nuclear reactions giving criteria for the formation process of expanded austenite,
13th Int. Conf. on Ion Beam Analysis (IBA-13), Lisboa, Portugal, July 1997

Behrisch, R., Grigull, S., Kreissig, U., Grötzschel, R.,
Influence of surface roughness on measuring depth profiles and the total amount of implanted ions by RBS and ERDA,
13th Int. Conf. on Ion Beam Analysis (IBA-13), Lisboa, Portugal, Aug. 1997

Beling, C.D., Fung, S., Cheung, S.H., Ling, C.C., Brauer, G.,
Positron mobility in semi-insulating 4H-SiC,
11th Int. Conf. on Positron Annihilation (ICPA-11), Kansas City, USA, May 25-30, 1997

Bischoff, L.,
Maskenlose schreibende Ionenimplantation mit massensepatiertem FIB,
19. Deutsches Nutzertreffen Ionenimplanation, Robert-Bosch GmbH, Reutlingen, April 24 - 25, 1997

Bischoff, L., Hausmann, S., Teichert, J., Borany, J. v.,
Mikro- und Nanostrukturierung mit Ionenfeinstrahlen,
Messe Technologie-Dialog Mikrosystemtechnik/Neue Materialien, Gera, April 9, 1997

Bischoff, L., Hausmann, S., Teichert, J., Borany, J. v.,
Mikro- und Nanostrukturierung mit Ionenfeinstrahlen,
Hannover Messe, April 1997

Bischoff, L., Hausmann, S., Teichert, J., Borany, J. v.,
Mikro- und Nanostrukturierung mit Ionenfeinstrahlen,
Forschungsforum '97, Leipzig, Sept. 20, 1997

Borany, J.von, Grötzschel, R., Heinig, K.-H., Markwitz, A., Möller, W., Rebohle, L., Schmidt, B., Skorupa, W.,
Photo-and electroluminescence from Ge implanted SiO_2 films,
Gordon Conference, New Hampshire, USA, August 1997

Borany, J. von, Grötzschel, R., Heinig, K.-H., Markwitz, A., Matz, W., Möller, W., Rebohle, L., Schmidt, B., Skorupa, W.,
Strong Blue Photo- and Electroluminescence from Ge implanted SiO_2 films,
Herbstschule Elektronenmikroskopie, Halle, Sept. 20 - 25, 1997

Brauer, G., Wendler, W., Büttig, H., Gabriel, F., Gippner, P., Gläser, W., Grosse, E., Guratzsch, H., Dönau, F., Höhnel, G., Janssen, D., Nething, U., Pobell, F., Prade, H., Pröhl, D., Schilling, K.D., Schlenk, R., Seidel, W., Stephan, J., vom Stein, P., Wenzel, M., Wustmann, B., Zahn, R.,
The ELBE radiation source project at the Research Center Rossendorf,
11th Int. Conf. on Positron Annihilation (ICPA-11), Kansas City, USA, May 25-30, 1997

Brenscheidt, F., Piekoszewski, J., Wieser, E., Langner, J., Grötzschel, R., Reuther, H.,
Modification of silicin nitride ceramics with high intensity pulsed ion beams,
Modification of Ceramics and Semiconductors by Ion Bombardment, Ciocco, Italy,
May 19-23, 1997

Brückner, J., Günzel, R., Richter, E., Möller, W.,
Metal plasma immersion ion implantation and deposition: chromium on magnesium,
SMMIB 97, Gatlinburg, TE, USA, Sept. 1997

Brückner, J., Günzel, R.,
Metall-Plasmaimmersions-Ionenimplantation und –abscheidung (MPIIID),
8. Bundesdeutsche Fachtagung Plasmatechnologie, Dresden, Sept. 14 - 17, 1997

Bürger, W., Friedrich, M., Turuc, S.,
Developments at the Rossendorf electrostatic accelerators,
31st SNEAP Symposium, Jülich, Oct. 13 . 15, 1997

Deshkovskaya, A.A., Richter, E., Komar, V., Skornyakov, I.,
Investigation of phase formation and liquidation in glass layers produced by ion beam synthesis,
VITT Minsk, Belarus, Sept. 1997

Deshkovskaya, A.A., Richter, E.,
Swelling and surface profil of glass surfaces after ion bombardment,
VITT Minsk, Belarus, Sept. 1997

Dobler, M., Reuther, H., Möller, W.,
CEMS- und AES-Untersuchungen an Eisensiliziden,
DPG-Frühjahrstagung, Münster, March 17 - 21, 1997

Dobler, M., Reuther, H., Betzl, M., Möller, W.,
Phase formation of iron silicides during ion beam synthesis,
Int. Conf. Appl. Mössbauer Effect, Rio de Janeiro, Sept. 14 - 20, 1997

Eichhorn, F., Mazur, K., Sass, J.,
X-ray scattering characterization of Si implanted with MeV Ge ions,
3th Autumn School on "X-ray scattering from surfaces and thin layers", Smolenice, Slovakia,
Oct. 1 - 4, 1997

Fichtner, P.F.P., Kaschny, J.R., Kling, A., Trinkaus, H., Yankov, R.A., Mücklich, A., Skorupa, W.,
Zawislak, F.C., Amaral, L., da Silva, M.F., Soares, J.C.,
Nucleation and growth of platelet bubble structures in helium implanted silicon,
13th Int. Conf. on Ion Beam Analysis (IBA-13), Lisboa, Portugal, July 27 - Aug 1, 1997

Friedrich, M., Bürger, W., Turuc, S.,
Operation and developments at the Rossendorf electrostatic accelerators,
12th Int. Conf. on Electrostatic Accelerators, Obninsk, Russia, Nov. 25 - 28, 1997

Fukarek, W.,
Simultaneous in situ ellipsometry and elastic recoil detection analysis during plasma processing,
ICSE-2, Charleston 1997

Fukarek, W., Kruse, O., Kolitsch, A.,
Untersuchungen zur Struktur von Bornitridschichten,
4. c-BN-Expertentreffen, Reichenau, June 23 - 24, 1997

Fukarek, W., Kruse, O., Kolitsch, A., Möller, W.,
Investigations on the structure of boron nitride films,
ICMCTF 97, San Diego, USA

Ganetsos, T., Mair, G.L.R., Teichert, J., Bischoff, L., Aidinis, C.,
Ion implantation of Ge in Si, characterization in $Si_{1-x}Ge_x$ structures,
XIIIrd Greek Conf. in Solid State Physics, Thessaloninki, Greece, Sept. 1997

Günzel, R., Möller, W., Parascandola, S., Richter, E.,
Diffusion behaviour, outgasing and absorption of nitrogen during plasma immersion ion implantation of stainless steel,
AEPSE '97, Seoul, Korea, Oct. 5-9, 1997

Günzel, R., Betzl, M., Alphonsa, I., Ganguly, B., John, P. I., Mukherjee, S.,
Plasma source ion implantation compared with glow discharge plasma nitriding of stainless steel,
AEPSE '97, Seoul, Korea, Oct. 5-9, 1997

Hausmann, S., Bischoff, L., Teichert, J., Grambole, D., Hermann, F., Möller, W.,
Investigation of dwell-time effects on the cobalt disilicide formation using focused ion beam implantation,
Int. Conf. Micro- and Nano-Engineering, MNE '97, Athens, Greece, Sept. 15 - 18, 1997

Hausmann, S., Bischoff, L., Teichert, J., Herrmann, F., Grambole, D.,
Co-Implantation in Si(111) bei Stromdichten größer 1 A/cm^2,
DPG-Frühjahrstagung, Münster, March 17 - 21, 1997

Heinig, K.-H., (invited)
Precipitation of nanoclusters with ion beam synthesis,
Gordon Research Conference "Materials Processing far from Equilibrium", Meriden , USA,
Aug. 17-22, 1997

Heinig, K.-H., (invited)
Fundamentals of ion beam synthesis of nanoclusters and buried layers,
European Conference on Accelerators in Applied Research and Technology (ECAART5),
Eindhoven, The Netherlands, Aug. 26-30, 1997

Heinig, K.-H., Strobel, M.,
Kinetic 3D lattice Monte-Carlo simulation of phase transformations at ion beam synthesis of nanoclusters,
E-MRS Spring Meeting, Strasbourg, France, June 16 - 20, 1997

Heinig, K.-H., Reiss, S., Strobel, M., Möller, W., (invited)
Ionenstrahlsynthese von Nanoclustern und Schichten: Kinetik von Keimbildung, Wachstum und Ostwald-Reifen,
Frühjahrstagung der DPG, Münster, Germany, March 17-21, 1997

Heinig, K.-H., Schmidt, B., Grötzschel, R., Markwitz, A., von Borany, J., Strobel, M.,
Self-organized Ge nanocrystals produced in SiO_2 layers by ion beam synthesis,
MRS Fall Meeting, Boston, USA, Dec. 1-5, 1997

Heinig, K.-H., Strobel, M., Palard, M., Schmidt, B., Grötzschel, R., Markwitz, A.,
Predictive simulations of high-dose ion implantation,
Int. Workshop on Challenges in Predictive Process Simulation (ChiPPS '97), Wandlitz, Germany,
Aug. 17-20, 1997

Heinig, K.-H., Strobel, M., Schmidt, B. ,
Phase transformations during ion beam synthesis: computational approaches to the kinetics of nucleation, growth, Ostwald ripening and coalescence,
MRS Fall Meeting, Boston, USA, Dec. 1-5, 1997

Hermann, S., Mahnke, H.-E., Spellmeyer, B., Wienecke, M., Reinhold, B., Yankov, R.A., Gumlich, H.-E.,
Pd defect complexes in ZnTe and CdTe and their interaction with group-V elements,
Int. Conf. on II-VI Compound Semiconductors, Grenoble, France, August 1997

Hilke R., Mändl, S.,
Increased tool cutting life of drills by ion implantation,
8th Int. Symp. Danube Adria Assoc. for Automation & Manufacturing, Dubrovnik, Croatia,
Oct. 23 – 25, 1997

Jäger, H.U., Weiler, M.,
Molecular-dynamics studies of a-C:H film growth by energetic hydrocarbon molecule impact,
8th European Conference on Diamond, Diamond-Like and Related Materials, Edinburgh, UK,
Aug. 3-8, 1997

Jankuhn, S., Butz, T., Flagmeyer, R.-H., Reinert, T., Vogt, J., Barckhausen, B., Hammerl, J., Protsch von Zieten, R., Grambole, D., Herrmann, F., Bethge, K.,
Ion microprobe analyses of ancient human bone,
13th Int. Conf. on Ion Beam Analysis (IBA-13), Lissabon, Portugal, July 27 - Aug. 1, 1997

Kaschny, J.R., Fichtner, P.F.P., Kreißig, U., Yankov, R.A., Mücklich, A., Skorupa, W.,
Helium bubbles in silicon: study of the residual helium content using elastic recoil detection analysis,
13th Int. Conf. on Ion Beam Analysis (IBA-13), Lissabon, Portugal, July 27 - Aug 1, 1997

Kaschny, J.R., Mücklich, A., Kreißig, U., Yankov, R.A., Kögler, R., Skorupa, W., Fichtner, P.F.P., Danilin, A.B.,
Helium induced cavities in silicon: their formation, microstructure and gettering ability,
MRS Spring Meeting, San Francisco, CA, USA, March 31 - April 4, 1997

Kharlamov, V.S., Kulikov, D.V., Trushin, Yu.V., Tsigankov, D.N., Yankov, R.A., Voelskow, M., Skorupa, W., Pezoldt, J.,
Computer-simulation and RBS/C studies of high-dose N^+ and Al^+ co-implantation in 6H-SiC,
Int. Workshop on New Approaches to Hi-Tech Materials'97 - Nondestructive Testing and Computer Simulations in Materials Science and Engineering, St. Petersburg, Russia, June 9 - 12, 1997

Kögler, R.,
Implantationsdefekte in Silizium: Der $R_p/2$-Effekt,
34. Treffen des Dt. Arbeitskreises"Punktdefekte", MPI-FKF, Stuttgart, Nov. 26 - 27, 1997

Kögler, R., Kaschny, J.R., Yankov, R.A., Skorupa, W., Werner, P., Danilin, A.B.,
Metal gettering by defective regions in carbon-implanted silicon,
7th Int. Conf. on Gettering and Defect Engineering in Semiconductor Technology, GADEST'97, Spa, Belgium, Oct. 5 - 10, 1997

Kögler, R., Posselt, M., Yankov, R.A., Kaschny, J.R., Mücklich, A., Skorupa, W., Danilin, A.B.,
Detection of metastable defective regions in ion-implanted silicon by means of metal gettering,
MRS Spring Meeting, San Francisco, CA, USA, March 31- April 4, 1997

Kolitsch, A., Möller, W.,
Growth and characterization of boron nitride thin films,
COST PISE, Final Meeting, Nancy, France, Sept. 1997

Kolitsch, A., Möller, W., Magula, V.,
Deposition by IBAD and characterization of CN_x films,
COST PISE, Final Meeting, Nancy, France, Sept. 1997

Kolitsch, A., Schöneich, J.,
Development of a user data base system for ion implanter operation,
4th DANFYSIK User Meeting, Ispra, Italy, Sept. 1997

Kreißig, U., Grigull, S., Lange, K., Nitzsche, P., Schmidt, B.,
In situ ERDA studies of ion drift processes during anodic bonding of alkali-borosilicate glasses to metal,
13th Int. Conf. on Ion Beam Analysis (IBA-13), Lissabon, Portugal, July 27 - Aug. 1, 1997

Kruijer, S., Dobler, M., Reuther, H., Keune, W.,
DCEMS-Tiefenanalyse der Phasenbildung in Fe-ionenimplantiertem Si,
DPG-Frühjahrstagung, Münster, March 17 - 21, 1997

Kruijer, S., Nikolov, O., Reuther, H., Keune, W., Weber, S., Scherrer, S.,
DCEMS-Tiefenanalyse der Phasenbildung in Al-ionenimplantierten Fe-Oberflächen,
DPG-Frühjahrstagung, Münster, March 17 - 21, 1997

Kruijer, S., Dobler, M., Reuther, H., Keune, W.,
Depth analysis of Fe-silicide formation after Fe-implantation into Si by DCEMS,
Int. Conf. Appl. Mössbauer Effect, Rio de Janeiro, Sept. 14 - 20, 1997

Kruse, O.,
High depth resolution ion scattering (ERDA and RBS) by means of an electrostatic spectrometer,
4th Int. Workshop on the Measurements, Characterization and Modeling of Ultra-Shallow Doping Profiles in Semiconductors, Research Triangle Park, North Carolina, USA, April 6 - 9, 1997

Kruse, O.,
Doppler broadening in high resolution ion scattering,
13th Int. Conf. on Ion Beam Analysis (IBA-13), Lisboa, Portugal, July 27 - Aug. 1, 1997

Kruse, O., Carstanjen, H. D.,
Hochauflösende Ionenstrahlanalytik unter Verwendung eines elektrostatischen Spektrometers,
Jahressitzg. d. HS-Arbeitsgruppe "Energiereiche atomare Stöße", Sonthofen, Jan. 27 - 13, 1997

Kruse, O., Carstanjen, H. D.,
Hochauflösende Ionenstrahlanalytik (ERDA, RBS) unter Verwendung elektrostatischer und magnetischer Spektrometer,
BMBF-Statusseminar zur Erforschung kondensierter Materie mit Neutronen, nuklearen Sonden, Ionen- und Synchrotronstrahlung, Kloster Seeon, Sept. 14 - 17, 1997

Mäder, M., Grambole, D., Herrmann, F., Neelmeijer, C., Schreiner, M., Woisetschläger, G.,
Non-destructive analysis of glass corrosion using external PIXE/PIGE,
13th Int. Conf. on Ion Beam Analysis (IBA-13), Lisboa, Portugal, July 27 - Aug. 1, 1997

Mäder, M., Neelmejier, C., Schramm, H.-P.,
Kolorierten Holzschnitten zerstörungsfrei auf der Spur,
Jahrestagung der GDCh, Archäometrie und Denkmalpflege, Vienna, Austria, March 24 - 26, 1997

Mändl, S., Günzel, R., Möller, W.,
Implantation in 3D-objects using plasma immersion ion implantation,
Spring Meeting, German Physical Society, Münster, Germany, March 17 – 21, 1997

Mändl, S., Günzel, R., Möller, W.,
Plasma immersion ion implantation of 3D-Objects,
8th German Meeting on Plasma Technology, Dresden, Germany, Sept. 15 – 17, 1997

Mändl, S., Günzel, R., Möller, W., Hilke, R., Knösel, E., Künanz, K.,
Characterization of drills implanted with nitrogen plasma immersion ion implantation, SMMIB 97, Gatlinburg, TE, USA, Sept. 1997

Markwitz, A., Mücklich, A., Borany, J. von, Matz, W., Schmidt, B., Möller, W.,
Cross-Section TEM analysis of Germanium nanoclusters in thin implanted SiO_2 films,
Tagung Elektronenmikroskopie, Regensburg , Sept. 7 - 12, 1997

Matz, W., Schell, N., Bernhard, G., Schlenk, R., Pröhl, D., Funke, H., Betzl, M., Brendler, V., Claußner, J., Dienel, S., Eichhorn, F., Hüttig, G., Krug, H., Neumann,W., Nitsche, H., Oehme, W., Prokert, F., Reich,T., Reichel, P., Strauch, U.,
ROBL - a CRG Beamline for Radiochemistry and Materials Research at the ESRF,
SR50 - Highlights in X-ray Synchrotron Radiation Research, Grenoble, France, Oct. 17 - 20, 1997

Matz, W., Schell, N., Prokert, F., Schlenk, R., Claußner, J., Pröhl,D., Betzl, M., Eichhorn, F., Dienel, S., Oehme, W., Bernhard, G., Funke, H.,
ROBL - ein Strahlrohr für Radiochemie und Materialforschung an der ESRF,
Gemeinsames Statusseminar im Kloster Seeon, Sept. 14 - 17, 1997

Mazur, K., Sass, J., Eichhorn, F.,
X-ray high resolution diffraction and reflectivity studies of the mechanical treatment related defects in opi-ready wafers,
3th Autumn School on "X-ray scattering from surfaces and thin layers", Smolenice, Slovakia,
Oct. 1 - 4, 1997

Möller, W., (invited)
Physik und Anwendungen der Plasma-Immersions-Ionenimplantation,
VDE/ITG-Seminar "Teilchenstrahl- und Plasmatechnik", Helmsdorf b. Dresden, March 7, 1997

Möller, W., (invited)
Plasma-Immersions-Ionenimplantation,
VDI/TZ-Statusseminar "Oberflächen- und Schichttechnologien", Würzburg, June 10, 1997

Möller, W., (invited)
Basic aspects and applications of plasma immersion ion implantation,
German-Japanese Seminar "Physics and Application of Low-Pressure Plasmas", Bad Honnef, June 18, 1997

Möller, W., (invited)
Ionenstrahlen zur Modifizierung und Analyse von Oberflächen,
GDCh-Tagung "Oberflächenanalytik", Chemnitz, June 25, 1997

Möller, W., Fukarek, W., Grigull, S., Kruse, O., Parascandola, S., (invited)
In-situ diagnostics using high-energy ion beam analysis,
13th Int. Conf. on Ion Beam Analysis (IBA-13), Lisboa, Portugal, July 1997

Müller, M., Grahl, H., Mattern, N., Schnell, B., Reibold, M., Reuther, H.,
Structure and magnetic properties in the low temperature annealing range of FeZrBCu-base alloys,
Soft Magnetic Materials 13, Grenoble, Sept. 24 - 26, 1997

Murthy, C.S., Posselt, M., Feudel, T.,
Physically-based modeling of 2d and 3d implantation profiles: influence of damage accumulation,
4th International Workshop on the Measurement, Characterization and Modeling of Ultra-Shallow Doping Profiles in Semiconductors, Research Triangle Park, USA, April 6-9, 1997

Nagy, D.L., Bottyan, L., Deak, L., Gerdau, E., Gittsovich, V.N., Korecki, J., Leupold, O., Reuther, H., Semenov, V.G., Szilagyi, E.,
Synchrotron Mössbauer reflectometry: feasibility of depth selective phase analysis of thin films and multilayers,
XXXII Zakopane School of Physics, May 10 - 17, 1997

Nakamura, K., Mändl, S., Brutscher, J., Günzel, R., Möller, W.,
Direct measurements of high-energy secondary electrons during plasma immersion ion implantation,
3rd Int. Conf. Reactive Plasmas, Nara, Japan, Jan. 21 – 24, 1997

Nangia, A., Kim, J.H., Weiss, A.H., Brauer, G.,
Experimental determination of positron related surface characteristics of 6H-SiC,
American Physical Society Meeting, Kansas City, USA, March 1997

Nangia, A., Kim, J.H., Weiss, A.H., Brauer, G.,
Experimental determination of positron related surface characteristics of 6H-SiC,
11th Int. Conf. on Positron Annihilation (ICPA-11), Kansas City, USA, May 25-30,1997

Nangia, A., Kim, J.H., Weiss, A.H., Brauer, G.,
Experimental determination of positron related surface characteristics of 6H-SiC,
American Vacuum Society - Texas Chapter (Symp. on Electronic Materials, Processing and Characterization), Austin, TX, USA, June 3 - 4, 1997

Neelmeijer, C., Mäder, M., Jarjis, R., Calligaro, T., Salomon, J., Schreiner, M., Gantz, T.,
Initial inter-laboratoring testing of the Rossendorf - Oxford (ROX97) secondary standard for X-ray analysis,
13. Int. Conf. on Ion Beam Analysis (IBA-13), Lisboa, Portugal, July 27 - Aug. 1, 1997

Nicht, E.-M., Brauer, G., Vostry, P., Cieslar, M., Blasek, P.,
Positron annihilation spectroscopy, electrical resistivity, and microstructural transmission electron microscopy studies of the CuMn system,
11th Int. Conf. on Positron Annihilation (ICPA-11), Kansas City, USA, May 25-30, 1997

Obara, K., Yiji, P., Chiba, K., Fukarek, W., Möller, W.,
Surface excitation processes of adsorbed gas molecules on metal surface,
ICRP-3/SPP-14, Nara, Jan. 1997

Palard, M., Strobel, M., Ruault, M.-O., Heinig, K.-H., Bernas, H.,
In situ TEM study of the evolution of $CoSi_2$ precipitates during annealing and ion irradiation,
10th International Conference on Microscopy of Semiconducting Materials, Oxford, UK, April 7 - 10, 1997

Parascandola, S., Anwand, W., Richter, E., Brauer, G., Coleman, P.G., Möller, W.,
Slow positron implantation spectroscopy of high current ion nitrided austenitic stainless steel,
13th Int. Conf. on Ion Beam Analysis (IBA-13), Lisboa, Portugal, July 27 - Aug 1, 1997

Parascandola, S., Günzel, R., Grötzschel, R., Richter, E., Möller, W.,
Stickstoffdiffusion in austenitischem Edelstahl unter Hochstrom-Ionenimplantation,
DPG Frühjahrstagung Münster, March 18, 1997

Parascandola, S., Richter, E., Möller, W.,
Nitriding transport during high current ion nitriding of austenitic stainless steel,
SMMIB 97, Gatlinburg, TE, USA, Sept. 1997

Pezoldt, J., Yankov, R.A., Fukarek, W., Hatzopoulos, N., Brauer, G., Anwand, W., Kreißig, U., Mücklich, A., Voelskow, M., Heera, V., Skorupa, W.,
Ion beam synthesis and characterization of buried $(SiC)_{1-x}(AlN)_x$ layers in 6H-SiC,
39th Electronic Materials Conf., Fort Collins, Colorado, USA, June 25-27, 1997

Pezoldt, J., Yankov, R.A., Fukarek, W., Hatzopoulos, N., Voelskow, M., Kreißig, U., Mücklich, A., Brauer, G., Anwand, W., Heera, V., Skorupa, W.,
Structural studies of buried $(SiC)_{1-x}(AlN)_x$ layers fabricated by co-implantation of nitrogen and aluminium ions in 6H-SiC,
7th Int. Conf. on Defect Recognition and Image Processing in Semiconductors (DRIP VII), Templin, Germany, Sept. 7 - 10, 1997

Plass, M.F., Fukarek, W., Kolitsch, A., Möller, W.,
Infrared investigation and ion beam analysis of boron nitride coatings,
E-MRS '97 Spring Meeting, Strasbourg, France, June 16-20, 1997

Plass, M.F., Fukarek, W., Kolitsch, A., Mücklich, A., Möller, W.,
Characterization of noncubic boron nitride films grown by a nonnormal angle of ion bombardment,
ICMCTF 97, San Diego, USA

Plass, M.F., Fukarek, W., Kolitsch, A., Möller, W.,
Growth and characterization of boron nitride thin films,
SMMIB 97, Gatlinburg, TE, USA, Sept. 1997

Posselt, M., (invited)
Computer simulation of random-to-channeling and blocking-to-channeling transitions,
Workshop on Channeling and Blocking Effects with Heavy Ion Beams, München, Germany,
April 18-19, 1997

Posselt, M., (invited)
Modeling of implantation damage in silicon,
Int. Workshop on Challenges in Predictive Process Simulation (ChiPPS'97), Wandlitz, Germany,
Aug. 17-20, 1997

Prokert, F., Betzl, M., Eichhorn, F., Matz, W., Schell, N.,
Das ROBL-Strahlrohr an der ESRF: (Röntgenoptik und Strahlcharakteristika, der MRH-Meßplatz),
Workshop "Strukturanalyse von Kristalloberflächen und dünnen Schichten mit Synchrotronstrahlung", LMU München, Oct. 8 - 10, 1997

Rebohle, L., Borany, J. v., Grötzschel, R., Markwitz, A., Schmidt, B., Tyschenko, I.E., Skorupa, W., Fröb, H., Leo, K.,
Strong blue photo-and electroluminescence from ion beam synthesized Ge-rich SiO_2-layers,
II. Int. Workshop on Light Emitting Low Dimensional Silicon Structures, Lagonissi-Attiki, Greece,
June 23 - 25, 1997

Rebohle, L., Tyschenko, I.E., Fröb, H., Leo, K., Yankov, R.A., Borany, J. v., Skorupa, W.,
Blue photoluminescence from high-dose Si^+- and Ge^+-implanted silicon-dioxide layers,
10th Biennial Conf. on Insulating Films on Semiconductors, Stenungsund, Sweden, June 11 - 14, 1997

Rebohle, L., Tyschenko, I.E., Fröb, H., Leo, K., Yankov, R.A., Skorupa, W.,
Erzeugung blauer Lumineszenzzentren durch Ionenstrahlsynthese,
DPG-Frühjahrstagung, Münster, March 17 - 21, 1997

Reiche, R., Oswald, S., Thomas, J., Schumann, J., Wetzig, K., Reuther, H., Dobler, M.,
XRS and TEM investigations on argon profiled metal-silicon thin films,
7th European Conf. Appl. Surf. Interface Analysis, Göteborg, Sweden, June 16 - 20, 1997

Reinert, T., Butz, T., Flagmeyer, R.-H., Jankuhn, S., Vogt, J., Gründer, W., Kanowski, M., Wagner, M., Werner, A., Grambole, D., Herrmann, F.,
Investigation of the calcium content in joint cartilage: Is it connected with (early arthrotic) changes in cartilage structure?,
13th Int. Conf. on Ion Beam Analysis (IBA-13), Lisboa, Portugal, July 27 - Aug. 1, 1997

Reuther, H., (invited)
Alloying by high dose ion implantation of iron into magnesium and aluminium,
Int. Conf. Appl. Mössbauer Effect, Rio de Janeiro, Brazil, Sept. 14 - 20, 1997

Reuther, H., Behr, G., Dobler, M., Teresiak, A.,
Angle dependent Mössbauer spectroscopy on β-$FeSi_2$ single crystals,
Int. Conf. Appl. Mössbauer Effect, Rio de Janeiro, Brazil, Sept. 14 - 20, 1997

Reuther, H., Betzl, M., Matz, W., Richter, E.,
Investigation of Fe-Mg-alloys produced by ion implantation,
10th Int. Conf. Surface Modification of Metals by Ion Beams, Gatlinburg, USA, Sept. 21 - 26, 1997

Richter, E., Reuther, H., Kreissig, U.,
The influence of heat treatment during the implantation of oxygen into magnesium,
SMMIB 97, Gatlinburg, TE, USA, Sept. 1997

Richter, E.,
Nitrierung austenitischer Edelstähle mittels Plasma-Immersions-Ionenimplantation,
OWT-97, Chemnitz, June 16-18, 1997

Romano-Rodriguez, A., Kögler, R., Bachrouri, A., Perez-Rodriguez, A., Serre, C., Reuther, H., Voelskow, M., Skorupa, W., Calvo-Barrio, L., Morante, J.R.,
Influence of the substrate structure (SIMOX,bulk Si) on the SiC synthesis by high dose carbon implantation,
7th Int. Conf. on Gettering and Defect Engineering in Semiconductor Technology, GADEST'97, Spa, Belgium, Oct. 5-10, 1997

Romano-Rodriguez, A., Perez-Rodriguez, A., Serre, C., Calvo-Barrio, L., Bachrouri, A., Gonzales-Varona, O., Morante, J.R., Kögler, R., Skorupa, W.,
TEM characterisation of carbon ion implantation into epitaxial $Si_{1-X}Ge_X$,
Int. Conf. on Microscopy of Semiconducting Materials, Oxford, England, April 1997

Schmidt, B., von Borany, J., Grötzschel, R., Heinig, K.-H., Markwitz, A., Matz, W., Nitzsche, P., Rebohle, L., Seifarth, H., Strobel, M., Skorupa, W.,
Dünnschichtsysteme für die Photo- und Elektrolumineszenz,
Photonik-Symposium, Würzburg, Oct. 8 - 10, 1997

Schmidt, B., Nitzsche, P., Lange, K., Grigull, S., Kreissig, U.,
In-situ investigation of ion drift processes in glass during anodic bonding,
EUROSENSORS XI, The 11th European Conference on Solid-State Transducers, Warsaw, Poland, Sept. 21 - 24, 1997

Schmidt, B., Posselt, M., Strecker, N., Feudel, T.,
Atomistic simulation of ion implantation into real 2d structures,
Int. Workshop on Challenges in Predictive Process Simulation (ChiPPS'97), Wandlitz, Germany, Aug. 17-20, 1997

Schmidt, B., Posselt, M., Strecker, N., Feudel, T.,
Atomistic modeling of ion implantation within a 2d process simulator,
MRS Fall Meeting, Boston, USA, Dec. 1 - 5, 1997

Seifarth, H., Grötzschel, R., Markwitz, A., Matz, W., Nitsche, P., Rebohle, L.,
Abscheidung von Si/SiO_2-Cluster-Schichten durch reaktives Magnetron-Sputtern,
8. Bundesdeutsche Fachtagung Plasmatechnologie, Dresden, Sept. 14 - 17, 1997

Segrouchni, Z., Betzl, M. Richter, E.,
Composition, structural and hardeness change of aluminium implanted with carbon,
SMMIB 97, Gatlinburg, TE, USA, Sept. 1997

Skorupa, W.,
MeV-Implantation in Silicium,
20. Dt. Nutzertreffen Ionenimplantation, SIMEC-Werk der Siemens AG, Dresden, Oct. 29 -30, 1997

Soltani-Farshi, M., Baumann, H., Bethge, K., Rück, D., Richter, E., Kreissig, U.,
Content of hydrogen in boron-, carbon-, nitrogen-, oxygen-, fluorine-, and neon-implanted titanium,
SMMIB 97, Gatlinburg, TE, USA, Sept. 1997

Spaeth, Kühn, M., Richter, F., Falke, U., Hietschold, M., Kilper, R., Kreissig, U.,
A comparative study of ERDA, EELS and XPS for structural analysis of amorphous carbon nitride films,
Int. Conf. Diamond '97

Strobel, M., Heinig, K.-H., Möller, W.,
Computersimulationen zur Evolution von Nanoclustern,
Frühjahrstagung der DPG, Münster, Germany, March 17-21, 1997

Strobel, M., Heinig, K.-H., Möller, W.,
A combination of atomic and continuum computational models describing the evolution of nanoclusters,
E-MRS Spring Meeting, Strasbourg, France, June 16 - 20, 1997

Strobel, M., Heinig, K.-H., Möller, W.,
Formation and self-organization of nanoclusters by ion beam synthesis: a combined atomistic and continuum description,
MRS Fall Meeting, Boston, USA, Dec. 1-5, 1997

Teichert, J., Bischoff, L., Hausmann, S., (invited)
Ion beam synthesis of cobalt disilicide using focused ion beam implantation,
Int. Seminar on Ion Nanobeams and Applications to Material Processing, Osaka, Japan, Nov. 16 - 20, 1997

Teichert, J., Voelskow, M., Bischoff, L., Hausmann, S.,(invited)
RBS and channeling analysis of cobalt disilicide layers produced by focused ion beam implantation,
10th Int. School on Vacuum, Electron and Ion Technologies, Varna, Bulgaria, Sept. 22 - 27, 1997

Trushin, Y.V., Yankov, R.A., Kharlamov, V.S., Kulikov, D.V., Tsigankov, D.N., Kreißig, U., Voelskow, M., Pezoldt, J., Skorupa, W.,
A computational model of the formation of $(SiC)_{1-x}(AlN)_x$ structures by hot, high-dose N^+ and Al^+ co-implants in 6H-SiC,
Int. Conf. on Silicon Carbide, III-Nitrides and Related Materials, Stockholm, Sweden,
Aug. 31 - Sept. 5, 1997

Turos, A., Wieteska, K., Wierzchowski, W. K., Wendler, E., Wesch, W., Strupinski, W., Grötzschel, R.,
Ion bombardment induced relaxation of strained AlGaAs/GaAs heterostructures studied by the complementary use of RBS-channeling and X-ray synchrotron radiation,
13th Int. Conf. on Ion Beam Analysis (IBA-13), Lisboa, Portugal, July 27 - Aug. 1, 1997

Tyschenko, I.E., Kachurin, G.A., Zhuravlev, K.S., Pazdnikov, N.A., Volodin, V.A., Gutakovsky, A.K., Leier, A.F., Fröb, H., Leo, K., Böhme, T., Rebohle, L., Yankov, R.A., Skorupa, W.,
Blue photoluminescence from high-dose Si^+- and Ge^+-implanted silicon-dioxide layers,
Int. Workshop des Innovationskollegs der TU Chemnitz "Methoden und Materialsysteme für den Nanometerbereich", Schöneck/Vogtl., March 3 - 5, 1997

Wang, X., Kolitsch, A., Prokert, F., Möller, W.,
Ion beam assisted deposition of AlN monolithic films and Al/AlN multilayers: A comparative study,
SMMIB 97, Gatlinburg, TE, USA, Sept. 1997

Werninghaus, T., Zahn, D.R.T., Yankov, R.A., Mücklich, A., Pezoldt, J.,
Cross-sectional micro-Raman Spectroscopy: a tool for structural investigations of thin polytypic SiC layers,
Int. Conf. on Silicon Carbide, III-Nitrides and Related Materials, Stockholm, Sweden,
Aug. 31 - Sept. 5, 1997

Wesch, W., Karmann, A., Börner, H.G., Jentschel, M., Heinig, K.-H.,
GRID spectroscopy - a new nuclear method for lattice localization of foreign atoms,
13th Int. Conf. on Ion Beam Analysis, Lissabon, Portugal, July 28 -August 2, 1997

Wieser, E., Richter, E., Grötzschel, R., Mücklich, A., Prokert, F.,
Microstructure and wear behaviour of aluminium implanted with nickel,
SMMIB 97, Gatlinburg, TE, USA, Sept. 1997

Wieteska, K., Wierzchowski, W. K., Turos, A., Grötzschel, R.,
Synchrotron X-ray studies of AlGaAs/GaAs epitaxial layers implanted with Se ions,
4th Symp. on Synchrotron Radiation, Krakow, PL, 1997

Wirth, H., Anwand, W., Brauer, G., Voelskow, M., Panknin, D., Skorupa, W., Coleman, P.G.,
Investigation of ion-implantation induced damage in 6H-SiC by RBS/C and Positron Annihilation Spectroscopy,
Int. Conf. on Silicon Carbide, III-Nitrides and Related Materials, Stockholm, Sweden,
Aug. 31 - Sept. 5, 1997

Wirth, H., Voelskow, M., Panknin, D., Skorupa, W.,
Kristallgitter-Einbau implantierter Ionen in 6H-SiC,
DPG-Frühjahrstagung, Münster, March 17 - 21, 1997

Witke, T., Siemroth, P., Brückner, J., Brutscher, J., Richter, E.,
Ionenimplantation aus Vakuumbogenplasmen,
8. Bundesdeutsche Fachtagung Plasmatechnologie, Dresden, Sept. 14 - 17, 1997

Yankov, R.A., Fukarek, W., Hatzopoulos, N., Voelskow, M., Kreißig, U., Brauer, G., Anwand, W., Heera, V., Skorupa, W.,
Ion beam synthesis: a novel method of producing $(SiC)_{1-x}(AlN)_x$ layers,
Int. Conf. on Silicon Carbide, III-Nitrides and Related Materials, Stockholm, Sweden,
Aug. 31 - Sept. 5, 1997

Yankov, R.A., Kaschny, J.R., Fichtner, P.L.F., Mücklich, A., Kreißig, U., Skorupa, W.,
Impurity gettering effects in separation-by-implanted-oxygen (SIMOX) structures - what getters what, where and how,
10th Biennial Conf. on Insulating Films on Semiconductors, Stenungsund, Sweden, June 11 - 14, 1997

Lectures

Albe, K.,
Computersimulationen zur Schichtabscheidung von Bornitrid,
Inst. f. Oberflächen- und Mikrostrukturphysik, TU Dresden, Dresden, Germany, August 1, 1997

Betzl, M.,
Neutronenstreuung am RFR,
Vortrag auf Kolloquium des VKTA - 40 Jahre Rossendorfer Forschungsreaktor RFR, Rossendorf, Dec. 16, 1997

Borany, J. von,
Zusammenarbeit mit industriellen Einrichtungen (Industriekooperation),
Vortrag zur Evaluierung durch den Wissenschaftlichen Beirat des FZR, Rossendorf, Apr. 29, 1997

Borany, J. von,
Ionenstrahlphysik und Technik im Forschungszentrum Rossendorf,
FernUniversität Hagen, FB Elektrotechnik, Jan. 31, 1997

Borany, J. von,
Ionenstrahlsynthese von Nanoclustern für elektrooptische Anwendungen,
1. Materialwissenschaftliche Tagung der WGL, Berlin, Oct. 14, 1997

Brauer, G.,
Positron studies of defects in ion-implanted and annealed SiC,
Lawrence Livermore National Lab, Physics and Space Technology, Livermore, USA, May 22, 1997

Brauer, G.,
Progress in the study of vacancy-type defects in ion implanted SiC by slow positron implantation spectroscopies,
Univ. of East Anglia (School of Physics), Norwich, Nov. 7, 1997

Friedrich, M.,
The Rossendorf electrostatic accelerator,
SINR Shanghai, Dept. of Physics, P. R. China, April 17, 1997

Fukarek, W.,
Ellipsometry as a diagnostic tool for thin film processing,
Institute of Polymer Physics, Charles University Prague, Nov. 27, 1997

Grambole, D.,
Möglichkeiten der Oberflächenanalytik mit Ionenstrahlverfahren im Forschungszentrum Rossendorf,
TU Dresden, Inst. f. Werkstoffwissenschaften, Aug. 13, 1997

Grötzschel, R.,
Grundlagen der Ionenstrahlanalytik,
TU Chemnitz, Graduiertenkolleg, Jan./Feb., 1997

Grötzschel, R.,
Recent developments of in situ ion beam analysis at Rossendorf,
Faure, South Africa, Nov. 19, 1997

Günzel, R.,
Plasma source ion implantation in the Forschungszentrum Rossendorf: state of the art and recent developments,
IPR, Ghandinagar, March 18, 1997

Günzel, R.,
Plasma source ion implantation compared with glow discharge plasma nitriding of stainless steel,
City University of Hong Kong, October 13, 1997

Günzel, R., Richter, E.,
Verschleißfester Edelstahl – ein Erfolg der Ionenstrahltechnik,
Workshop "Werkstoffe innovativ", Hannovermesse 1997

Heera, V.,
Implantations- und Ausheileffekte in SiC,
Institutsseminar FWI-FZR, Rossendorf, June 5, 1997

Heinig, K.-H.,
Grundlagen der Synthese von Nanoclustern und dünnen Schichten mit Ionenstrahlen,
Seminar am ISI des Forschungszentrum Jülich, Jülich, Germany, February 27, 1997

Heinig, K.-H.,
Theoretische Grundlagen der Ionenstrahlsynthese: Beschreibungen basierend auf Ratengleichungen,
Seminar an der TU Chemnitz, Chemnitz, Germany, May 6, 1997

Heinig, K.-H.,
Theoretische Grundlagen der Ionenstrahlsynthese: Computersimulationen auf atomarer Ebene,
Seminar an der TU Chemnitz, Chemnitz, Germany, May 13, 1997

Kögler, R.,
Detektion von Defektzonen in ionenimplantiertem Si,
MLU Halle-Wittenberg, FB Physik, Halle (Saale), Apr. 10, 1997

Kögler, R.,
Defective zones in Si detected by means of metal gettering,
Univ. Barcelona, Dept. Fisica Aplicada i Electronica, Barcelona, Spain, Nov. 10, 1997

Mändl, S.,
Plasma immersion ion implantation,
City University of Hongkong, Oct. 13, 1997

Mändl, S.,
Basics and applications of plasma immersion ion implantation,
University of Augsburg, Nov. 20, 1997

Matz, W.,
ROBL: Strahlrohr und Experimentierausrüstung,
Nutzertreffen ROBL, FZR, Rossendorf, June 19, 1997

Matz, W., Prokert, F., Eichhorn, F., Schell, N., Betzl, M.,
Experimente der Materialforschung an ROBL
Nutzertreffen ROBL, FZR, Rossendorf, June 19, 1997

Matz, W.,
Der Materialforschungsmeßplatz der Rossendorfer Beamline an der Europäischen Synchrotronstrahlungsquelle in Grenoble
TU Dresden, Institut für Kristallographie und Festkörperphysik, Nov. 11, 1997

Matz, W.,
Synchrotronstrahlung: Eigenschaften, Quellen, Anwendungen,
Zentrumsseminar FZR, Nov. 20, 1997

Matz, W.,
Das Rossendorfer Strahlrohr ROBL an der ESRF,
Zentrumsseminar FZR, Dec. 4, 1997

Möller, W.,
Physik und Anwendungen der Plasma-Immersions-Ionenimplantation,
Elektrotechnisches Kolloquium der Univ. Stuttgart, Jan. 23, 1997

Möller, W.,
Ion beam analysis in Europe and Germany,
Univ. of Surrey, Dept. Electrica Engineering, Guildford, U.K., Feb. 4, 1997

Möller, W.,
Ionenstrahlen in Forschung und Technik,
Physikalisches Kolloquium des Inst. für Physikalische Hochtechnologie, Jena, June 4, 1997

Nicht, E.-M.,
Recent positron annihilation studies of the CuMn-system,
Lehrstuhl für Tieftemperaturphysik, Univ. Prag, Oct. 30, 1997

Parascandola, S.,
Aufstickung von austenitischem Edelstahl durch Hochstrom-Ionenimplantation,
TU Bergakademie Freiberg, May 5, 1997

Posselt, M.,
Theoretische Beschreibung von Implantationsprozessen: Grundlagen,
Methoden, Anwendungen,
Sommerschule "Nukleare Sonden und Ionen", Bad Blankenburg, Germany, Sept. 1-5, 1997

Rebohle, L.,
Erzeugung blauer Lumineszenz-Zentren in SiO_2 durch Ionenstrahlsynthese,
Vortrag zur Evaluierung durch den Wissenschaftlichen Beirat des FZR, Rossendorf, Apr. 4, 1997

Rebohle, L.,
Strong blue and violet light emission from silicon- and germanium-implanted silicon dioxide,
Bell Labs, Lucent Technologies, Murray Hill, NJ, USA, Dec. 8, 1997

Richter, E., Chudoba, T., Wieser, E.,
Verschleißschutz von Alumnium- und Magnesiumlegierungen durch Ionenimplantation,
Innovative Verfahren der Oberflächenvergütung von Leichtmetallen, Essen, June 5, 1997

Skorupa, W.,
Strong blue photo-and electroluminescence from ion beam synthesized Ge-rich SiO_2-layers,
Dept. de Fisica Aplicada i Electronica, Univ.Barcelona, Spain, Nov. 11, 1997

Skorupa, W.,
Ionenstrahlmodifizierung von Halbleitermaterialien: Forschungsaktivitäten am Institut für Ionenstrahlphysik und Materialforschung,
Vortrag zur Evaluierung durch den Wissenschaftlichen Beirat des FZR, Rossendorf, Apr. 29, 1997

Skorupa, W.,
Hochenergieimplantation in Silicium: Defekt-Engineering und Gettern,
Institut für Physik, FSU Jena, May 16, 1997

Skorupa, W.,
Defectengineering and gettering by high energy implantation into Silicon,
Center for Analysis of Substances, Moscow, Russia, May 26, 1997

Skorupa, W.,
Ionenstrahlmodifizierung von Halbleitermaterialien: Forschungsaktivitäten am Institut für Ionenstrahlphysik und Materialforschung,
Treffen der Dresdener Forschungsinstitute mit der Sächsischen Industrie, Dresden, June 27, 1997

Skorupa, W.,
Blaue Lumineszenz hoher Intensität aus implantierten SiO_2-Schichten: Nanocluster oder ....?
Innovationskolleg "Methoden und Materialsysteme für den Nanometerbereich", Institut für Physik, TU Chemnitz, Oct. 24, 1997

Skorupa, W.,
Strong blue photo-and electroluminescence from ion beam synthesized Ge-rich SiO_2-layers,
Naval Res. Lab, Electronics Division, Washington, D.C., USA, Nov. 26, 1997

Skorupa, W.,
Ion beam processing of Semiconductors: Research activities at the Forschungszentrum Rossendorf,
VARIAN Company, Gloucester, MA, USA, Dec. 4, 1997

Skorupa, W.,
High energy implantation into silicon: Gettering and Defect Engineering,
Bell Labs, Lucent Technologies, Murray Hill, NJ, USA, Dec. 8, 1997

Strobel, M.,
Monte-Carlo and rate-equation simulations describing the evolution of nanoclusters in high-dose ion implantation,
Solid State Division, Oak Ridge National Laboratory, Oak Ridge, USA, Oct. 23, 1997

Teichert, J.,
Flüssigmetall-Ionenquellen und ihre Anwendung in Ionenfeinstrahlanlagen,
Univ. Magdeburg, Inst. f. experimentelle Physik, Nov. 27, 1997

Wieser, E.,
Bestimmung von Ni-Tiefenprofilen in Al und Aufklärung der Phasenbildung bei Ionenimplantation in Al,
Seminar des Sonderforschungsbereiches "Strukturbildung und Eigenschaften in Grenzschichten", Dresden,
Nov. 20, 1997

Wirth, H.,
Ionenimplantation in 6H-SiC; Elektrische Untersuchungen und Sublimation,
Daimler-Benz-AG, FZ Frankfurt/M., Jan. 8, 1997

Wirth, H.,
Effekte bei der Implantationsdotierung von Bor und Aluminium in 6H-SiC,
Daimler-Benz-AG, FZ Frankfurt/M., Oct. 29, 1997

Yankov, R.A.,
Proximity gettering of transition-metal impurities in separation-by-implanted-oxygen (SIMOX) structures
using buried carbon- and helium-implanted layers,
Naval Res. Lab, Electronics Division, Washington D.C., USA, Nov. 26, 1997

Yankov, R.A.,
Interaction of high-energy ion beams with silicon: buried layers, gettering and defect engineering,
VARIAN Company, Gloucester, MA, USA, Dec. 4, 1997

Yankov, R.A.,
Impurity gettering effects in separation-by-implanted-oxygen (SIMOX) structures: what getters what, where
and how,
Bell Labs, Lucent Technologies, Murray Hill, NJ, USA, Dec. 8, 1997

Reports

Böhmert, J., Brauer, G.,
Abschlußbericht zum Verbundprojekt "Strukturelle Ursachen und Mechanismen der bestrahlungsinduzierten
Versprödung in Reaktordruckbehälterstählen",
Verbundprojekt Forschungsförderung SMWK 1994, 4-7541.83 - FZR/403
Berichtsdatum: 15.01.1997

Fontaine, F., Borany, J.v., Heera, V.,
Dotierte und undotierte Diamantfilme,
SMWK: 4-7531.50-03-IFW/602, Zwischenberichte 25.6.1997, 11.12.1997

Nitzsche, P., Lange, K., Schmidt, B., Grigull, S., Kreissig, U., Huber, H., Assmann, W., Thomas, B.,
Herzog, K.,
Ionendriftprozesse in Borosilikatgläsern während des anodischen Bondens,
FZR-Report, FZR-184, Juli 1997

Noll, K., Döbeli, M., Tobler, L, Grambole, D., Krähenbühl, U.,
Fluorine profiles in antarctic meteorites by nuclear reaction analysis,
Annual Report 1996, Labor f. Radio- u. Umweltchemie der Univ. Bern u. des PSI

Schmidt, B., Lange, K., Harz, M., Nitzsche, P.,
Schlußbericht: Anwendungsgerechte Systemintegration und Zuverlässigkeit für die intelligente mikromechanische Sensorik (AN-SYS), Teilvorhaben: Silizium-Glas- und Silizium-Silizium-Bonden, BMBF-Vergundprojekt, Förderkennzeichen 13 MV 0266, Mai 1997

Siemroth, P., Richter, E., Schülke, T., Witke, T., Brückner, J. Brutscher, J.,
Hochstromionenquelle für Dünnschichttechnologien,
SMWK 4-7541.83-IWS/504

Teichert, J., Hausmann, S.,
Entwicklung eines Permeable Base Transistors mit Kobaltdisilizid-Gate auf der Basis maskenloser Implantation mit feinfokussiertem Ionenstrahl,
DFG-Te 250/1-1, Zwischenbericht, 12/97

Wolf, D., Oberhänsli, R., Grambole, D., Gruner, T.,
Morphologie, chemische Heterogenität und Lumineszenz von Zirkonen und ihre Bedeutung für petrogenetische Typologie und Genchronologie,
DFG-Abschlußbericht zur Sachbeihilfe Wo 489/2 - 2

Laboratory Visits

Anwand, W.,
University of East Anglia, School of Physiks, Norwich, UK, Feb. 5 - 21; Oct. 29 - Nov. 14, 1997

Betzl, M.
European Synchrotron Radiation Facility, Grenoble, France, Oct. 19 - 30, Nov. 19 -28, 1997

Bischoff, L.,
Robert-Bosch GmbH, Reutlingen, Apr. 24-25, 1997

Boede, W.
European Synchrotron Radiation Facility, Grenoble, France, Oct. 19 - 30, 1997

Brauer , G.,
Karls-Universität Prag, Tieftemperaturlabor, Oct. 7-9, 1997

Brauer, G.,
University of East Anglia, School of Physiks, Norwich, UK, Feb. 5 - 21; Oct. 29 - Nov. 14, 1997

Eichhorn, F.,
European Synchrotron Radiation Facility, Grenoble, France, June 23 - July 4, Oct. 8 - 17, Nov. 16 - 25, 1997

Eichhorn, F.,
Institut of Electronic Materials Technology, Warsaw, June 3 - 7, 1997

Eichhorn, F.,
HASYLAB Hamburg, Feb. 27 - March 3, 1997

Grötzschel, R.,
National Accelerator Centre, Faure, South Africa, Nov. 14 - 20, 1997

Günzel, R.,
Institute for Plasma Research, Gandhinagar, India, Feb. 18 – March 28, 1997

Günzel, R.,
City University of Hong Kong, Oct. 1997

Heinig, K.-H.,
ISI, FZ Jülich, Jülich, Germany, February 27, and December 17-18, 1997

Heinig, K.-H.,
ILL Grenoble, Grenoble, France, November 19-23, 1997

Heinig, K.-H.,
CSNSM-CNRS, Orsay/Paris, France, December 18-20, 1997

Kruse, O.,
MPI Stuttgart, Oct. 25 - 28, 1997

Mäder, M.,
L.A.R.N. Namur, Belgium, Feb. 17 - 20, 1997

Mäder, M.,
Akademie d. Bildenden Künste, Vienna, Austria, June 8 - 13, 1997

Mändl, S.,
City University of Hong Kong, October 7 – 22, 1997

Markwitz, A.,
L.A.R.N. Namur, Belgien, Jan. 27 - 31, April 1 - 4, 1997

Markwitz, A.,
Inst. f. Kernphysik, J. W. Goethe-Universität, Frankfurt/M., Feb. 7, Aug. 28 - 29, 1997

Markwitz, A.,
MPI für Microstrukturphysik, Halle, July 15 - 17, 1997

Matz, W.,
European Synchrotron Radiation Facility, Grenoble, France, Feb. 3 - 6; April 21 - 25; June 9 - 12; 23 - 27; Sept. 15 - 23; Nov. 16 - 19, 1997

Matz, W.,
Oxford Instruments, Accelerator Technology Group, Oxford, UK, March 10 - 14, 1997

Mücklich, A.,
Material Science Division, Argonne National Lab., Argonne, IL, USA, May 27 - June 4, 1997

Prokert, F.,
Oxford Instruments, Accelerator Technology Group, Oxford, UK, March 10 - 14, 1997

Prokert, F.,
European Synchrotron Radiation Facility, Grenoble, France, June 26 - July 4; Sept. 17 - 26; Dez. 1 - 11, 1997

Prokert, F.,
Institut f. Kristallographie, Universität Tübingen, Sept. 30 - Okt. 2, 1997

Reichel, P.,
European Synchrotron Radiation Facility, Grenoble, France, Oct. 19 - 30; Nov. 19 - 28, 1997

Reuther, H.,
Universität Duisburg, Oct. 28 - 29, 1997

Skorupa, W.,
Institut für Physik, FSU Jena, May 15-17, 1997

Skorupa, W.,
Center for Analysis of Substances, Moscow, Russia, May 23-28, 1997

Skorupa, W.,
Dept. de Fisica Aplicada i Electronica, Universitat de Barcelona, Spain, Nov.8 - 13, 1997

Skorupa, W.,
Electronics Division, Naval Research Laboratory, Washington, D.C., USA, Nov. 25-27,1997

Skorupa, W.,
Revesz Associates Consulting, Bethesda, Maryland, USA, Nov. 27-29, 1997

Skorupa, W.,
VARIAN Ion Implant Systems, Gloucester, Mass., USA, Dec. 4-5, 1997

Skorupa, W.,
Bell Laboratories, Murray Hill, New Jersey, USA, Dec.7-9, 1997

Strobel, M.,
Solid State Division, Oak Ridge National Laboratory, Oak Ridge, USA, October 20- November 28, 1997

Strobel, M.,
CSNSM-CNRS, Orsay/Paris, France, Dec. 18 - 19, 1997

Tyrroff, H.,
Argonne National Lab, Tandem Laboratory, USA, May 27 - June 4, 1997

Yankov, R.A.,
Center for Analysis of Substances, Moscow, Russia, May 23-28, 1997

Yankov, R.A.,
Electronics Division, Naval Research Laboratory, Washington, D.C., USA, Nov.25-27,1997

Yankov, R.A.,
Revesz Associates Consulting, Bethesda, Maryland, USA, Nov. 27-29, 1997

Yankov, R.A.,
VARIAN Ion Implant Systems, Gloucester, Mass., USA, Dec. 4-5, 1997

Yankov, R.A.,
Bell Laboratories, Murray Hill, New Jersey, USA, Dec. 7-9, 1997

Guests

A. Antons,
ISI, FZ Jülich, Jülich, Germany, April 1- June 6, and August 4-16, 1997

Dr. N. Barradas,
University of Surrey, U.K.

Dr. F. Becvar,
Karlsuniversität Prag, Tschechien, March 10-14; Oct. 6-11, 1997

Prof. M. Behar,
Dept. of Physics, Univ. of Rio Grande dol Sul, Porto Allegre, Brazil, July 14-17, 1997

A. Birner,
MPI für Mikrostrukturphysik, Halle/Saale, Oct.18-19, 1997

Dr. V. Borodin,
Russian Research Center, Kurchatov Institute of Atomic Energy, Moscow, Russia, Sept. 29 - Nov. 29, 1997

Prof. G. L. Catchen,
Pennsylvania State University, USA, Apr. 14-18, 1997

Dr.A. Danilin,
Centre for Analysis of Substances, Moskau, Oct.15-20, 1997

A.A. Deshkovskaya,
Belarussian State University of Informatic and Electronics, Minsk, Belarus

Dr. G. Dollinger,
TU München, Oct. 26 - 27, 1997

J. Engeldinger,
Univ. des Saarlandes, Inst. f. Physikalische Chemie, Sept. 15 - 19, 1997

Dr. J. Esteve,
Centro Nacionale de Microelectronica, Barcelona, Spain, Dec. 17-21, 1997

Prof. P. Fichtner,
Dept. of Metallurgy, Univ. Rio Grande dol Sul, Porto Allegre, Brazil, Aug. 19-27, 1997

J. Gaca,
Institut of Electronic Materials Technology, Warsaw, March 17 - 21, Sept. 22 - 27, 1997

T. Ganetsos,
Department of Physics, University of Athens, Greece, Jan.2-30, 1997

B. Groß,
Univ. des Saarlandes, Inst. f. Physikalische Chemie, Sept. 15 - 19, 1997

S. Herrmann,
Hahn-Meitner-Institut Berlin, Feb. 7; July 14 - 15; Sept. 11 - 12, 1997

Dr. A. Ivanov,
NIIEFA St. Petersburg, Russia, Nov. 2 - 7, 1997

S. Jankuhn,
Univ. Leipzig, Fak. f. Physik und Geowiss., June 16 - 20, 1997

Dr. R. Jarjis,
University of Oxford, Nuclear Physics Laboratory, Feb. 19 - March 22; Sept. 7 - Oct. 18, 1997

D.A. Karpov,
Efremov Scientific Research Institute of Electrophysical Apparatus, St. Petersburg, Russia

Dr. J. Kaschny,
Dept. of Physics, Univ. of Rio Grande dol Sul, Porto Allegre, Brazil, Jan.1 - Dec.21, 1997

V. Kharlamov,
Ioffe-Institut, St. Petersburg, Russia, Nov. 3 - Dec. 14, 1997

Dr. J. Krynicki,
Inst. of Nuclear Chemistry and Technology, Warsaw, PL, Nov. 25 - 29, 1997

D.V. Kulikov,
A.F. Ioffe Physicotechnical Institute, St. Petersburg, Russia

V. Magula,
Welding Research Institute, Bratislava, Slovakia

Dr. V. Makarov,
Centre for Analysis of Substances, Moskau, Oct. 15-20, 1997

A. Malygin,
IPPE Obninsk, Russia, Sept. 1 - Dec. 31, 1997

D. Manova,
Bulgarian Academy of Sciences, Institute of Solid State Physics, Sofia, Bulgaria

Dr. K. Mazur,
Institut of Electronic Materials Technology, Warsaw, June 16 - 21; Nov. 24 - 29, 1997

Dr. T. Michely,
FZ Jülich, Inst. f. Oberflächenforschung u. Vakuumphysik, Nov. 27 - 28, 1997

S. El sayed Soliman Mohamed,
Ain Shams University Cairo, Egypt, Jan. 1 - Dec. 31, 1997

A. Näser,
TU Berlin, Sept. 11 - 12, 1997

K. Noll,
Univ. Bern, Inst. f. Anorganische Chemie, CH, June 26 - July 4, 1997

A. Peeva,
Institute of Solid State Physics, Bulg.Acad.of Sciences, Sofia, Nov. 27 - Dec. 5, 1997

Dr. A. Perez-Rodriguez,
Dept. de Fisica Aplicada i Electronica, Universitat de Barcelona, Spain, March 11-16; Dec.17-21, 1997

Dr. J. Petzoldt,
Institut für Festkörperelektronik, TU Ilmenau, March 18 - 20; July 17-18, 1997

Dr. Prichodko,
Russian Research Center, Kurchatov Institute of Atomic Energy, Moscow Russia, Dez. 8 - 12, 1997

Dr. V. Prozesky,
National Accelerator Centre, Van de Graaff Group, Faure, South Africa, Aug. 2 - 6, 1997

T. Reinert,
Univ. Leipzig, Fak. f. Physik und Geowiss., June 16 - 20, 1997

Dr. A. Romano-Rodriguez,
Dept. de Fisica Aplicada i Electronica, Universitat de Barcelona, Spain, July 18 - Aug. 8, 1997

J. Sass,
Institut of Electronic Materials Technology, Warsaw, June 16 - 21, Nov. 24 - 29, 1997

Z. Segrouchny,
Strasbourg, France

Dr. C. Serre,
Dept. de Fisica Aplicada i Electronica, Universitat de Barcelona, Spain, March 11-16, 1997

Prof. M. Svinin,
NIIEFA St. Petersburg, Russia, Nov. 2 - 7, 1997

T.A. Telbizova,
Bulgarian Academy of Sciences, Institute of Solid State Physics, Sofia, Bulgaria

Prof. Y. V. Trushin,
A.F.Joffe-Physical-Technical-Institute, St.Petersburg, Russia, March 13 - Apr. 14; Nov. 7 - 21, 1997

Prof. A. Turos,
Inst. of Electronic Materials Technology, Warsaw, PL, Feb. 9 - 11; July 1 - 5, 1997

Dr. I. E. Tyschenko,
Institut for Semiconductor Physics, Novosibirsk, Russia, Sept. 15 - Dec. 14, 1997

X. Wang,
Shanghai Institute of Metallurgy, Chinese Academy of Sciences, Shanghai, PR China

Dr. S. Warchol,
Inst. of Nuclear Chemistry and Technology, Warsaw, PL, Nov. 25 - 29, 1997

M. Wojzik,
Institut of Electronic Materials Technology, Warsaw, March 17 - 21; Sept. 22 - 27, 1997

Dr. R. A. Yankov,
TU Ilmenau and Bulg.Acad. of Sciences., Sofia, Jan. 1 - July 31; Sept. 1 - Dec. 31, 1997

Awards

Albe, K.,
E-MRS Spring Meeting, Symposium D, Strasbourg, France
Young scientist award

Jentschel, M.,
Doktorandenpreis des FZ Rossendorf 1997

PhD Theses

Brenscheidt, F.,
Modifizierung der tribologischen, mechanischen und korrosiven Eigenschaften von Siliziumnitrid-Keramik mittels Ionenimplantation
TU Dresden, December 1997

Grigull, S.,
Transport und Strukturmodifikation bei der Stickstoffimplantation in amorphen Kohlenstoff,
TU Dresden, July 1997

Henkel, T.,
Ionenstrahlinduzierte Wachstumsprozesse amorpher Schichten in Silizium,
TU Dresden, March 1997

Jentschel, M.,
Crystal-GRID: Eine neue nukleare Sonde zur Untersuchung atomarer Bewegung im Festkörper,
TU Dresden, April 1997

Mändl, S.,
Die Randschichtausbreitung bei der Plasma-Immersions-Ionenimplantation,
TU Dresden, December 1997

Möller, D.,
Synthese schwermetallionensensitiver Membranen für ISFETs mittels Ionenimplantation,
TU Dresden, July 1997

Diploma Thesis

Schwieger, T.,
TRIDYN-Computersimulationen zur Schicht-Deposition von BN und zur Hochdosisimplantation in Si,
Friedrich-Schiller-Universität Jena, April 1997

Meetings Organized by the Institute

Summer School "Nuclear Probes and Ion Beams", Bad Blankenburg/Thuringia, Sept. 1 - 6, 1997
Organizers: Dr. E. Mahnke, Dr. H. Homeyer (HMI Berlin), Dr. R. Grötzschel, Prof. W. Möller (FZ Rossendorf)

8th German Topical Conference on Plasma Technology, Dresden, Sept. 14 - 17, 1997
Chairman: Prof .W. Möller (FZ Rossendorf)
Local Organizers: W. Fukarek, I. Heidel, W. Möller (FZ Rossendorf); S. Schiller, M. Wünsche (FhG-FEP Dresden); B. Schultrich, T. Witke (FhG-IWS Dresden)

Patents

Günzel, R.,
Modulator für die Plasma-Immersions-Ionenimplantation,
OS 197 02 294.4

Heera, V., Skorupa, W.,
Verfahren zur gezielten Herstellung von n-leitenden Bereichen in Diamantschichten mittels Ionenimplantation,
ha 1135, Institutsakte 9711-IN, Aktenzeichen Patentamt 197 30 083.9, 14.7.97

Heera, V., Skorupa, W.,
Verfahren zur Erzeugung einer dotierten Schicht in Siliziumkarbid,
ha 1134, Institutsakte 9713-IN, Aktenzeichen Patentamt 197 41 725.6, 22.9.97

Pham, M.T., Steiner, G., Salzer, R.,
Kompositmaterial zur Resonanzverstärkung optischer Signale und Verfahren zu dessen Herstellung,
DP, AZ: 196 30 538.1, 1997

Wirth, H., Skorupa, W., Wondrak, W.,
Verfahren zum Abtragen einer Oberfläche eines Körpers,
07/97, DE 197 27 911.2

New Projects

- Sensoren für extreme Bedingungen (BMBF)
- Dotierung von Diamant (SMWK)
- Oxidationskinetik von Hochtemperatur-Legierungen (VW)
- c-BN im Mikrometer-Bereich (DFG)
- Harte Schichten auf Kohlenstoff-Basis (EU-TMR)
- Leerstellendiagnostik mit Positronen (SMWK)
- Plasma-Immersions-Implantation für Präzisionswerkzeuge (EU - BRITE/EURAM)
- Aktivierung von Dotanden (SMWA)
- Fenster für Abgasreaktoren (EU - COPERNICUS)

Research Center Rossendorf

Institute of Ion Beam Physics and Materials Research (FWI)

Postfach 510119
D-01314 Dresden

Tel. 0351-260-2245
Fax 0351-260-3285

DIRECTOR: **Prof. Dr. W. Möller** 2245
DEPUTEE: **Prof. Dr. E. Wieser** 3096

NEW MATERIALS (FWIM)
Dr. W. Skorupa 3612
- Semiconductors
- Optical Applications
- Defect Engineering
- Submicron Ion Beam

INDUSTRIAL CONTACTS (FWIK)
Dr. J. von Borany 3378

ION IMPLANTATION (FWII)
Dr. E. Richter 3326
- Surface Properties
- Ion Beam Assisted Deposition
- Plasma Immersion Implantation
- Operation of Implanters

MEV ACCELERATORS (FWIB)
Dr. M. Friedrich 3284
- Operation of MeV Accelerators
- Accelerator Mass Spectrometry

ION BEAM ANALYSIS (FWIA)
Dr. R. Grötzschel 2802
- High-Energy Ion Beam Analysis
- Elementary Processes of Ion-Surface-Interaction

STRUCTURAL DIAGNOSTICS
Dr. W. Matz 3122 (FWIS)
- Transmission Electron Microscopy
- X-ray Diagnostics
- Electron Spectroscopies
- Rossendorf Beamline at ESRF

THEORY (FWIT)
Dr. M. Posselt 3279
- Computer Simulation
- Reaction-Diffusion-Calculations
- Defects
- Precipitation

PREPARATION (FWIP)
Dr. B. Schmidt 2726
- PVD Coatings
- Reactive Ion Etching
- Wet Chemical Processing
- Annealing

Experimental Equipment

1. Accelarators, Ion Implanters and Ion-Assisted-Deposition

- ❑ van de Graaf accelerator — 1,8 MeV
- ❑ Tandem accelerator — 5 MV, Russian
- ❑ Tandetron accelerator — 3 MV, HIGH VOLTAGE, NL
- ❑ Ion implanter — 80 kV (Own construction)
- ❑ Ion implanter — 180 kV, medium current, SCANIBAL, FL
- ❑ High current ion implanter — 200 kV, high current, DANFYSIK, DK
- ❑ High energy ion implanter — 500 kV, HIGH VOLTAGE, NL
- ❑ Plasmaimmersion implantation — 5-60 keV
- ❑ Fine focused ion beam — 50 keV, 100 nm, 10 A/cm^2
- ❑ Ion beam assisted deposition
- ❑ Plasma enhanced chemical vapour deposition

2. Particle and Photon Based Analytical Techniques

❑	RBS	Rutherford backscattering	p,α: 1-6 MeV
❑	ERDA	Elastic recoil detection analysis	35 MeV, ^{35}Cl
❑	PIXE	Proton induced X-ray analysis	+ PIGE-option, external beam
❑		Nuclear microprobe	MeV, > 2 μm
❑	NRA	Nuclear reaction analysis	^{1}H(^{15}N,$\alpha\gamma$)^{12}C
❑	TEM	Transmission electron microscope	+ STEM-EDX, 300 kV, PHILIPS, NL
❑	STM	Scanning tunneling microscope	+ AFM-option, DME, DK
❑	AES	Auger electron spectroscopy	+ XPS-option, FISIONS, GB
❑		Mössbauer spectroscopy	
❑	XRD	X-ray diffraction	
❑		Spectroscopic ellipsometry	250-1700 nm, WOOLLAM, USA
❑	FTIR	Fourier transform infrared spectrometry	600-7000 cm^{-1}, NICOLET, USA

3. Other Analytical and Mesuring Techniques

- ❑ Surface profilometer — Dektak, VEECO, USA
- ❑ Micro indenter — SHIMATSU, J
- ❑ Scratch tester — SHIMATSU, J
- ❑ Spreading resistance measuring station — SENTECH, D
- ❑ Hall-effect equipment (< 600°C) — BIO-RAD, GB ; KEITHLEY, USA
- ❑ I-U and C-U- analyzer — KEITHLEY, USA

4. Preparation Techniques

- ❑ Wet chemical etching and cleaning — incl. anisotropic selective KOH-etching
- ❑ Photoliothographic patterning — 5 µm-level
- ❑ Thermal treatment — RT - 2000°C; Furnace, Flash lamp unit, Rapid thermal annealing, RF-Heating (Vacuum)
- ❑ Physical deposition — Sputtering DC / RF, Evaporation
- ❑ Dry etching — Plasma and RIE mode
- ❑ Bonding techniques — Anodic, Si-Si and WireBonding

List of Personnel

Director: Prof. W. Möller

Deputy Director: Prof. E. Wieser

Scientific Staff:
Permanent:

Dr. M. Betzl
Dr. L. Bischoff
Dr. J. von Borany
Dr. W. Bürger
Dr. F. Eichhorn
Dr. M. Friedrich
Dr. W. Fukarek
Dr. D. Grambole
Dr. R. Grötzschel
Dr. R. Günzel
Dr. V. Heera
Dr. K.-H. Heinig
Dr. H.-U. Jäger
Dr. A. Kolitsch
Dr. R. Kögler
Dr. U. Kreißig
Dr. W. Matz
Dr. A. Mücklich
Dr. C. Neelmeijer
Dr. D. Panknin
Dr. M.T. Pham
Dr. M. Posselt
Dr. F. Prokert
Dr. H. Reuther
Dr. E. Richter
Dr. B. Schmidt
Dr. J. Schöneich
Dr. H. Seifarth
Dr. W. Skorupa
Dr. J. Teichert
Dr. H. Tyrroff
Dr. M. Voelskow

Post Docs:

Dr. J. Brückner
Dr. J. Brutscher
Dr. A. Markwitz
Dr. N. Schell
Dr. M. Weiler
Dr. H. Weishart

Projects:

Dr. F. Fontaine
T. Gehring
Dr. S. Hengst
Dr. J. Hüller
Dr. O. Kruse
M. Mäder
Dr. M. Seidel

PhD Students:

K. Albe
F. Brenscheidt
M. Dobler
C. Fitz
S. Grigull
S. Hausmann
A. Höfgen
U. Hornauer
M. Jentschel
T. Koch
S. Mändl
D. Möller
I. Mrotschek
J. Noetzel
S. Parascandola
M.F. Plass
L. Rebohle
Br. Schmidt
M. Strobel
H. Wirth

Diploma Students:

T. Gebel
T. Schwieger

Technical Staff:
Permanent:

J. Altmann
R. Aniol
G. Anwand
I. Beatus
W. Boede
K.-D. Butter
W. Gäßner
B. Gebauer
H.-J. Grahl
P. Hartmann
F. Herrmann
G. Hofmann
M. Iseke
S. Klare
R. Kliemann
L. Kumpf
A. Kunz
G. Küster
D. Maul
M. Mißbach
K. Müller
F. Nötzold
W. Probst
E. Quaritsch
P. Reichel
B. Richter
M. Roch
E. Rost
B. Scheumann
H. Schluttig
E. Schmidt
G. Schnabel
J. Schneider
A. Scholz
C. Schulenberg
K. Sommerfeld
U. Strauch
K. Thiemig
S. Turuc
A. Vetter
A. Weise
I. Winkler

Projects:

G. Grunert
S. Scharfe
A. Schneider
H. Seifert
G. Winkler